https://ntrs.nasa.gov/search.jsp?R=19700001409 2020-03-12T04:19:09+00:00Z

46121
N70-10713
CR-106585

RESEARCH ON DIGITAL TRANSDUCER PRINCIPLES

Volume X.

THIN FILM TITANIUM DIOXIDE BY CHEMICAL VAPOR DEPOSITION

CASE FILE COPY

ELECTRONIC MATERIALS RESEARCH LABORATORY

THE UNIVERSITY OF TEXAS

COLLEGE OF ENGINEERING

AUSTIN

RESEARCH ON DIGITAL TRANSDUCER PRINCIPLES

Volume X.

THIN FILM TITANIUM DIOXIDE BY CHEMICAL VAPOR DEPOSITION

for the

NATIONAL AERONAUTICS AND SPACE ADMINISTRATION

GRANT NGL 44-012-043

Covering the Period

July 1, 1968 - December 31, 1968

by

Dale R. Harbison

H. Lyndon Taylor

William H. Hartwig

The University of Texas at Austin

Austin, Texas 78712

Page intentionally left blank

PREFACE

The discontinuous V-I characteristic of thin film MIS structures has been regarded as potentially productive of digital transducer action. The missing element is an active dielectric film which responds to external stimuli. At the outset, considerable research has been conducted by the senior author with a view to development of such "exotic" dielectrics. The justification is much broader, however, since new dielectric films are potentially useful in many microelectronics and integrated circuits areas.

Thin dielectric film formation by chemical vapor deposition (CVD) remains to be investigated as thoroughly as sputtering, evaporation, and oxidation. Chemical vapor deposition offers several advantages over other methods of dielectric film growth. Titanium dioxide has promise as a dielectric material in integrated circuits because of its high dielectric constant. Present emphasis on microelectronics and integrated circuits indicates a need for new materials to improve the performance of existing devices and to aid in new developments. High dielectric constant materials offer the advantage of higher capacitance without the necessity for larger areas or thinner films which lead to pin holes and device failure. This dissertation investigates using CVD of titanium organometallics to form thin films of TiO_2, followed by a study of the physical and electrical properties of the films.

The work described in this report received partial support from NASA Grant NGL 44-012-043, and from the NSF (Grant GK 1395) and the Joint Services Electronics Program (Grant AF-AFOSR-766-76).

ABSTRACT

The hydrolysis of titanium organometallics using hydrogen and carbon dioxide at 900°C forms a thin film of titanium dioxide with desirable properties. The frequency effects in the C-V curves of the dielectric differ for tetraisopropyl titanate and polymerized tetrabutyl titanate.

The 1 kHz capacitance per unit area is 0.21μF/cm^2 for a 2000 Å film on silicon. The dielectric constant of this film ranges from 50 on silicon to 80 on platinum. The dissipation factor ranges from 1% to 10%. The breakdown strength is 5×10^5 volts/cm. Capacitance-voltage data on MIS structures indicate an oxide space charge of approximately 10^{12} states/cm^2 with a flat-band voltage of zero volts. Measurements of the change in voltage required to maintain the flat band condition as the temperature is lowered give a density of fast interface surface states of less than 10^{12} states/eV-cm^2. Shifts in C-V curves with gate electrode material and SiO_2-TiO_2 mixtures suggests promising device applications. Current-voltage data indicate that the dominant conduction mechanism is Poole-Frenkel emission from donor and acceptor sites and traps within the bulk of the TiO_2 film. The activation energy is 0.11 eV and the conduction barrier height is 0.25 eV.

TABLE OF CONTENTS

Chapter		Page
	Preface	iv
	Abstract	vi
	Table of Contents	vii
	List of Illustrations	ix
	List of Symbols	xi
I.	Introduction	1
	A. Other Work on Titanium Dioxide	1
	B. Significance of this Work	3
	C. Experimental Techniques	4
II.	Film Formation Techniques	6
	A. Sputtering	7
	B. Vacuum Evaporation	8
	C. Thermal Deposition	9
	D. Chemical Vapor Deposition	9
III.	Fundamentals of CVD	13
	A. Vapor Plating Requirements	13
	B. Basic Kinetic Considerations	13
	C. Chemical Reactions	14
IV.	Experimental Techniques and Film Properties	18
	A. Apparatus	18
	B. Substrates	18
	C. Deposition Conditions	21
	D. Film Composition	22
	E. Appearance and Structure	23
	F. Adherence and Stability	23
	G. Thickness and Refractive Index	23
	H. Electrical Measurements	25
V.	Conduction Properties of Titanium Dioxide	27
	A. Conduction Mechanisms	27
	1. Ionic Flow	28
	2. Tunneling	28
	3. Space Charge Limited Current	29
	4. Thermionic Emission - Schottky Emission and Poole-Frenkel Emission	32
	B. Experimental Results and Discussion	40

Chapter		Page

VI Capacitance-Voltage Properties of Metal-TiO_2-Silicon 55

A. Theory of the M-O-S Structure 55
1. Accumulation 55
2. Flat Band 56
3. Depletion 56
4. Inversion 58
5. Effect of Surface States 60
6. Effect of Interface Contact Polarization Potentials 66
7. Effect of Work Function Difference 66

B. Experimental Results and Discussion 67
1. Dielectric Constant 67
2. Surface Charge and Surface States 68
a. Oxide Space Charge, Q_{so} 68
b. Fast Interface Surface States, Q_{FS} 73
3. Frequency Effects 83
4. C-V Shifts 85

VIII Summary and Conclusions 89

Appendix-Attempts to Grow Lead Titanate 92

Bibliography 94

LIST OF ILLUSTRATIONS

Figure		Page
1.	Deposition Apparatus	19
2.	Capacitance Measurement System	26
3.	Current-Voltage Measurement System	26
4.	Various Ways Tunneling Can Occur	29
5.	Energy Band Shape	30
6.	Mechanisms of Schottky and Poole-Frenkel Effects	33
7.	Restoring Force on an Escaping Electron	35
8.	Current vs. Temperature	41
9.	Current vs. $(\text{Voltage})^{1/2}$ for MIM Device	42
10.	Voltage vs. Film Thickness	44
11.	Current vs. $(\text{Voltage})^{1/2}$ for MIS Device	45
12.	Effect of Deposition Temperature on Conductivity	49
13.	Current vs. $(\text{Voltage})^{1/2}$ for MIS Device	51
14.	Conductivity vs. $(\text{Voltage})^{1/2}$	53
15.	Energy Bands and Charge Distribution for MIS Structure	56
16.	Charge Distribution and Capacitance Variation	59
17.	Surface State Occupancy	61
18.	Effect of a Charge Sheet within the Insulator	63
19.	Effect of Surface States and Work Function on C-V Curve	65
20.	Effect of Metal-Semiconductor Work Function Difference	65
21.	Capacitance and Dissipation Factor vs. Bias	69
22.	Capacitance vs. Bias for p-type Sample	71
23.	Capacitance vs. Bias for n-type Sample	74
24.	Flat-band Voltage vs. Change in Fermi Level with Temperature	77

Figure | Page

25. Equivalent Circuit of MIS Capacitor 80

26. Capacitance vs. Bias for "PB" Prepared Samples 84

27. Electrode Effects on Capacitance vs. Bias 86

28. SiO_2 Effects on Capacitance vs. Bias 87

LIST OF SYMBOLS

A	Area (cm)
C_T	Total Capacitance (farads)
C_o	Oxide capacitance (farads)
C_{sp}	Space charge capacitance (farads)
C_{SFB}	Capacitance of space charge layer at flat band (farads)
C_{FB}	Flat-band capacitance (farads)
C_s	Surface state capacitance (farads)
C_p	Equivalent parallel capacitance (farads)
C_m	Measured capacitance (farads)
d	Film thickness (cm)
e	Charge on an electron = 1.6×10^{-19} (coulombs)
E_F	Fermi energy (eV)
E_c	Lowest energy in conduction band (eV)
E_v	Highest energy in valence band (eV)
E_d	Energy of donor sites (eV)
E_A	Energy of acceptor sites (eV)
F	Free energy (kilo-cal)
G_m	Measured conductance (mhos)
G_s	Surface conductance (mhos)
G_p	Equivalent parallel conductance (mhos)
h	Planck's constant = 6.62×10^{-34} (joule-sec)
H	Heat content of the system at constant pressure (kilo-cal)
I	Current (amps)
J	Current density (amps/cm^2)
k	Boltzmann's constant = 1.38×10^{-23} (joule/^{o}K)

L_D Debye length (cm)

m Slope of the Schottky type plot $(m/volt)^{1/2}$

m^* Effective mass (kg)

N_A Acceptor concentration (cm^{-3})

N_D Donor concentration (cm^{-3})

N_C Effective density of states in conduction band (cm^{-3})

N_V Effective density of states in valence band (cm^{-3})

n Concentration of free carriers (cm^{-3})

n_i Intrinsic carrier concentration (cm^{-3})

n_o Density of states in conduction band, including concentration of traps (cm^{-3})

N_{so} Oxide space charge density $(states/cm^2)$

N_{FS} Interface state charge density $(states/ev\text{-}cm^2)$

q Charge on the carriers (coulomb)

Q_{so} Oxide space charge $(coulombs/cm^2)$

Q_{FS} Interface state charge $(coulombs/cm^2)$

Q_s Surface state density $(coulombs/cm^2)$

r Parameter ranging between 1 and 2 depending on degree of compensation

S Entropy (cal/degree-mole)

T Temperature ($^\circ$K)

U Electron hole pair generation rate (carriers/sec)

u_b Bulk potential (volts)

u_s Surface potential (volts)

V_{FB} Flat-band voltage (volts)

V Voltage (volts)

X_d Depletion layer width in semiconductor (cm)

X_m Space charge width in insulator (cm)

ε	High frequency dielectric constant of dielectric
ε_o	Permittivity of free space = 8.85×10^{12} (farads/m)
ξ	Electric field (volts/cm)
ε_d	Activation energy (eV)
κ	Low frequency dielectric constant of dielectric
κ_s	Dielectric constant of semiconductor
λ	Wavelength (cm)
$\Delta\phi_{PF}$	Barrier lowering for Poole-Frenkel emission (eV)
$\Delta\phi_s$	Barrier lowering for Schottky emission (eV)
ϕ_{ms}	Metal-semiconductor work function (volts)
ϕ_m	Metal work function (volts)
ϕ_s	Semiconductor work function (volts)
ϕ_o	Potential barrier at the interface (eV)
ϕ_{max}	Maximum barrier at the interface (eV)
ϕ	Energy difference between emission site and bottom of conduction band (eV)
ψ_m	Metal potential barrier (eV)
ψ_s	Semiconductor potential barrier (eV)
ψ_i	Insulator potential barrier (eV)
ρ	Charge density (coulomb/cm^3)
σ	Conductivity (mhos/cm)
$\tan \delta$	Dissipation factor
μ	Mobility of carriers (cm^2/volt-sec)
χ	$\psi_i - E_F$ (eV)
ω	Frequency = $2\pi f$ (radians/sec)
τ	Majority carrier time constant (sec)
τ_o	Effective carrier lifetime in depletion region (sec)

CHAPTER I.

INTRODUCTION

Present efforts on dielectric thin films emphasize their formation by oxidation, anodization, evaporation, and sputtering. Chemical vapor deposition offers several advantages over other methods of dielectric film growth, such as versatility in choice of substrate, homogenous oxide film, a sharper and cleaner interface, greater control over the composition of the film, and more control over the thickness and growth rate.

To be compatible with integrated circuits, a thin film capacitor must satisfy several criteria, including low dissipation factor, high stability during integrated circuit processing, voltage insensitivity, and high yield. Many materials currently used as capacitor dielectrics for thin film microcircuits exhibit low dielectric constants or low breakdown voltage. Titanium dioxide is attractive as a dielectric material in integrated circuits since the dielectric constant in rutile parallel to the C-axis is 170[19]. High dielectric constant materials offer the advantage of higher capacitance without the necessity for larger areas or thinner films which lead to pin holes and device failure.

In the present work organometallics of titanium in an oxidizing atmosphere containing water vapor from hydrogen and carbon dioxide form thin films of titanium dioxide with desirable dielectric properties on metals and on silicon.

A. Other Work on Titanium Dioxide.

Titanium dioxide films for optical applications were first prepared by oxidation of the metal in air and anodization of the metal[63]. Titanium dioxide films for dielectric applications have been prepared by anodization[74], chemical vapor deposition of titanium tetrachloride and tetraisopropyl

titanate with water vapor (steam) at a substrate temperature of 150°C[49,50], chemical vapor deposition of tetraisopropyl titanate in an oxygen atmosphere at 700°C[138], glow discharge,[89] reactive sputtering,[81] and by direct evaporation of titanium dioxide by heating in a vacuum[65].

Martin[89], in 1962, reported the formation of TiO_2 films by glow discharge. Leaking reactive gases into an evacuated bell jar in the vicinity of the discharge forms the films. The films were amorphous with a dielectric constant of 90, but became crystalline with a dielectric constant of 40 when heat treated at 350°C for one-half hour. For 2500 Å films at 1 kHz the capacitance per unit was .15μF/cm^2, with a dissipation factor of 2.6% and a breakdown strength of 4×10^5 volts/cm.

Lakshmanan[81], in 1963-65, used reactive sputtering to form films of titanium oxide. Pure titanium cathodes in an oxygen-argon gas mixture forms the films. Capacitance of .30μF/cm^2 and dissipation factors of 5.5% at 1 kHz are reported for films between 1000 Å and 1600 Å thick.

Von Hippel[132], in 1964, reported on the growth and structure of titanium films on alkali halide crystals and the effect of controlled oxidation of these films while van Raalte,[131] of the same laboratory, reported on conduction phenomena in rutile single crystals. He reported an increasing conductivity with time due to increased effective carrier mobility caused by the filling of shallow traps and due to an increased positive space charge throughout the bulk of the crystal, enhancing electron injection.

In the 1963-64 Feuersanger[49,50] formed thin films of TiO_2 by the vapor reaction of titanium tetrachloride or tetraisopropyl titanate with water vapor at a substrate temperature of 150°C. The water vapor is introduced in the form of steam from oxygen or nitrogen bubbled through hot water. These films have dielectric constants of 80 and capacitances of 0.5μF/cm^2

with a dissipation factor of 2.3% and a breakdown strength of 2-7 x 10^5 volts/cm.

Very recently Yokozawa[138] formed thin films of titanium dioxide by the decomposition of tetraisopropyl titanate in a dry oxygen atmosphere at 700°C. The films were porous and easily etched by diluted HF. The films consist of fine crystallites of anatase. The refractive index is 2.0. No electrical data is reported for these films.

In 1965 Peterson [103,104] deposited titanium dioxide films by the reaction of tetraisopropyl titanate with oxygen at a substrate temperature of from 300-500°C. However, he discontinued this work because of low dielectric strength (3 x 10^5 volts/cm) and instability of the film to electrical stress. The anodized films of TiO_2 form only on titanium substrates and show a dielectric constant of about 40. Direct evaporation of titanium dioxide by heating in a vacuum results in a loss of oxygen of the evaporant. Such deposits are semiconducting rather than insulating.

The above authors report only a limited amount of electrical data. Maserjian and Mead[90] describe the electrical properties of thin film sandwiches of Al-TiO_2-Al with evaporated films varying in thickness from 100 to 410 Å. Their results are interpreted in terms of a large ionic space charge in the TiO_2 films. These films have a dielectric constant of 27.

B. Significance of this Work.

A knowledge of the conduction behavior of titanium dioxide films on silicon and metal coated quartz substrates with different contacts is the expected result of this work. The existence of a large ionic space charge as observed by Maserjian[90] for very thin evaporated films would not necessarily be expected for these thicker films formed by CVD due to the difference in processing. This type of data and these results have been unexplored prior to this work[67].

The capacitance-voltage data yield information about the outer oxide surface state density, the fast interface surface state density, frequency effects due to the various source materials, electrode effects, and SiO_2-TiO_2 mixture effects that have not been reported by other investigators[67].

The experimental technique resembles that of Feuersanger[50] and Yokozawa[138], but is different in that hydrogen and carbon dioxide form the water vapor in preference to bubbling the carrier gas through heated water[50] or dry O_2[138]. Feuersanger's[50] technique has the advantage of low deposition temperature (150°C versus 900°C), however, the hydrogen and carbon dioxide seems to be more desirable for reasons enumerated in Chapter III.

C. Experimental Techniques.

The main experimental technique applicable to thin film dielectrics is a study of their electrical properties. The experimental program involves making metal-insulator-metal (MIM)structures and metal-insulator-semiconductor (MIS) structures and measuring their capacitance and conduction.

Two basic techniques apply to the study of the electrical properties: Capacitance versus bias versus frequency and dc current transport. Capacitance data give information about the interface states, oxide surface states, and dielectric constants. The current-voltage measurements at various temperatures yield information about the breakdown strength of the material, uniformity of the films, various conduction mechanisms, barrier heights, and trap levels in the energy band.

A knowledge of current-voltage characteristics helps the device engineer, as well as supplying basic information about the material. These characteristics relate to the design of field effect transistors (FET)[33]. The leakage current of the dielectric affects the characteristics and must be considered in design. This leakage current also provides warning as the

dielectric approaches breakdown. This current-voltage behavior is also of importance to the design of new surface state and interface digital transducer concepts described by Hartwig[72].

Surface-state densities gained from capacitance-voltage data is also of importance to device engineers. More fast surface states can decrease the channel mobility causing lower gain-bandwidth products in MOSFET's. They also increase the switching voltage of enhancement mode FET's. Fast surface states affect MOS performance by altering the reactance of the MOS varactors by filling and emptying of charge in and out of these states at the ac measurement frequency. Also, the charge in the states is an added component to the surface charge at the insulator-semiconductor interface. Oxide surface-state density is a parameter which controls the threshold of MOS enhancement mode FET switches, the operating point of MOS depletion mode FET amplifiers, the PNP transistor collector junction leakage, and parasitic surface capacitance[33].

CHAPTER II

FILM FORMATION TECHNIQUES

Several techniques exist for forming dielectric thin films. All the dielectric film formation techniques have both advantages and disadvantages. Surface reactions like oxidation depend on an appropriate starting material, but process easily. Vacuum evaporation readily forms films of materials which vaporize congruently at "reasonable" temperatures, but most dielectrics do not evaporate congruently. Flash evaporation avoids atomic species separation, but requires special apparatus and a solid powder form of source material.

The multiple forms of sputtering made it a wide ranging technique. DC sputtering works for metallic anode materials. RF or AC sputtering can avoid space charge build-up on insulating source materials by neutralization from the plasma electrons. The greatest versatility of sputtering arises through chemical reaction at the source, in the gas, or at the target in the process of reactive sputtering. Multiple-electrode sputtering offers another way to form films containing several atomic species, but requires fairly complex processing.

Chemical vapor deposition uses a basically simple reaction chamber for any kind of reaction. The process complications arise in obtaining gaseous reactants, controlling the flow of reactants and carrier gases, and optimizing the flow of gases around the substrate. In principle, however, nearly any material can be formed on nearly any other material that is thermally and chemically compatible.

The detailed characteristics of dielectric films may depend significantly on the formation process. This section discusses these processes in greater detail.

A. Sputtering.

Sputtering is a process whereby the impact of a stream of accelerated ions vaporizes a target. In dc sputtering, several thousand volts dc are placed between two electrodes in a vacuum of 10^{-3} to 10^{-1} torr. The resulting glow discharge contains high energy ions, accelerated by the high field, which strike the cathode and dislodge neutral atoms or molecules. These nuetral species radiate outwards from the target surface and deposit on a substrate[45]. This technique requires the target to be a conductor as otherwise the initial bombarding ions create a region of positive space charge in the vicinity of the target thereby shielding the target from further bombardment. RF sputtering techniques avoid this by applying an RF voltage to the target with respect to the plasma. On alternate half cycles, the positive space charge building up is neutralized by plasma electrons. RF sputtering is a useful technique for the deposition of insulators[42] with the limitation that the atomic species in the film deposited is the same as that of the target. In reactive sputtering, some chemical reaction takes place prior to sputtering (the surface of the target is altered to possess a thin reacted surface layer), during sputtering (the species dislodged during bombardment is reacted chemically during its transport to the substrate surface)[121] or after sputtering (the film deposited on the substrate surface is altered through some chemical reaction).

Non-reactive sputtering is suitable for the deposition of metals and conductors while reactive sputtering is suitable for the deposition of dielectrics. The requirement of maintaining a gas discharge limits the practical range of gas pressure and influencesthe useful range of gas mixtures.

Advantages of sputtering include the fact that the substrate temperature can be lower than in CVD. This allows the films to be deposited on substrates which would melt at high temperatures (i.e., Al).

The cleaning of surfaces to be coated by physical vapor deposition methods is more difficult than that required for CVD[6]. No vigorous chemical action occurs at the surface as an inherent part of the coating process as in CVD. Sputtering does produce more adherent films than vacuum evaporation because of the greater ion energies. The substrate temperature is normally sufficiently low during deposition that little diffusion of the deposit into the substrate occurs.

B. Vacuum Evaporation.

Vacuum evaporation is basically simple in theory and in many applications[65]. The material to be applied is heated in a high vacuum to a temperature at which its vapor pressure is about 10^{-2} torr or greater. Thus, this process involves the transfer of material and the formation of coatings by physical means alone. In the evaporation of non-elemental material (i.e., compounds), dissociation or incongruent evaporation may occur, followed by varying degrees of recombination of the compounds at the place of impingement[6]. Since no chemical reaction occurs at the surface as an inherent part of this process, the cleaning of surfaces is difficult with this technique.

One obvious advantage to this technique is the low substrate temperature required. Other vacuum methods are available for the deposition of compounds. One of these is flash evaporation. Films of $BaTiO_3$ and $SrTiO_3$ have been prepared[97,98] by this method. Individual grains of the compound are fed onto a hot surface at a rate such that one volatilizes completely before the next one arrives. This method does not offer much desirable variation in the composition of the deposited film. The deposition of compounds by co-deposition from multiple vapor sources requires accurate knowledge and control of vapor source temperature, areas, and vaporization rates. Because of the difficulties involved in securing and maintaining these conditions, this technique

has not been used to any great extent[6].

C. Thermal Deposition.

Thermal oxidation is an important technique for forming thin films[35]. Silicon dioxide thermally grown on silicon is the best example of this technique. Thermal oxidation disadvantages include film not structurally perfect, film purity not perfect, high temperature required, abnormal transition regions at metal-insulator or semiconductor-insulator interface, and the composition of the film is limited by the substrate. The main objections really stem from the fact that years of technological development have yet to make these materials perform as satisfactorily as device reliability and performance criteria demand.

D. Chemical Vapor Deposition.

In CVD solid deposits are formed by chemical reactions which take place on, at, or near the deposition surface. Vapor deposited materials are of great importance at present and promise even greater importance because the deposition process is an extremely versatile and usefully inexpensive method of molecular forming[6]. While in physical vapor deposition the medium is a vacuum or a rarefied gas, in CVD the medium is a chemically reactive gas mixture which is thermally activated to deposit material. CVD has the disadvantage that the substrate must be heated to relatively high temperatures, but these temperatures would not be detrimental in many applications. It has the advantage that it is applicable to the widest range of materials[6].

In CVD and in physical vapor deposition feed vapors are generated by evaporation from a surface and the volatilized material is then transported to a substrate on which it condenses or decomposes.

With CVD it is possible to volatilize selectively a feed material, transport it to the desired location, and precipitate it as a controlled

structure. Further purification can be achieved in the chemical transport system by separate distillation of the volatile intermediates, as well as selective reaction either at the source or at the heated substrate.

By reason of the very large number of available chemical reactions, CVD is seen to be a process of great versatility and flexibility[6]. It does not require the use of ionizable compounds or any degree of electrical conductivity in the substrate or deposit. Highly insulating materials are deposited as readily as pure metals. Also, CVD can be used to deposit compounds which are too unstable to be deposited without marked change in composition by physical vapor deposition. CVD can be carried out over a pressure range from super-atmospheric down to pressures characteristic of physical vapor deposition.

Blocher[112] recently enumerated three main differences in CVD and simple condensation. (1) Simple condensation is exothermic and most useful CVD reactions are endothermic. By the use of endothermic processes, the reactions can be delayed more effectively until the reactant gases reach the heated substrate. The use of endothermic reactions generally introduces an appreciable energy barrier to the kinetics of the reaction, but at the higher pressures and temperatures of CVD equilibrium is more easily approached than in simple condensation. (2) Though vacuum evaporation-condensation plating processes operate at pressures in the molecular flow region, CVD operates in the viscous flow region with associated carrier gases through which the reactant must diffuse to reach the substrate. Carlton and Oxley[112] thoroughly discuss this subject. This diffusion barrier places an upper limit on the attainable nucleation density. However, the ratio of the nucleation rate to growth rate depends on the nature of the system and the temperature and can be varied to increase nucleation. (3) Whereas only the condensable vapor of

the material being deposited need be considered in a clean condensation system, CVD involves other chemical species. These intrinsic impurities are considered to have a number of possible effects depending on the nature of the impurity, the adsorbed monomer and the substrate. Since such effects would be specific to the system in question and would operate in many directions, it is impossible to account for them quantitatively.

The expitaxial growth of elemental semiconductors by chemical vapor deposition is now a well established technique[2,35,36,79,114,128], in spite of its slow initial acceptance. Two major vapor phase systems used for the elemental semiconductor growth are pyrolytic decomposition of halides or hydrides and the hydrogen reduction of halides.

The production of pigments and reinforcing agents is the largest application of CVD to date[6]. Carbon blacks and pigment-grade titanium dioxide made by burning $TiCl_4$ are the largest items of importance. Next in importance are the carbonyl metals, particularly nickel.

The need for refractory materials in the aerospace industry is an important application of CVD. Niobium, molybdenum, tantalum, and tungsten are conveniently deposited by hydrogen reduction of the corresponding halide vapors. Refractory metal carbides are obtained by reaction of the metal halides with hydrocarbons.

Many metals have been successfully deposited by CVD. Powell[6] gives summaries of the conditions used to prepare deposits of Al, As, Sb, Bi, Cr, Co, Cu, Ge, Au, Fe, Pb, Mo, Ni, Ta, Pt, Re, Sn, Ti, W, U, V, and Zr. Numerous references are given for each metal. Powell[6] also gives a similar treatment for chemically deposited nonmetals such as boron and borides[55,57], carbon and carbides, nitrides, silicon and silicides, and oxides. Of great importance in the microelectronics field is the recent work in CVD of SiC[30,76],

Si_3N_4[29,40,121,136] and SiO[28,91]. Powell[6] lists references for CVD of various oxides, including Al_2O_3, Cr_2O_3, GeO, Fe_2O_3, SiO_2, TiO_2, and others.

Chemical vapor deposition offers several advantages over other methods. Some of these advantages are:

1. Much versatility is possible since films can be deposited on metals, semiconductors, or other dielectrics.
2. The oxide film should be very homogeneous since the reactant emanates from a source with preservable integrity.
3. The composition of the film can be controlled independently of the composition of the substrate.
4. The processes involved generally can be carried out at lower temperatures than those required for deposition in inorganic systems.
5. The reactant and product vapors of the organic systems are usually less reactive and corrosive than those of the inorganic systems.
6. Coating thickness can be varied, and fairly well controlled over a wide range.
7. The very large number of available chemical reactions assures chemical vapor deposition to be a process of great versatility and flexibility.
8. The organic reactions are more suitable for the preparation of high purity oxides.
9. Due to the large number of variables, such as gas temperature, gas flow rate, substrate temperature and time, greater control over film composition is possible.

CHAPTER III

FUNDAMENTALS OF CVD

A. Vapor Plating Requirements.

The general requirements for any gas plating reaction may be summarized as follows:

1. The reactants must be in the gaseous or vapor state;
2. the product to be deposited must be condensible at the substrate; and
3. the by-products formed in the reaction chamber must be sufficiently volatile to allow their ready removal.

In addition to these general requirements, the thermodynamics and kinetics of any particular vapor plating reactions impose restraints upon the deposition temperature and reactant concentrations which are unique to the reaction under consideration[6].

B. Basic Kinetic Considerations.

A number of steps must occur for the overall deposition[6]: Diffusion of the reactant through the static layer adjacent to the substrate; adsorption onto the substrate; diffusion of the adsorbed species across the surface to active sites; the chemical reaction; deposition of the non-volatile products; desorption of the volatile products; and their diffusion away from the vicinity of the substrate. The first and last steps are generally not independent, since the diffusion rate of the reactants affects the diffusion rate of the products, and stoichiometry influences the two steps of the reaction, and both affect the chemical reaction rate. The complex intermediate steps normally involve surface and gaseous reactions, as well as simultaneous adsorption-desorption and nucleation processes. Any of the above steps may determine the rate of deposition. Each step has a temperature dependence

which determines its relative importance. In the low-temperature range ($< 350^{\circ}C$) the deposition rate depends predominately on the chemical kinetics. That is, the deposition rate is relatively insensitive to the flow except at very low flows, but is strongly dependent on deposition temperature. In the high temperature range ($> 350^{\circ}C$) the major limiting factor is gas-phase diffusion. In this case, the rate of deposition depends strongly upon the geometry of the deposition system and upon the flow. The deposition rate is relatively insensitive to the temperature.

In establishing the overall kinetics of the deposition, one needs to treat the experimental data so as to evaluate the relative influence of the diffusion flux and the chemical kinetics, and to develop expressions for calculating their simultaneous influences on deposition rate.

C. Chemical Reactions.

The free-energy function provides a true measure of the chemical affinity of a reaction. The free-energy change in a chemical reaction is defined as $\Delta F = F$ (products) - F (reactants). When the free energy change is zero, the system is in a state of equilibrium. When the free-energy change is positive for a proposed reaction, net work must be put into the system to effect the reaction. When the free-energy change is negative, the reaction can proceed spontaneously with the accomplishment of the net work.

For processes occurring at constant temperature and constant pressure:

$$F = H - TS$$

The free-energy F is equal to the difference in enthalpy or heat content H of the system at constant pressure and the product of the system temperature T and the entropy S.

The deposition process depends on the decomposition of the vapors of organometallic compounds. This decomposition takes place at atmospheric

pressure in an oxidizing atmosphere containing H_2O to control the stoichiometry of the resulting oxide. The oxygen is introduced in the form of water vapor generated by the reaction

$$H_2 + CO_2 = H_2O + CO \quad [1]$$

at the substrate. This reaction is not surface catalyzed and proceeds readily in the forward direction provided the temperature of the gases is greater than 800°C. The water-gas reaction is incorporated primarily to reduce the premature hydrolysis of the organometallics since they would react with any water vapor that exists in the vapor space forming finely suspended alkoxides. Thus, it is essential that all components retain their individual identities until they reach the substrate where they spontaneously react[6].

Various organometallics supplied by duPont as "Tyzor" organic titanates[130] were used, including the alkyls [tetraisopropyl titanate (TPT), tetrabutyl titanate (TBT), polymerized tetrabutyl titanate (PB)], and a chelate [titanium acetyl acetonate (AA)]. Tetraisopropyl titanate exhibits the highest vapor pressure of any of the tetraalkyl titanates and thus is the most suitable candidate for vapor phase applications. On exposure to water, moist air, or substances containing water the alkyl titanates hydrolyze. "Tyzor" PB is a partially hydrolyzed titanate and is a prepolymer of the ultimate polymerization product, titanium dioxide. The titanium chelates are much less reactive than simple alkyl titanates and proved ineffective in forming TiO_2. The tetrabutyl titanate has such a low vapor pressure that it condenses into a powdery deposit in the room temperature flow lines between the vaporizer and the deposition chamber. Both TPT and PB work satisfactorily, however, the PB requires a source temperature 2-3 times greater than the TPT. The reaction that follows equation 1 above for TPT is

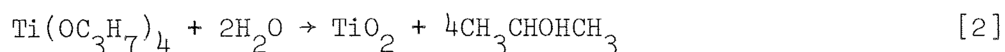

$$Ti(OC_3H_7)_4 + 2H_2O \rightarrow TiO_2 + 4CH_3CHOHCH_3 \quad [2]$$

The titanium compound above is liquid at room temperature and has sufficient vapor pressure to permit the rate of delivery of the respective gas to the reactor to be controlled by regulation of the flow of hydrogen over the liquid, rather than bubbling through the liquid. This is desirable in order to prevent the formation of spray droplets which may collect downstream, producing a variable and too concentrated a plating atmosphere. They may also tend to nucleate growth defects on the surface of the substrate[6]. This would appear to be a disadvantage in the water-bubbler system used by Feuersanger[50].

For the reactions under consideration the standard free energies are negative at room temperature, but the reactions will not occur at this temperature because they are dependent upon the water vapor being produced by the water-gas reaction, equation 1.

Work on various metal-organic compounds presented at a Symposium on Metal-Organic Compounds at the Miami meeting of the American Chemical Society in April, 1957, appears in book form[13]. From papers presented by Herman and Beachman of the National Lead Co. and Hasham of duPont at this conference and from work of Bradley[14], Brill[16], and other published data[15], one gains an insight into the chemistry of titanium organic compounds.

The alkyl titanates may be considered the esters of orthotitanic acid [$Ti(OH)_4$] in which the four hydrogens of that hypothetical acid are replaced by four alkyl groups. Thus $Ti(OR)_4$ is the general formula for an alkyl titanate, R representing the alkyl group.

On exposure to water, moist air, or substances containing water or hydroxyl groups the alkyl titanates hydrolyze. Isopropyl titanate hydrolyzes very rapidly, sec-butyl titanate hydrolyzes rapidly, butyl titanate

hydrolyzes and 2-ethylbutyl and 2-ethylhexyl titanates hydrolyze relatively slowly, thus affording the researcher an opportunity to vary rates of hydrolysis, as well as the type of hydrolysis product. The extent and rate of the reaction are mainly dependent upon the ratio of water to alkyl titanate. In all cases the eventual result of the complete hydrolysis is the formation of titanium hydrate and released alcohol. The mechanism is believed[16] to involve the formation of an intermediate complex between the ester and water.

The hydroxyl ester cannot be isolated since it immediately reacts to give the dimer. The hydrolysis proceeds stepwise as shown in the following reaction[16,130]:

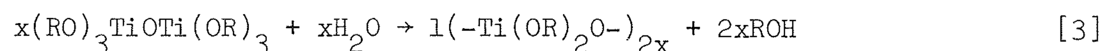

$$x(RO)_3TiOTi(OR)_3 + xH_2O \rightarrow 1(-Ti(OR)_2O-)_{2x} + 2xROH \qquad [3]$$

and continues as follows

$$(-Ti(OR)_2O-)_x + xH_2O \rightarrow xTiO_2 + 2xROH \qquad [4]$$

giving as the end result a clear amorphous film of TiO_2. As pointed out previously, the water-gas reaction, equation 1, will make this reaction more controllable and prevent deposition of the TiO_2 prematurely before reaching the substrate.

The alkyl titanates, when heated, pyrolyze to yield relatively hard glassy products[16]. In the case of tetraisopropyl titanate, the reaction can be illustrated as:

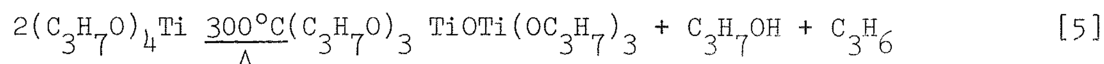

$$2(C_3H_7O)_4Ti \xrightarrow[\Delta]{300^{\circ}C} (C_3H_7O)_3\ TiOTi(OC_3H_7)_3 + C_3H_7OH + C_3H_6 \qquad [5]$$

The primary decomposition products of isopropyl titanate seem to be propylene, isopropyl alcohol, and titanium dioxide[13].

Current-voltage data presented in Chapter V show the high temperature hydrolysis films to be superior to the lower temperature pyrolysis films.

CHAPTER IV.

EXPERIMENTAL TECHNIQUES AND FILM PROPERTIES

Chemical vapor deposition (CVD) utilizing the reaction of titanium organometallics in an oxidizing atmosphere containing water vapor forms the titanium dioxide films of this work. Chapter II discusses CVD as a film formation technique in relation to other techniques. Chapter III discusses the organometallic compounds used and the reactions involved.

A. Apparatus.

Figure 1 illustrates the deposition apparatus. It provides a means for regulation of the reactant concentrations at the plating zone, a means of dispersing the reactants evenly over the substrate, and a means for the regulation of the substrate temperature. The temperature sensor is an Ircon infrared radiation pyrometer focused through a quartz window onto the substrate surface. The substrate rests on a graphite susceptor inductively heated at 300 kHz. The water jacket surrounding the reaction chamber keeps the quartz wall temperature low enough to limit the deposition to the susceptor and substrate. Pressure regulators, regulating valves, and flow meters provide the necessary regulation and control. A gas washing bottle serves as a vaporizer for the reactant which is liquid at room temperature. Quartz, stainless steel, and teflon lines, valves, and fittings help insure purity of the deposit.

B. Substrates.

Substrates are platinum-coated quartz and polished silicon. The silicon is 10 ohm-cm p-type [111] and 20 ohm-cm n-type [111] mechanically polished. The slices are one inch diameter and eleven mils thick. The quartz discs are one inch diameter and 1/16 inch thick. A glass cleaning solution consisting of 35 cc saturated potassium dichromate in 1 liter of concentrated

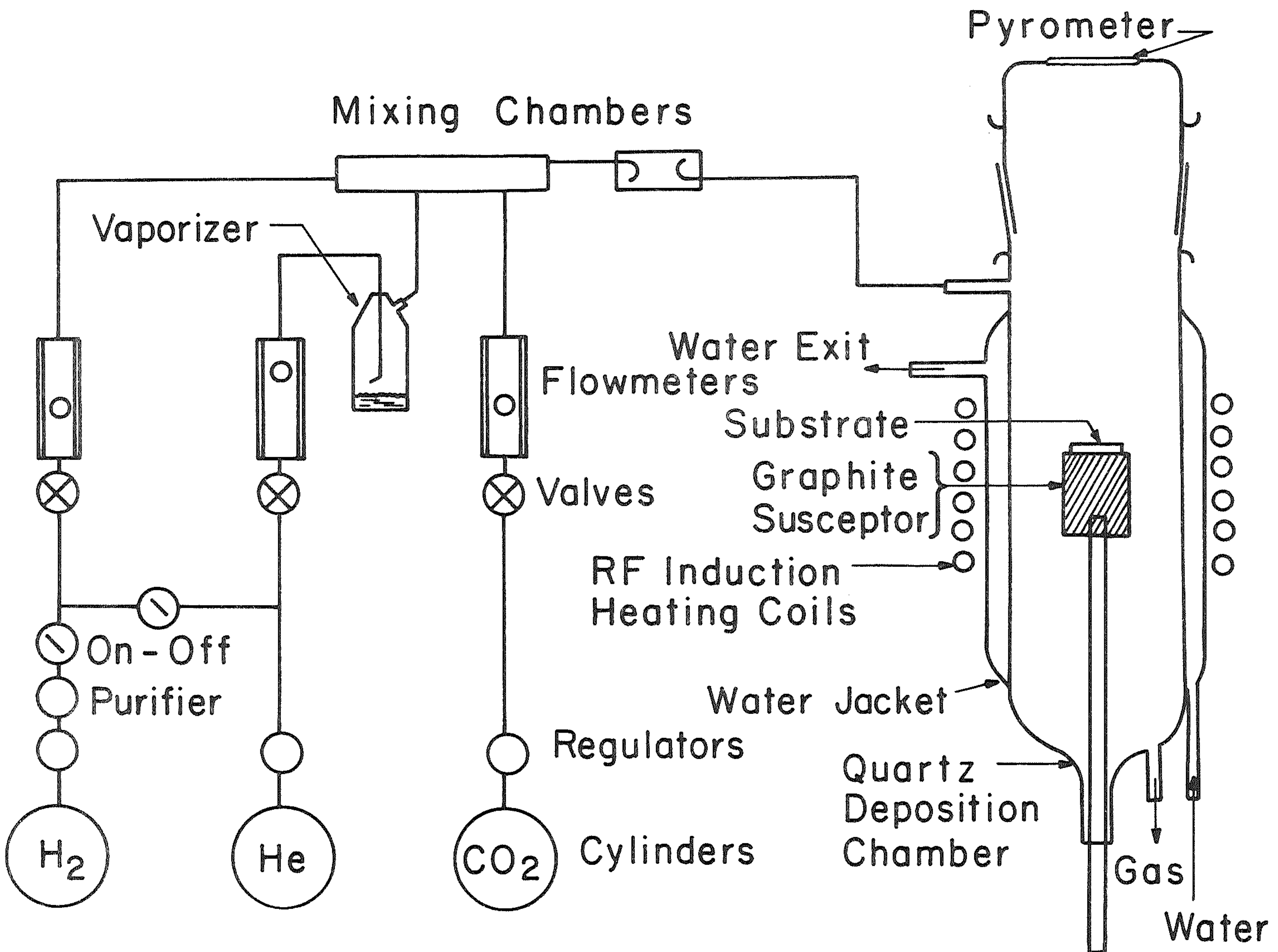

Fig. 1 Deposition Apparatus

sulfuric acid, followed by rinses in deionized water, methanol, and trichlolethylene cleans the quartz discs. The platinum evaporates onto the quartz disc from a tungsten filament at a pressure of 10^{-5} torr in a diffusion pumped system. Eight mil wire, tightly wound onto the filament, serves as the evaporation material. The cleaning procedure[135] for the silicon slices is:

1. Use deionized water in all cleaning steps.
2. Clean all glassware and other hardware to be used with a nonionic detergent or cleaning compound.
3. Scrub the wafers with detergent.
4. Place each wafer in a 50 ml beaker and flush with water five times.
5. Cover the wafer with methyl alcohol and ultra-sonically agitate for 30 seconds.
6. Pour off methyl alcohol and cover with trichloroethylene.
7. Heat the trichloroethylene until boiling has been observed for 30 seconds.
8. Pour off the trichloroethylene and repeat step 7.
9. Pour off the trichloroethylene and cover with methanol.
10. Pour off the methanol and flush beaker with water five times.
11. Fill the beaker half full of concentrated nitric acid and heat at 80°C for approximately 20 minutes.
12. Pour off the nitric acid and flush with water five times.
13. Cover with 48% hydrofluoric acid for two minutes to remove any silicon oxide.
14. Rinse with water five times.
15. Cover with methyl alcohol for 30 seconds.
16. Pour off methyl alcohol and store in trichloroethylene.

C. Deposition Conditions.

After cleaning and placing the sample in the deposition chamber, flushing the system with helium gas precedes heating. After heating the sample to the desired temperature in a hydrogen atmosphere for three minutes, the gases are introduced as follows:

H_2: 530 cm^3/min

CO_2: 240 cm^3/min

He across $Ti(OC_3H_7)_4$: 4600 cm^3/min

Temperature of $Ti(OC_3H_7)_4$: 100°C

Temperature of substrate: 900-950°C

Growth rate: 100 Å/min

Observing the color of the interference fringes gives the film thickness during deposition. At the desired thickness, the He and CO_2 are shut off, but the hydrogen remains. Cooling the substrate in hydrogen precedes a final helium flush. The commonly used thickness is 2000 angstroms. Evaporated aluminum or platinum dots with 1 mm^2 area form the upper metal electrode at 10^{-5} torr. Deposition temperatures ranged from 400°C to 1000°C, however, the films formed at temperatures below 850°C exhibit poor electrical properties as shown in Chapter V and appear by fast neutron activation analysis[26] to be oxygen deficient and not stoichiometric TiO_2. The thickness of the deposited film increases linearly with time. The deposition rate is constant, since the film is deposited from a chemical reaction, and not diffusion limited in the solid, as is the case of thermally grown oxides. The deposition rate is dependent on the flow rates of the gases and on the temperature of the organometallic, but is relatively independent of the substrate temperature. This agrees with the thermodynamic predictions of Chapter III. No observable differences occur in the deposition of the film on platinum or silicon substrates.

D. Film Composition.

Fast neutron activation analysis determined the stoichiometry of the films[26]. The irradiation and measurements of ^{16}N activity used in the oxygen determination were made at the Texas Nuclear Corporation on a 150 KeV positive ion accelerator and the measurements of the ^{48}Sc activity used in the titanium determination were made with a Triga Reactor in the Neutron Activation Analysis Laboratory of the Nuclear Reactor Laboratory of The University of Texas at Austin. The determination of activity induced in titanium is simplier because of the longer half-life. Comparison of the radioactivity produced between that produced in the deposited thin films and that in standard mixtures having known proportions of titanium and oxygen determines the proportion of titanium and oxygen in the deposited film. The technique has the advantage of being rapid and non-destructive. The technique is based on the principle that when a material is irradiated by the neutrons from a nuclear reactor, particle accelerator, or other suitable source, some of the atoms present in the material will interact with the neutrons and be converted into different isotopes of the same element or isotopes of different elements depending on the nature of the interaction. In many cases, the isotopes produced are radioactive. If each different kind of radioactivity can be distinguished or separated from all the radioactivities produced, then the amount of each activity is a measure of the quantity of the parent isotope present in the material.

Meaningful results require the presence of a rather large quantity of titanium dioxide. Therefore, special samples were prepared with 2 to 3 microns of titanium dioxide by both the low temperature process (550°C) and the high temperature process (850°C). Additional 550°C and 850°C samples were oxidized in dry oxygen at 800°C for two hours and analyzed. The low temperature samples give a ratio of Ti:O of about 2:3 and suggest the presence of

the compound Ti_2O_3. The high temperature samples and the oxidized samples give a ratio of about 1:2 and suggest the presence of the compound TiO_2.

E. Appearance and Structure.

The deposited films appear smooth and reflective, much like films of SiO_2. An x-ray diffraction powder pattern identifies the film to be titanium dioxide and this, with a Laue diffraction pattern, shows the film to be polycrystalline. The films used in the x-ray diffraction experiments were approximately one micron thick deposited on silicon.

F. Adherence and Stability.

The TiO_2 film adherence to the substrate is entirely satisfactory. The film does not show any tendency to pull away from the substrate during the classic "scotch tape test" used in the semiconductor industry. The occasional occurrence of peeling during etching indicates that the TiO_2 is not as adherent as SiO_2 or Si_3N_4. Forty-eight per cent hydrofluoric acid etches the film at about 700 angstroms per minute. The TiO_2 film maintains reproducable electrical characteristics after prolonged storange in a desiccator or in the room atmosphere and after dunking in water. The films are relatively hard, but are not as resistant to scratching as SiO_2 or Si_3N_4.

G. Thickness and Refractive Index.

The refractive index, as determined by ellipsometry, is about 2.0. This is lower than the value of 2.6 for rutile[19] and is probably due to the presence of SiO_2, with a refractive index of 1.46 at the interface between the silicon and the TiO_2. However, values from 1.96 to 2.6 have been reported [50,63,81,89,90,132] for the index of refraction of thin films of TiO_2. The ellipsometer also determines the thickness of the films. This agrees with the thickness determination using the color of the interference fringes with a value of 2.0 for the index of refraction. The method of ellipsometry is non-

destructive and capable of extremely high accuracy. Ellipsometry measures the effect of reflection on the state of polarization of light. The polarization state of light is characterized by the phase and amplitude relations between the two component plane waves of the electric field vector into which polarized light may be resolved. One component (p) lies in the plane of incidence and the other component(s) projects normal to the plane of incidence. Reflection causes a change in the relative phases of the p and s waves and a change in the ratio of their amplitudes. In the Gaertner ellipsometer used here, the incident monochromatic light (λ = 5461 Å) passes in sequence through the collimator, the polarizer, and the quarter-wave-plate. The azimuthal orientations of the polarizer and the quarter-wave-plate determine the relative amplitudes and phase difference between the p and s components of the incident beam. These orientations are adjusted so that the difference in phase just compensates that which results from reflection. The plane polarized beam is then reflected off the sample at an angle and transmitted by the analyzer through a telescope to the detector. With the polarizer and quarter-wave-plate oriented for compensation, the analyzer is adjusted to extinguish the reflected beam. Then from the angles determined by the polarizer, the quarter-wave-plate, and the analyzer settings, values of thickness and index of refraction are found using the SDS 930 research computer and a program written by Grady Rylander III, of this laboratory[108]. The program originates from Snell's law of refraction, the Murmann-Forsterling formulae, and the Fresnel reflection coefficients, and the fundamental equation of ellipsometry originally used by McCrackin[92]. This program gives the thickness and index of refraction directly rather than in terms of assumed thickness and index of refraction as presented by McCrackin which required curve fitting with families of curves. These measurements were used to

establish a color chart and to provide a spot check on thickness values normally obtained from the color of interference fringes.

H. Electrical Measurements.

Figure 2 shows a block diagram of the capacitance measurement system. A General Radio 1615A capacitance bridge measures the capacitance to six significant figures and the dissipation factor (tan δ) to four significant figures with a frequency range of 20 Hz to 100 kHz. Both dc bias and ac signal must be applied to the sample. Keeping the ac signal level low, about 10 millivolts, gives the ac capacitance at various values of applied dc bias with high accuracy. The equation $C = \kappa\varepsilon_o A/d$ yields the dielectric constant of the film. Chapter VI discusses the results of the capacitance-voltage data.

Figure 3 shows a block diagram of the current-voltage measurement system. A Keithley 610B electrometer or Hewlett-Packard 425A micromicroammeter measures the current and a HP 413A dc voltmeter measures the voltage. Chapter V discusses the results of the current-voltage data.

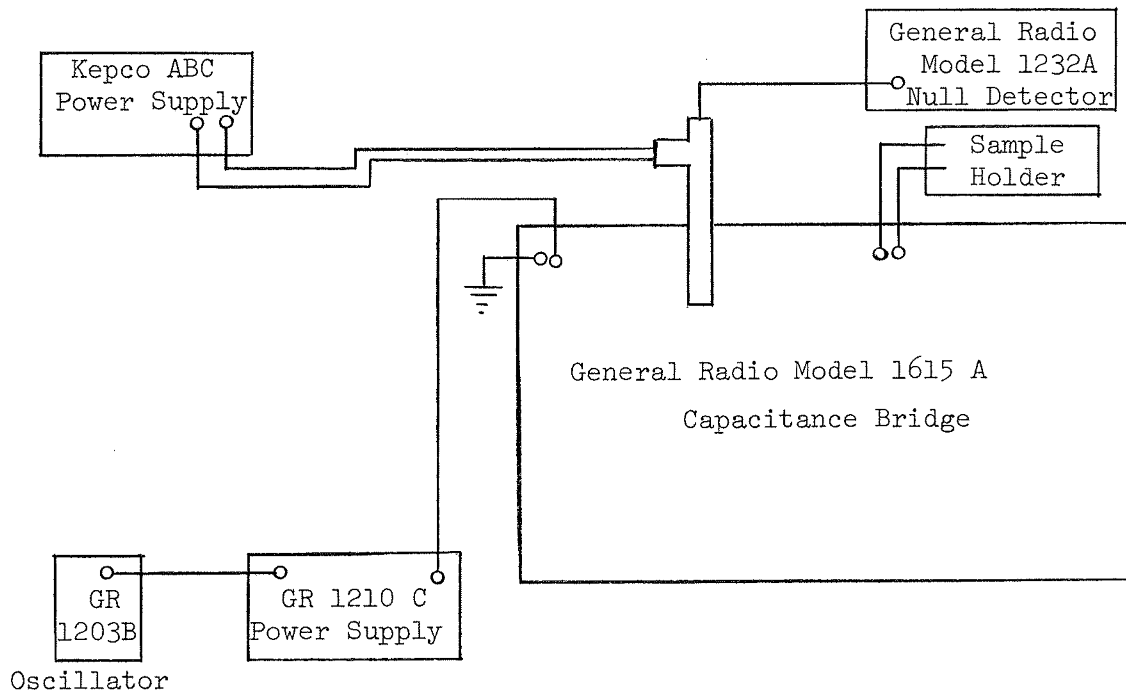

Fig. 2 Capacitance Measurement System

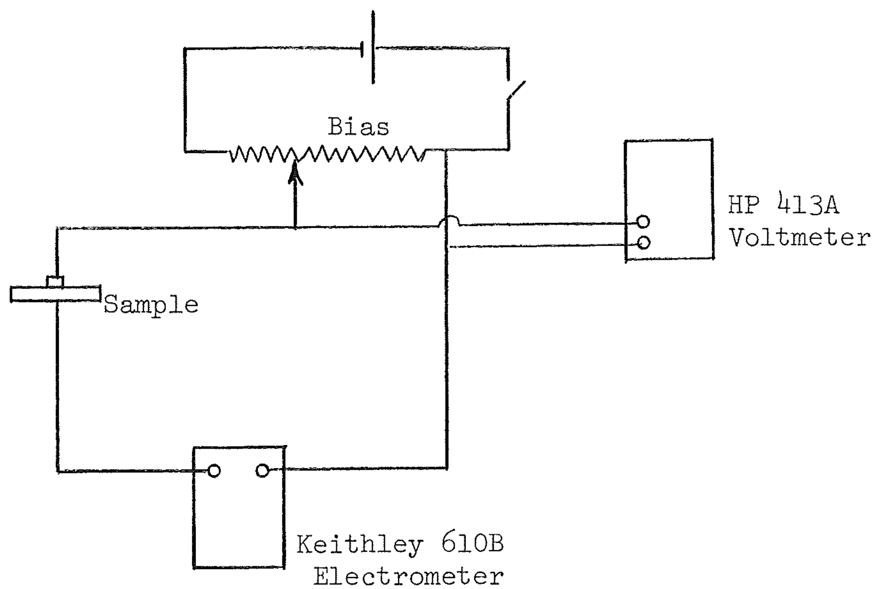

Fig. 3 Current-Voltage Measurement System

CHAPTER V.

CONDUCTION PROPERTIES OF TITANIUM DIOXIDE

A. Conduction Mechanisms:

Conduction properties in thin dielectric films have been studied extensively in recent years[34,47,82,93,94,96,117,137]. A large number of nearly amorphous insulating materials are known which, when a high electric field is applied to thin films of the substance, exhibit a current flow which increases roughly exponentially with applied voltage over many decades. The voltage required for a given current in many of these materials decreases monotonically with absolute temperature. Current mechanisms which might exist in thin film dielectrics include ionic flow, tunneling, space charge limited flow with distributed traps, Schottky emission, and Poole-Frenkel emission.

Imperfections in any real material allow states to exist in the forbidden band. These states (traps)affect the conduction process by capturing and emitting carriers to the conduction and valence bands. In insulators, traps collecting carriers compensate for traps contributing free carriers to the conduction process, i.e., acceptor traps compensate donor traps. Insulating materials with a large number of localized states (traps) remain insulating because of a high degree of compensation, or the energy difference between the traps and the nearer band is large compared to the thermal energy.

Significant current may flow in insulators at high temperatures and high fields due to the increasing quantity of free carriers. The carrier injection mechanism determines to a large extent the electric properties of the material and is therefore of great importance to device designers. Consider now some of these conduction mechanisms:

1. Ionic Flow.

In an ionic crystal, such as the alkali halides, currents occur as a result of the migration of ions under the influence of an electric field[44], similar to the electrolytic conduction of aqueous solutions of salts. Ionic conduction would exhibit an exponential volt-ampere characteristic and a decreasing voltage-temperature characteristic[93]. Maserjian and Mean[90] interpret their results on evaporated thin films (100-400 Å) of TiO_2 in terms of a large ionic space charge in the TiO_2 films. For ionic conduction the transient time for ions should be quite large and there should be a transport of material from one electrode to the other. Ionic flow is eliminated as a possible mechanism in this work because large currents were maintained in the samples for extended periods of time without observation of current decay due to ionic build-up near an electrode. One should note mechanical changes or plating of one electrode material onto the other electrode if ionic currents were present. Also, it is generally believed that ionic currents of the required magnitude to explain the results in thin films could not be supported in thin films for more than an instant without material breakdown[93].

2. Tunneling.

Tunneling occurs when the barrier becomes thin enough for appreciable quantities of electrons to penetrate the barrier and emerge to the other side[94,116,118,123]. Figure 4 shows three ways tunneling occurs:

(a) Tunneling from the conduction band of the metal into the conduction band of the insulator;

(b) direct tunneling from the conduction band of one metal into the conduction band of the other;

(c) tunneling from the valence band of the insulator directly into

the conduction band of the insulator.

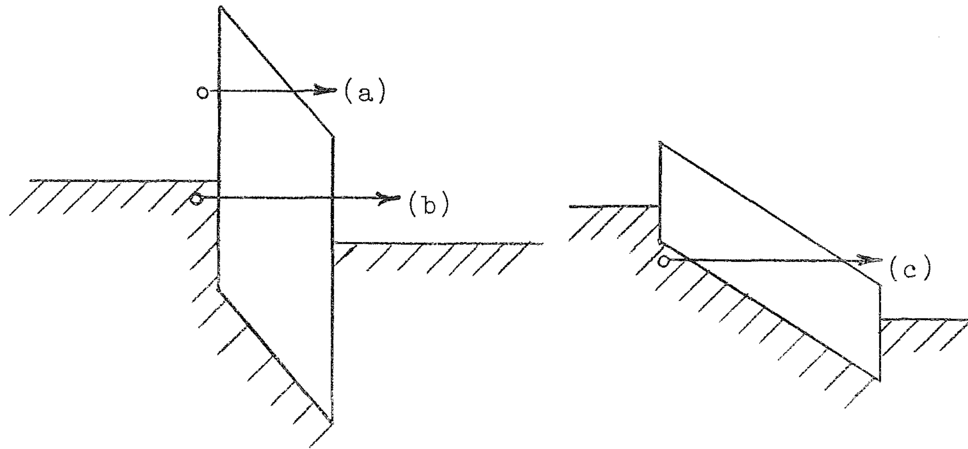

Fig. 4 Various Ways Tunneling Can Occur

Mechanism (c) occurs only at very large fields. Mechanism (b) is unlikely for films > 50 Å, but mechanism (a) occurs for thicker films due to narrowing of the barrier by the electric field. Simmons[116] gives an expression for mechanism (a) which is of the form

$$J = A_1 \xi^2 \exp(-A_2/\xi) \qquad [6]$$

where A_1 and A_2 are constants and ξ is the electric field. Stratton[123] gives an expression showing a T^2 temperature dependence of the current for tunneling. Hartman and Chivian[71] confirm this T^2 dependence and report that the tunneling current drops to 30 to 50 per cent of its room temperature value at liquid nitrogen temperatures.

Tunneling is eliminated from consideration here because of the thickness of the films and because tunneling would not show the large temperature dependence observed. No T^2 dependence or dependence on E given by equation 6 is observed.

3. Space charge limited current.

When an insulator is brought into contact with metal electrodes,

electrons are injected from the layers of initially high Fermi level into the layers of low Fermi level to satisfy thermal equilibrium. In the example of figure 5, electrons will diffuse from metal 2 to metal 1 (since $\psi_{m1} > \psi_{m2}$) and the dielectric will gain electrons from both of the adjoining electrodes. This results in a negative space-charge density in the region of the insulator adjacent to the contact. An equal amount of positive charge remains on the contact resulting in a field causing a gradual rise in the potential barrier from ϕ_o at the interface to a larger value inside the insulator, as shown in figure 5.

An equally valid case pointed out by Schmidlin[111] occurs when the Fermi level of the insulator is higher than the Fermi level of the metals. Then the dielectric will lose electrons to the adjoining electrodes. Thus the dielectric does not necessarily have to gain electrons.

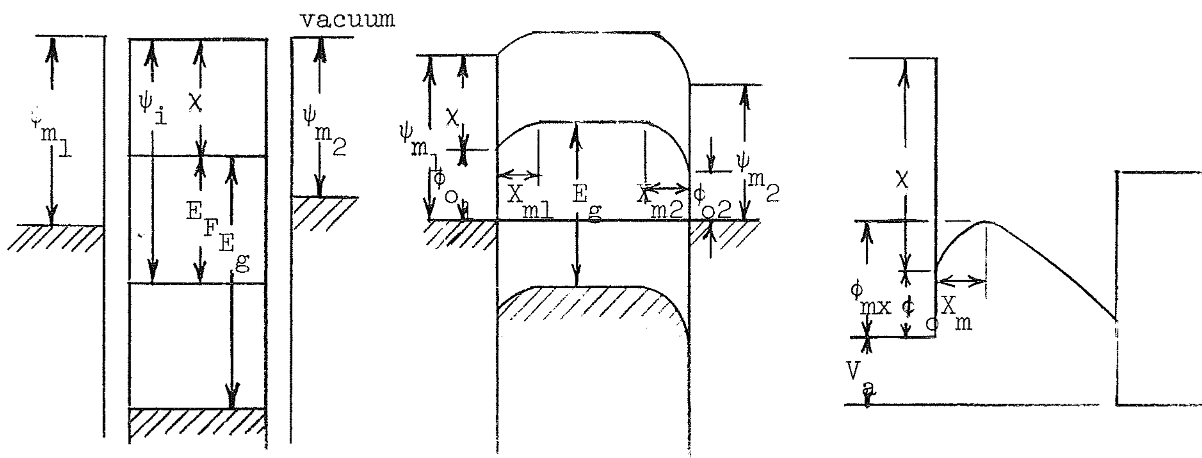

Fig. 5 Energy Band Shape

(a) Before Contact (b) Zero Bias (c) With Bias

The application of a bias to the system results in the appearance of an additional positive charge on the anode and an equal amount of negative charge in the insulator as a space charge[52]. It is this space charge which carries the current. The charge distribution in the system under applied bias consists of a positive charge on the cathode originating from thermal equilibrium requirements, a positive charge on the anode maintained by the applied bias, and a negative space charge in the insulator equal in magnitude to the sum of the positive charges on the cathode and anode.

The current flow in the system described above is space charge limited with the current in the cathode region flowing primarily by diffusion and that in the anode region primarily by drift. For an unlimited supply of carriers, the expression for one-carrier, trap-free, space charge limited current (SCLC) is of the form[52]

$$J \propto V^2 \qquad [7]$$

In general, the assumption of an unlimited supply of carriers does not hold and traps cause important effects on the current. This V^2 dependence is not observed for these TiO_2 films.

Space charge limited currents affect the field distribution which in turn affects the injection process. Frank and Simmons[52] consider the effects of space charge on emission-limited current flow in insulators. They find that after the current reaches the value in equation 7, as the voltage is increased, resulting in an increasing negative charge in the insulator, positive charge is removed from the cathode, reducing the barrier height ϕ_{max} at the metal-insulator interface, and allowing more current to flow. When this positive charge is depleted, ϕ_{max} is equal to ϕ_o, and the contact is no longer ohmic and emission limited current sets in. Negative charge now begins to appear on the cathode, as well as in the insulator and the contact

changes from an ohmic contact to a blocking contact so the current becomes contact or emission limited rather than bulk limited. This blocking effect (Schottky emission) does not occur as the bias is increased for these films eliminating SCLC as a possible mechanism.

4. Thermionic Emission - Schottky Emission and Poole-Frenkel Emission

Thermionic emission occurs when the carrier receives enough thermal energy from the lattice to surmount the restraining potential barrier separating its energy state from the lowest available state in the conduction band of the insulator. Thermionic emission subdivides further into electrode and bulk-controlled phenomena.

The Poole-Frenkel and Schottky effects result from the lowering of a coulombic potential barrier by an applied electric field. The Schottky effect is associated with the barrier at the surface of a metal and a semiconductor. The Poole-Frenkel effect is associated with barriers in the bulk of the material. Donor sites, acceptor sites, and traps, as well as electrons in the valence band experience the Poole-Frenkel effect. For a trap to experience the effect[117], it must be neutral when filled and positive when empty, otherwise, due to the absence of the coulomb potential the trap will not experience the effect.

Figure 6 shows the mechanisms of these effects. The solid line represents the coulombic barrier without the field. The dashed line shows the effect of an electric field on the barrier. The dash-dot line is proportional to the applied field.

Consider first the mechanism of Schottky emission over the metal-insulator interface shown in figure 6a. This resembles closely the case of thermionic emission into a vacuum and with no electric field present follows the Richardson-Dushman equation

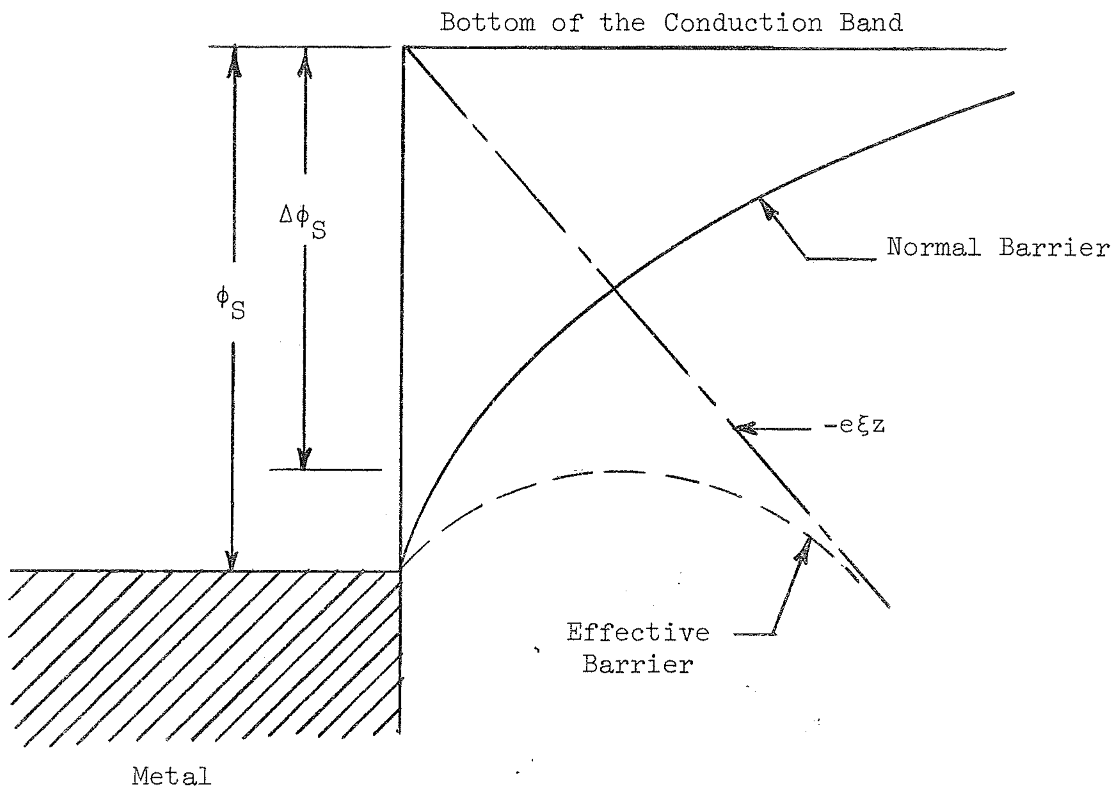

(a) Schottky Mechanism

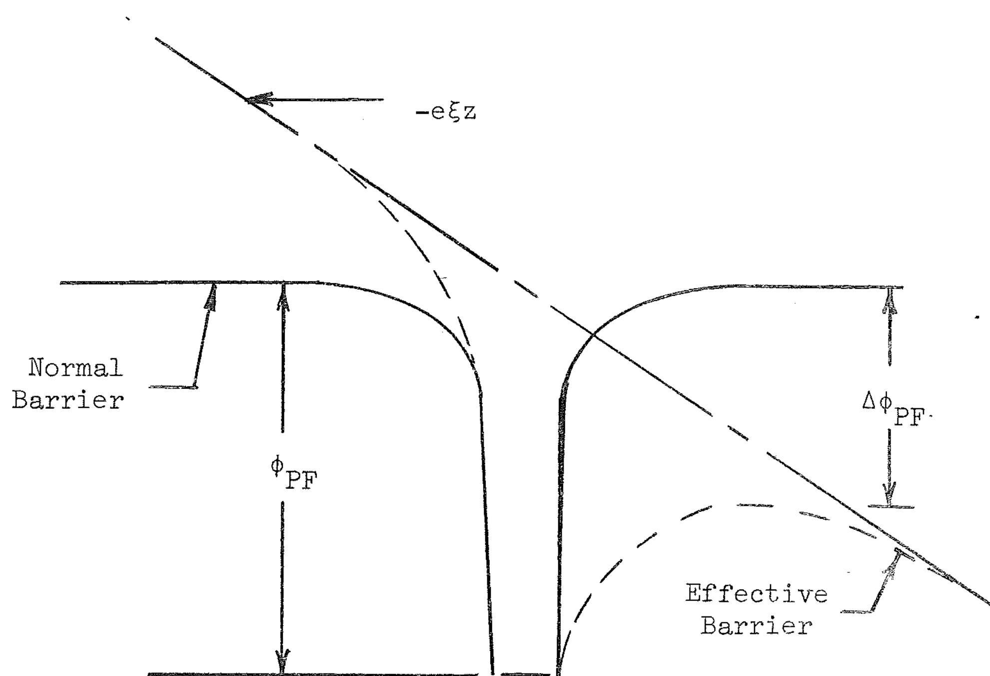

(b) Poole-Frenkel Mechanism

Fig. 6 Mechanisms of the Schottky and Poole-Frenkel Effects

$$J = A_S T^2 \exp(-\phi_S/kT) \qquad [8]$$

where

$$A_S = \frac{2em^*k^2}{(2\pi)^2 h^3} = 120 \frac{m_o}{m^*} \text{ amp/(cm-degree)}^2 \qquad [9]$$

The thermionic current is negligible at normal temperature. However, application of an electric field lowers the barrier height and increases the current by giving the electrons additional acceleration. The emitted electron sees an electrostatic force of attraction between itself and the emission surface caused by the image charge appearing within the conducting surface when the electron is emitted, as shown in figure 7a. The magnitude of this image force, is

$$F = \frac{e^2}{4\pi\varepsilon\varepsilon_o(2z)^2} \text{ newtons} \qquad [10]$$

An applied external electric field exerts a force on the electron given by

$$F = q\xi \qquad [11]$$

This results in a barrier lowering given by

$$\Delta\phi_S = (e^3\xi/4\pi\varepsilon\varepsilon_o)^{1/2} = \beta_S \xi^{1/2} \qquad [12]$$

resulting in an effective barrier

$$\phi_{eff} = \phi_S - \Delta\phi_S \qquad [13]$$

which gives the equation for Schottky emission as

$$J_S = A_S T^2 \exp[-(\phi_S - \Delta\phi_S)/kT] \qquad [14]$$

The proper dielectric constant is the electronic component (square of the index of refraction) since the electron is immediately collected by the field and does not polarize the ions in the vicinity.

Consider now the Poole-Frenkel mechanism. Deviations in the slope of the log J vs. $\xi^{1/2}$ curves from the value predicted by Schottky emission

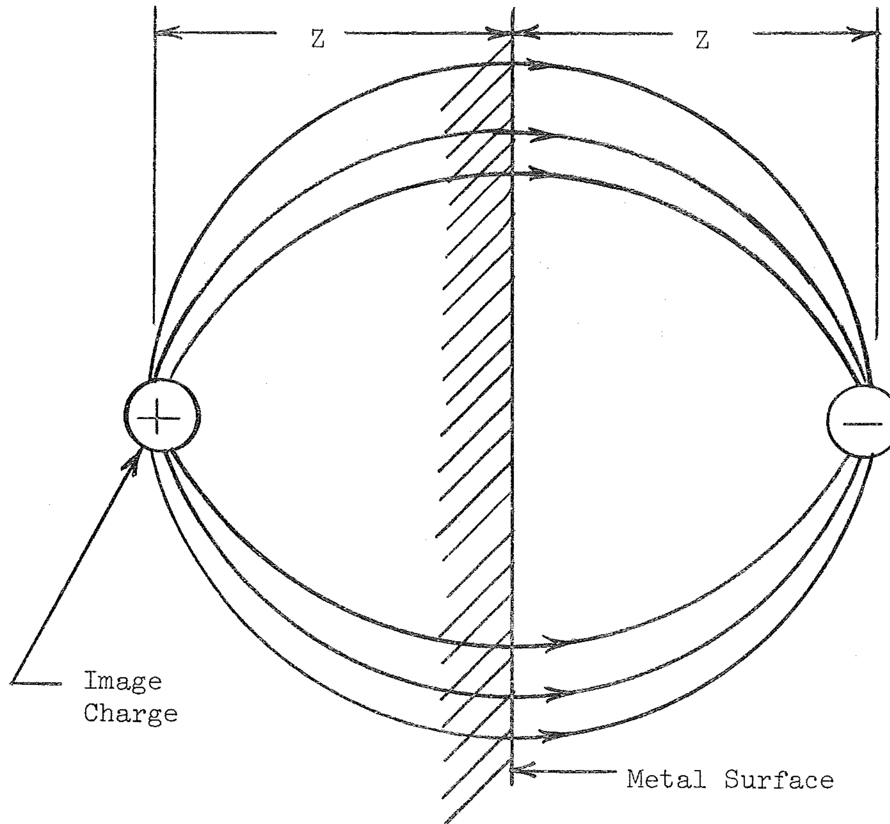

(a) Schottky Effect

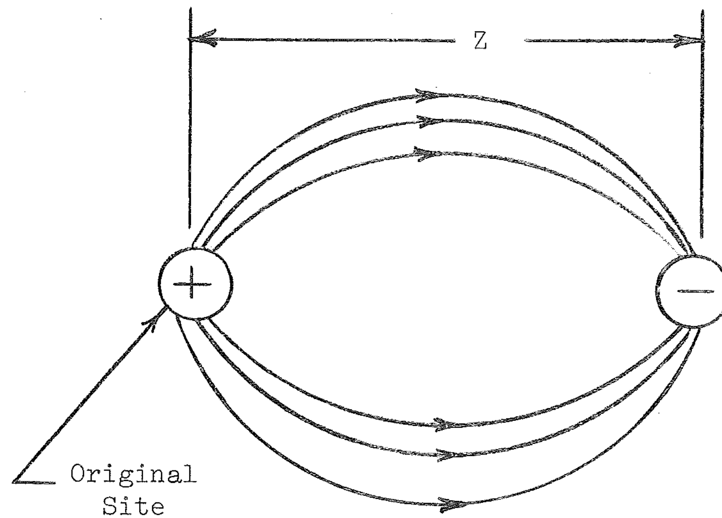

(b) Poole-Frenkel Effect

Fig. 7 Restoring Force on Escaping Electron

(equation 14) are explained by a model first proposed by Frenkel[54] based on internal, field assisted, thermal emission. Several authors[54,77,93,124] find that it best explains their data. Recently, O'Dwyer[102] and Emtage[46] introduced new models, based on tunneling mechanisms, which attempt to account for the slope differences. A recent paper by Simmons[117] considering a Poole-Frenkel type model with neutral traps lying above the Fermi level and donor states lying below the Fermi level, significantly clarifies the theory. Hu, et al.[73], in a short paper, modified the Poole-Frenkel model to account for differences in the slopes of the log σ vs. $\xi^{1/2}$ curves. Yeargan[137] extended the Poole-Frenkel model to include the effects of compensation showing that the relative densities of donor and acceptor sites control the slope of the log J vs. $\xi^{1/2}$ plots.

The current density expression for Poole-Frenkel emission arises from the expression for the conductivity of a material

$$\sigma = ne\mu \quad \text{ohm-cm} \qquad [15]$$

The concentration of free electrons in the material is

$$n = n_o \exp(-\phi/rkT) \qquad [16]$$

where r is a parameter ranging between 1 and 2 depending on the relative densities of donors and acceptors. The potential difference, ϕ, exists between the trap level and the lowest state in the conduction band. Using the energy band model with a single level each for donor and acceptor traps in the forbidden band of the insulator, the concentration of free carriers for an intrinsic material is[119]

$$n = (N_c N_v)^{1/2} \exp[-(E_c - E_v)/2kT] \qquad [17]$$

For n-type material with no acceptor sites[119]

$$n = \left(\frac{N_c N_d}{2}\right)^{1/2} \exp[-(E_c - E_d)/2kT] = n_1 \exp(-\phi/2kT) \qquad [18]$$

where $N_a << N_d$, $N_a << n$.

However, when traps or acceptor sites are present[137] these levels are lower in energy than the bottom of the conduction band so they tend to fill first causing a change in the above expressions. When the number of electrons in the conduction band is small compared to either the donor or acceptor density, then the concentration of free electrons is[119]

$$n = \frac{N_c(N_d - N_a)}{2N_a} \exp\left[-(E_c - E_d)/kT\right] = n_2 \exp(-\phi/kT) \qquad [19]$$

where $n \ll N_d$, $n \ll N_a$.

The application of an applied field as shown in figure 6b lowers the potential required to excite thermally an electron into the conduction band. Frenkel[54] calculates the barrier lowering as

$$\Delta\phi_{PF} = (e^3\xi/\pi\varepsilon\varepsilon_o)^{1/2} = \beta_{PF}\xi^{1/2} \qquad [20]$$

Note that the Poole-Frenkel effect results in a barrier lowering twice as great as for the Schottky effect because the positive image charge is fixed for the Poole-Frenkel barriers, but mobile with Schottky emission as shown in figure 7. The effective force contributing to the escape barrier for Poole-Frenkel emission from the ionized trap is

$$F = \frac{e^2}{4\pi\varepsilon\varepsilon_o(z)^2} \quad \text{Newtons} \qquad [21]$$

in contrast to equation 10.

This results in an effective barrier

$$\phi_{eff} = \phi_{PF} - \Delta\phi_{PF} \qquad [22]$$

Hence, the current is

$$J = \sigma\,\xi = ne\mu\xi \qquad [23]$$

where n is given by equation 18 or 19.

Therefore, the Poole-Frenkel equation becomes

Case I $\quad N_a \ll N_d,\ N_a \ll n$

$$J_{PF} = e\mu n_1 \xi \ \exp\ [-(\phi_{PF} - \Delta\phi_{PF})/2kT] \qquad [24]$$

Case II $\quad n \ll N_d,\ n \ll N_a$

$$J_{PF} = e\mu n_2 \xi \ \exp\ [-(\phi_{PF} - \Delta\phi_{PF})/kT] \qquad [25]$$

These equations may be written as

$$J_{PF} = \sigma_o \xi \ \exp\ (\Delta\phi_{PF}/2kT) = \sigma_o \xi \ \exp\ (\Delta\phi_s/kT) \qquad [26]$$

with only one type of site present, and

$$J_{PF} = \sigma_o \xi \ \exp\ (\Delta\phi_{PF}/kT) = \sigma_o \xi \ \exp\ (2\Delta\phi_s/kT) \qquad [27]$$

with compensation, where $\sigma_o = ne\mu$.

Therefore, both the Poole-Frenkel and Schottky mechanisms yield straight lines on plots of log J vs. $\xi^{1/2}$ and both may exhibit the same slope on these plots depending on conditions within the insulator. Both effects are likewise exponentially dependent on 1/T. These criteria are then insufficient for unique identification[137].

Rewriting the Schottky equation as

$$J_S = J_o \ \exp\ (\Delta\phi_s/kT) \qquad [28]$$

note that J_o is exponentially dependent on the barrier height at the metal-insulator interface (figure 6) while σ_o is exponentially dependent on the barrier of the donor sites within the insulator. Therefore, the current characteristics of MIM devices using metals with different work functions will be highly asymmetric for Schottky emission and symmetric for Poole-Frenkel emission.

The barrier height can further verify the presence of Schottky emission[70]. The ordinate intercept of a log J vs. $\xi^{1/2}$ plot yields ϕ_s and the

slope of a plot of log J/T^2 vs. $1/T$ yields $\phi_s - \Delta\phi_s$, however, equation 12 gives $\Delta\phi_s$. The barrier ϕ_s should agree when obtained by these two methods.

For Poole-Frenkel emission, analysis of the log σ vs. $\xi^{1/2}$ curves begins by noting the limiting slope values of

$$m = \left(\frac{e^3}{\pi\varepsilon\varepsilon_o}\right)^{1/2}/2kT \quad [29]$$

with donors only present, and

$$m = \left(\frac{e^3}{\pi\varepsilon\varepsilon_o}\right)^{1/2}/kT \quad [30]$$

with compensation.

An independent measure of ε, the high frequency dielectric constant, then determines if compensation is present. A knowledge of the degree of compensation now allows the barrier height ϕ_{PF} to be determined. Biasing the dielectric to a suitable value of current and varying the temperature at a constant bias yields data which exhibits a straight line plot of log I versus 1/T. The slope of this line is proportional to the activation energy, ε_d from

$$J = A_1 e^{-\varepsilon_d/kT} \quad [31]$$

The activation energy is related to the barrier height by

$$\varepsilon_d = -\frac{1}{r}\left[\phi_{PF} - \left(\frac{e^3\xi}{\pi\varepsilon\varepsilon_o}\right)^{1/2}\right] \quad [32]$$

where r = 2 with donors only present and r = 1 with compensation. A knowledge of the degree of compensation, r, obtained by comparing the measured slope with the limiting values from equations 29 and 30 and the barrier height gives information about the density of traps. The intercept of the log σ versus $\xi^{1/2}$ curve is a measure of σ_o, which is a function of the trap density. The barrier height of the traps results from the log I versus 1/T variation.

B. Experimental Results and Discussion.

Mead[93], with Ta_2O_5 films, and Sze[124], with Si_3N_4, identify three components of current. They find that a) Poole-Frenkel or internal Schottky emission dominates at high fields and high temperatures, b) field ionization dominates at high fields and low temperatures, and c) thermal hopping of carriers from one isolated state to another dominates at low fields and moderate temperatures. The thermal hopping mechanism yields an ohmic characteristic, exponentially dependent on temperature, but Mead[93] states that at higher temperatures, this mechanism would normally be expected to contribute much less current than mechanism (a). The field ionization mechanism yields a current-voltage characteristic independent of temperature. Figure 8 shows the current variation with temperature for these devices yielding an activation energy of 0.11 eV. Mead suggests that such a low activation energy might be due to some electron hopping from one trap to another with low mobility. However, no ohmic behavior is observed experimentally to support this suggestion. This exponential dependence of the current on temperature is further evidence that tunneling is not observed here.

Figure 9 shows that experimentally the current is proportional to exp $(m\xi^{1/2})$ where m is a constant and ξ the electric field. This behavior can be explained either on the basis of Schottky emission (equation 13) or Poole-Frenkel emission (equations 24 and 25). Schottky emission depends strongly on the barrier between the metal and insulator and should vary with the metal work function. Figure 9 shows that such dependence does not appear experimentally for MIM structures. If Schottky emission dominates, a difference of only 0.06 eV in the barrier heights at the two metal-insulator-interfaces results in a decade of current difference at equal and opposite fields. The device of figure 9 has platinum and aluminum electrodes which have a work

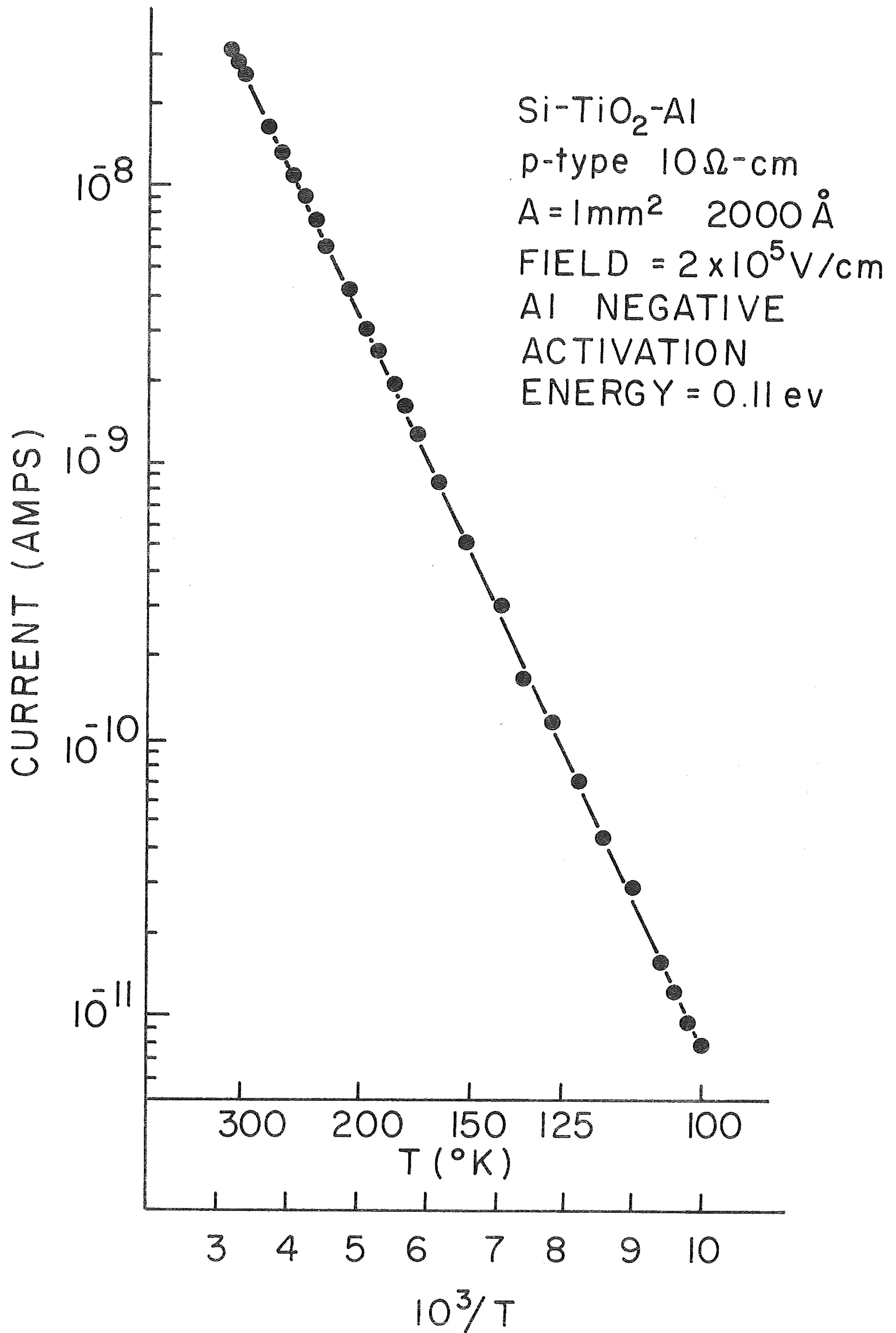

Fig. 8 Current vs. Temperature

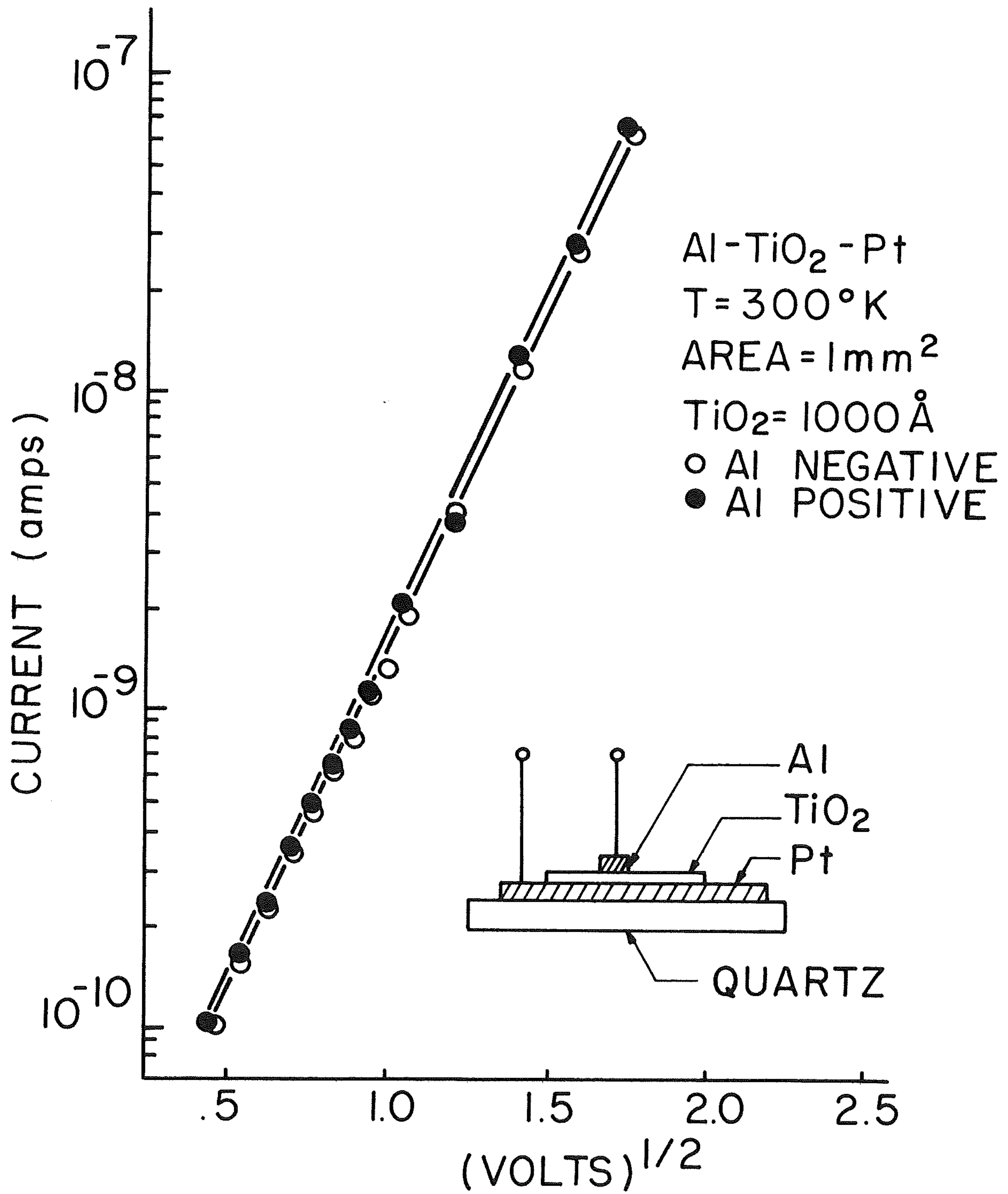

Fig. 9 Current vs. $(\text{Voltage})^{1/2}$ for MIM Device

function difference of approximately 1 eV. The Poole-Frenkel effect is associated with barriers in the bulk of the material, and the polarity independence, exponential dependence with 1/T, and exponential dependence with $V^{1/2}$, imply that Poole-Frenkel is definitely the dominant mechanism.

Figure 10 presents the voltage required to produce 10^{-7} amperes through films of various thicknesses. According to Mead[93], the linearity of such a plot indicates that the observed currents are not space-charge limited due to traps. The space-charge limited current for a quasi-continuum of trapping states between the Fermi level and the conduction band is nonlinear in terms of film thickness. Also, any model in which the electrodes cause rate limiting in the transport process predicts a deviation from linearity due to low mobility. Mead[93] concludes that the linearity of such a plot implies that the bulk of the material limits the current and not the potential barriers at the electrodes. Also, the passage of this curve through the origin definitely implies a bulk controlled mechanism.

On MIS devices (figure 11) a polarity difference exists, suggesting a penetration of the electric field into a surface or depletion layer of the semiconductor with reverse bias, rather than variations in the barrier heights. In the forward direction, the field within the insulator dominates the current which increases exponentially with bias voltage as for the Poole-Frenkel effect.

Wang[133] recently studied this saturation effect with reverse bias for a metal-polymer-silicon (n-type) (MPS) structure using polymerized silicone diffusion pump oil and interpreted the results in terms of the proportion of the voltage drop across the polymer and the semiconductor to the total bias voltage. J.D. Trotter, of this laboratory, proposed a model whereby the generation of electron-hole pairs in the depletion layer of the semiconductor

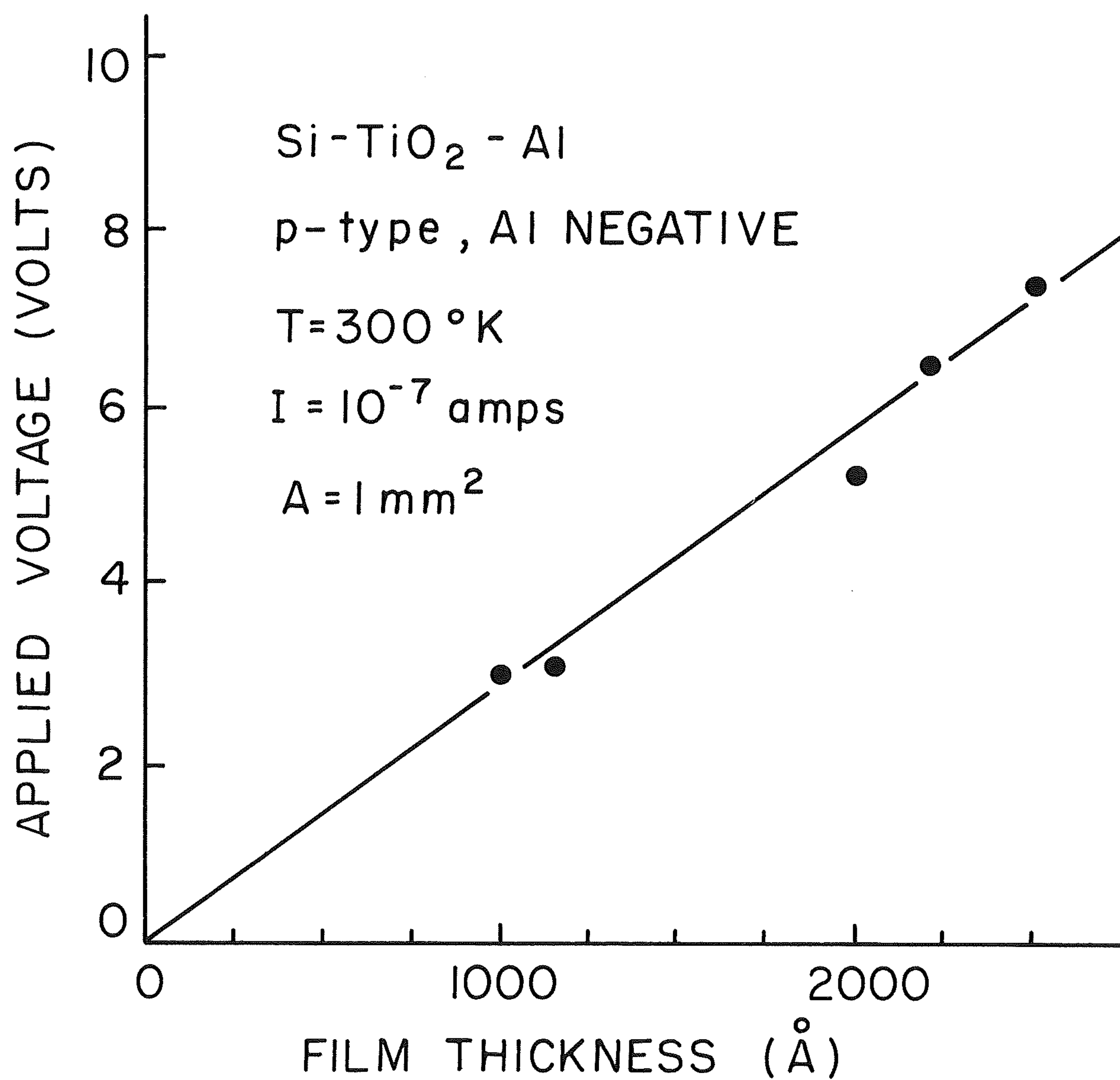

Fig. 10 Voltage vs. Film Thickness

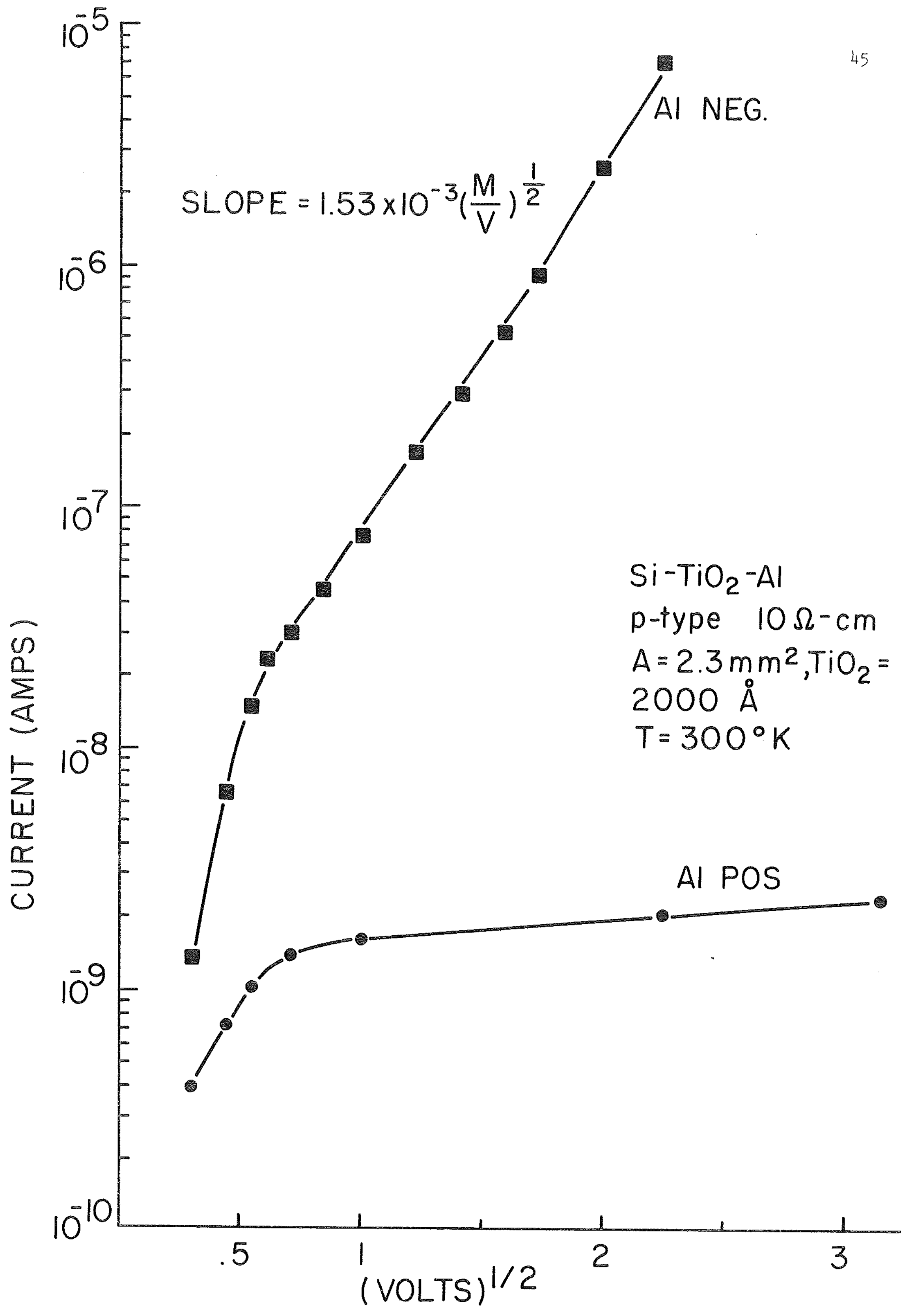

Fig. 11 Current vs. $(Voltage)^{1/2}$ for MIS Device

limits the current flow in the reverse bias condition causing saturation. Two "impedances" corresponding to the voltage drop across the dielectric and semiconductor are associated with the MIS device. At low bias, essentially all the applied voltage appears across the dielectric. As the reverse bias increases, the drop across the semiconductor begins to appear as the semiconductor forms a depletion layer. At some voltage, the impedance of the semiconductor increases to a value equal to that of the dielectric and the voltage is shared equally between them. Thereafter, more of the voltage falls across the semiconductor. Figure 11 shows that this saturation begins to occur for TiO_2 at approximately 0.5 volt which, as will be shown in Chapter VI, is at least as great as the voltage that the capacitance-voltage curve shows for the formation of an inversion layer. The formation of an inversion layer causes the capacitance to approach a minimum value. Actually, there is a field induced p-n junction at the semiconductor surface. For the case of Wang[133], using n-type material, this p-n junction causes injected electrons from the negative voltage on the insulator electrode to combine with the holes in the inversion layer. Until the inversion layer becomes strongly inverted, the recombination rate is not high and the mean free path of the injected electrons in this layer is longer than the width of the inversion layer allowing a large number of electrons to pass into the neutral n-region. As the inversion layer becomes strongly inverted, the charge in this layer is strongly increased. Now the recombination rate in the inversion layer limits the current passing through the MIS device because the holes in the inversion layer capture electrons entering from the insulator. Since the current flow has to be maintained in the device, holes from the depletion region have to be supplied to the inversion region and an equal number of electrons in the depletion layer have to move into the neutral n-type region; however, the current

is limited by the generation-recombination processes that take place in the field-induced junction.

For the present case of TiO_2 on p-type silicon, the situation is somewhat simplified. For n-type silicon, the surface must be strongly inverted and the inversion layer must contain a sufficient supply of holes to trap all of the electrons injected by the negative bias on the dielectric. For the p-type silicon, the surface is inverted when there is a positive bias on the dielectric. Therefore, electrons in the inversion region supplied by electron-hole pair generation in the depletion region are the only source of electrons reaching the positive terminal on the TiO_2. The number of electron-hole pairs generated (and hence the number of electrons available for conduction in the TiO_2 and consequently the current) depends on the volume of the depletion region. Since the width of the depletion region continues to increase a small amount as the voltage is increased, the current continues to increase slightly. In addition, surface leakage currents may be present in silicon p-n junctions[109]. These surface currents may increase with voltage depending on the condition of the surface. For this reason, a flatter saturation current should imply less surface currents. Not all of the devices measured exhibit a saturation current as flat as that shown in figure 11, but this curve was chosen for purposes of quantifying the above model because the surface current effect is small.

In the reverse bias case of a p-n junction, the current consists of the generation-recombination current in the depletion region and the diffusion current generated in the neutral n and p regions. From Sah[109] for the case of a reverse biased silicon diode, the current generated in the depletion region is extremely large compared to the diffusion current. Sah's model for the total recombination current for this case is

$$I_{gr} = qUX_dA \qquad [33]$$

where X_d is the width of the depletion region and U is the generation rate given by

$$U = -\ n_i/2\tau_o \qquad [34]$$

where τ_o is the effective carrier lifetime within the depletion region. Thus, the current flowing due to this effect is

$$I_{gr} = qn_iX_dA/2\tau_o \qquad [35]$$

The lifetime is the only quantity on the righthand side of equation 35 which is not known exactly. From measurements[61,109] on p-n junctions of similar material, a lifetime of 1μ second seems appropriate. Using this value with $n_i = 1.45 \times 10^{10} cm^{-3}$, and X_d = 1 micron yields $I_{gr} = 10^{-9}$ amps which agrees closely with the experimental value of the saturation current from figure 11.

The generation current is dependent upon the width of the depletion layer. For higher resistivity semiconductors, the doping density is lower, thus the width is larger and a higher saturation current level should be observed. Wang[133] did not observe this saturation for resistivities less than 70Ω-cm or for p-type material. Wang probably did not observe this saturation for p-type material because the polymer, like SiO_2, inverts p-type silicon causing appreciable surface currents to flow in the inverted channel and overriding the saturation current. It is significant that this saturation is observed on 10Ω-cm p-type material with titanium dioxide. This verifies the fact that the polymer inverts p-type silicon while titanium dioxide does not. As shown in Chapter VI titanium dioxide tends to invert n-type silicon creating a p-type surface channel. This would imply that surface currents in the channel could prevent n-type saturation with TiO_2 and this is seen to be true.

Figure 12 shows that the film deposition temperature has a strong effect on the conductivity. The films prepared at 500°C, described as not

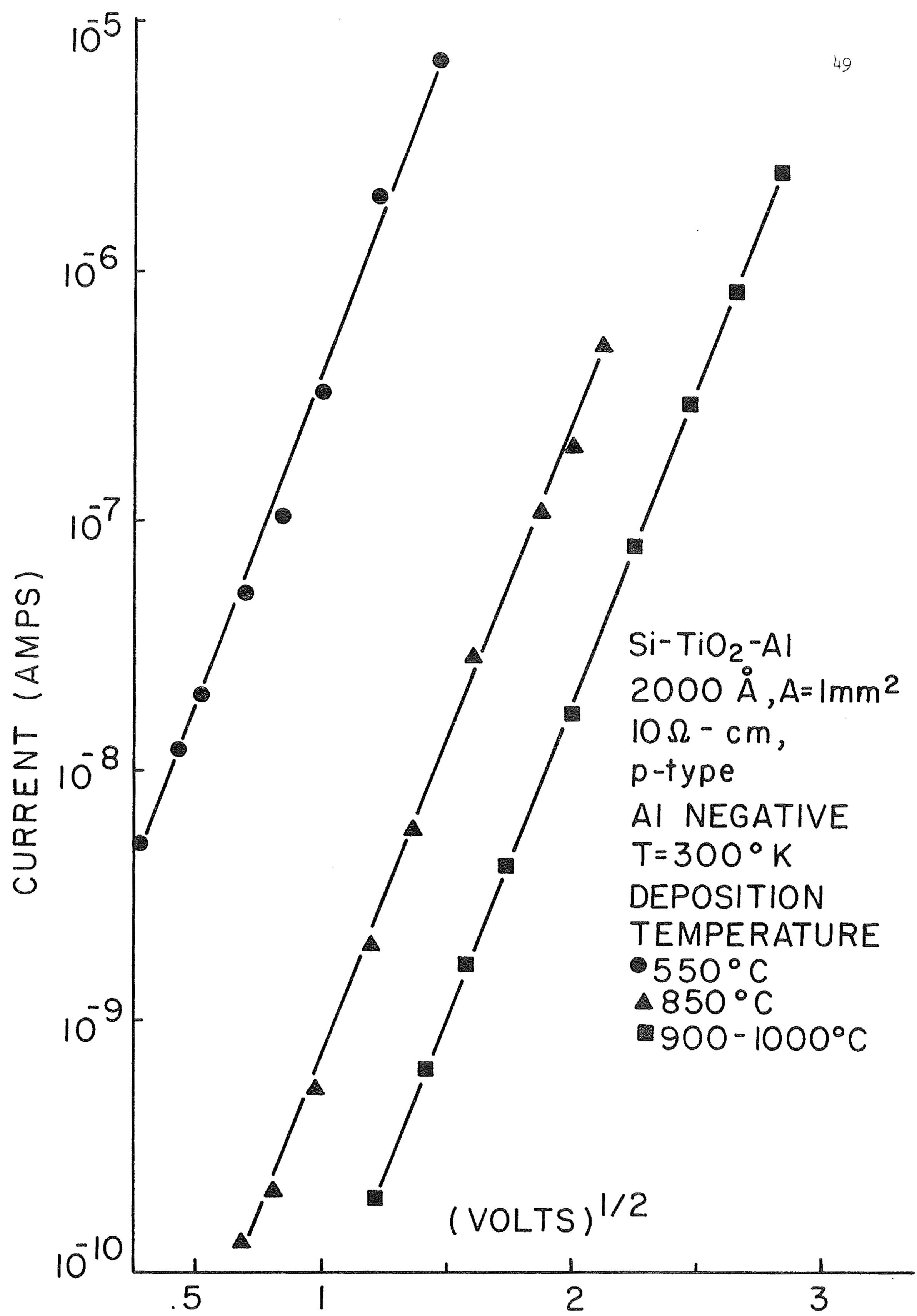

Fig. 12 Effect of Deposition Temperature on Conductivity

stoichiometric TiO_2 in Chapter IV, have a current density about 10^4 times greater than the 900°C films at a given field strength. This gives some further evidence of a bulk conduction mechanism. The breakdown strength of these 550°C films is only about 2 volts for a 2000 Å film. The 850°C films exhibit a conductivity an order of magnitude greater than the 900°C films and a breakdown strength of about 5 volts. The 900°C films have a breakdown strength of 10 volts which corresponds to a field strength of 5×10^5 volts/cm. Films formed between 900°C to 1000°C show similar characteristics. When the 550°C films and the 850°C films are oxidized for two hours in dry O_2 at 800°C, as described in Chapter IV, the properties of these films become equivalent to the 900°C samples suggesting that the oxygen anneal replaces missing oxygen and restores the film to stoichiometric TiO_2.

Figure 11 shows that at low fields when the work function of the positive electrode is higher than that of the negative one, Poole-Frenkel mechanism is effectively cut off by the negative electric field at applied voltages less than the difference in barrier heights, and electron hopping from one site to another may occur. Mead[93] observes this for Ta_2O_5 films, and he observes an ohmic characteristic at very low fields. Mead finds that somehow this ohmic behavior occurs at such low fields and low currents that it is difficult to observe experimentally. Figure 13 shows that for n-type material where the work function of the positive electrode is lower than that of the negative one, the Poole-Frenkel mechanism is not cut off by the field.

Equations 29 and 30 yield m as the expected slope of ln I vs. $\xi^{1/2}$ if Schottky or Poole-Frenkel mechanisms are present. The slope should fall between

$$0.73 \times 10^{-3} \leq m \leq 1.46 \times 10^{-3} \qquad (m/volt)^{1/2} \qquad [36]$$

using a dielectric constant of 4 (square of the index of refraction). The

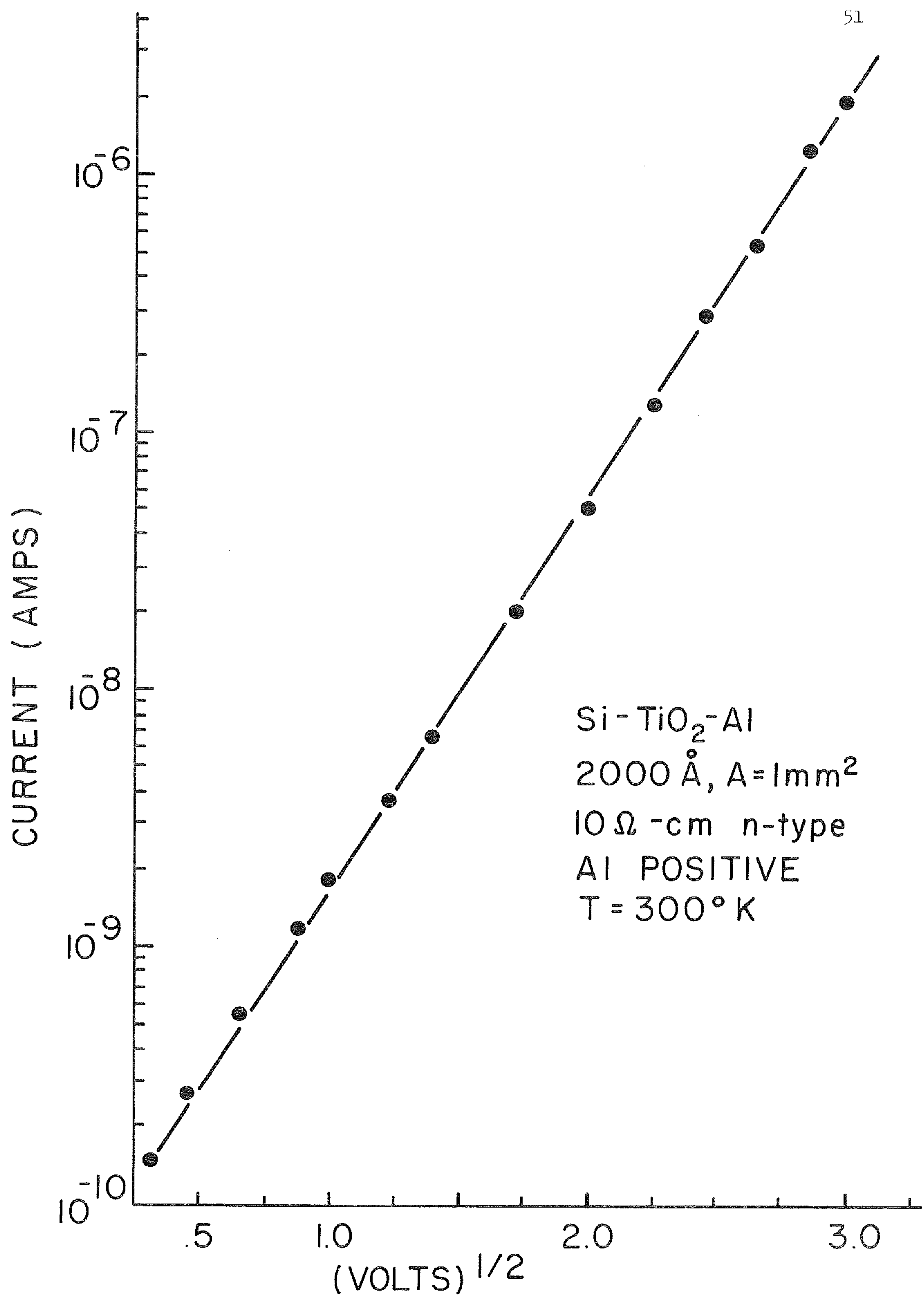

Fig. 13 Current vs $(\text{Voltage})^{1/2}$ for MIS Device

lower limit applies for Schottky emission (equation 12) and for Poole-Frenkel emission with only one type of carrier present. The upper limit applies for Poole-Frenkel emission with compensation (both donor and acceptor sites). The value of m from figure 9 and figure 11 are the expected values for Poole-Frenkel emission with compensation ($\simeq 1.5 \times 10^{-3}$). The slope would be one-half this for Schottky emission. The slope of the curves of figure 12 ($\simeq 2.4 \times 10^{-3}$) are about 50% larger than one would expect for Poole-Frenkel emission. Several possible explanations arise for this: a) Part of the field appears across the thin SiO_2 layer under the TiO_2; b) Mead[93] notes that in the majority of his thicker films some mechanism, possibly concentration of the field in small regions of the material due to a change in the structure of the film, raised the experimental m; c) the low activation energy (0.11 eV) suggest that perhaps some electron hopping from one trap to another with low mobility is occurring in combination with the Poole-Frenkel mechanism[93]; d) examination of the Poole-Frenkel effect expression, equation 24 and 25, shows that for accurate comparison, experimental values of ln (I/V) should be plotted versus $V^{1/2}$. Figure 14 shows the result of this for the 900°C sample of figure 12. The experimental slope is lowered from 2.4×10^{-3} to about 1.9×10^{-3} because of the moderate fields involved. The experimental slope is now only slightly higher than the predicted value. For very high fields as many authors use for Si_3N_4 this correction is negligibly small; e) although the measurements presented here are apparently steady-state values, a decay in current lasting from a few seconds to a minute was observed after increasing the voltage and if space charge regions associated with the contacts persist, their width will decrease the effective thickness of the films causing the slope, m, to be high[34].

The barrier height ϕ_s determined by the ordinate intercept of ln J

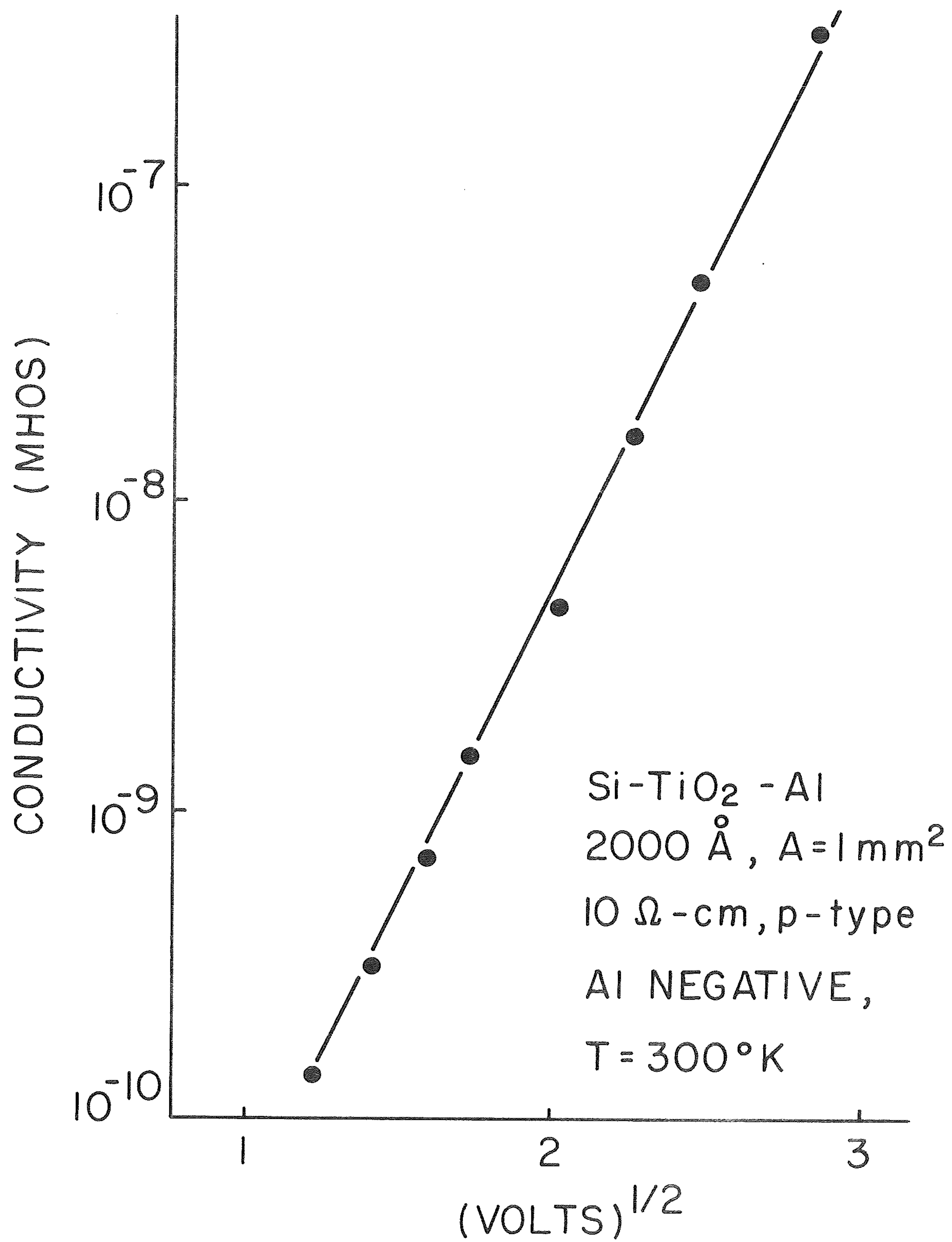

Fig. 14 Conductivity vs. $(Voltage)^{1/2}$

vs. $\xi^{1/2}$ plots (equation 13, $\xi = 0$) differs from that determined by the current variation with temperature (equations 24,25 and 26). This is further evidence that Poole-Frenkel is the dominant mechanism rather than Schottky. The value of this low field activation energy ranges from 1.08 eV for the high resistivity TiO_2 samples to approximately 0.83 eV for the more conductive samples when calculated from ln J vs. $\xi^{1/2}$, but it is 0.25 eV when calculated from ln J vs. 1/T. Therefore, this activation energy is equal to the energy difference between the emission sites and the band edge[34] and is equal to approximately 0.25 eV.

These considerations indicate that the dominant conduction mechanism in titanium dioxide is Poole-Frenkel emission from donor and acceptor sites and traps within the bulk of the TiO_2 film. The sites lie approximately 0.25 eV from the band edge. Both donor and acceptor sites are present creating a compensating effect.

CHAPTER VI.

CAPACITANCE-VOLTAGE PROPERTIES OF METAL-TiO_2-SILICON

The MOS capacitor structure sensitively reflects the electrical properties of the silicon-titanium dioxide system. A major discontinuity exists at the interface between the ordered semiconductor crystal lattice and the oxide layer. Energy states appear in the forbidden band of the interface where, as localized allowed energy levels, they become sources of charge strongly affecting the devices properties. Capacitance measurements yield information concerning these states.

The literature contains extensive reports on MOS work using silicon dioxide and, more recently, silicon nitride as the insulator. Terman[125] did the first major work on the MOS structure in 1961 at Stanford University. In late 1961, Lindner[84] reported on the MOS surface varactor. Lehovec[83], Grove[62], Garrett and Brattain[56], Marcus[88], Gray and Brown[33], and many others have made significant contributions toward understanding MOS phenomena.

A. Theory of the MOS Structure.

Numerous authors report the detailed mathematical analysis of the theory of the MOS device. This section gives a qualitative discussion of this theory. Consider the device of figure 15 using a p-type semiconductor. Bias application consists of a dc potential applied to the device with a superimposed ac component. The capacitance bridge requires the ac component in the measurement. The ac component is less than 10 millivolts. The potential is called a dc bias, however, the fact that an ac capacitance is actually measured is of great importance in the high frequency case. The following discussion is for the ideal case with no surface states or work function effects:

1. Accumulation Region.

Consider the situation of the metal biased negative with respect to

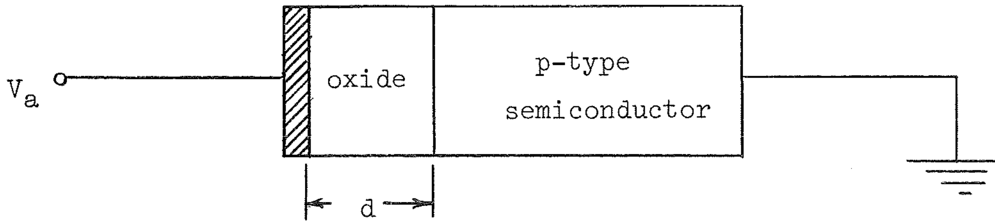

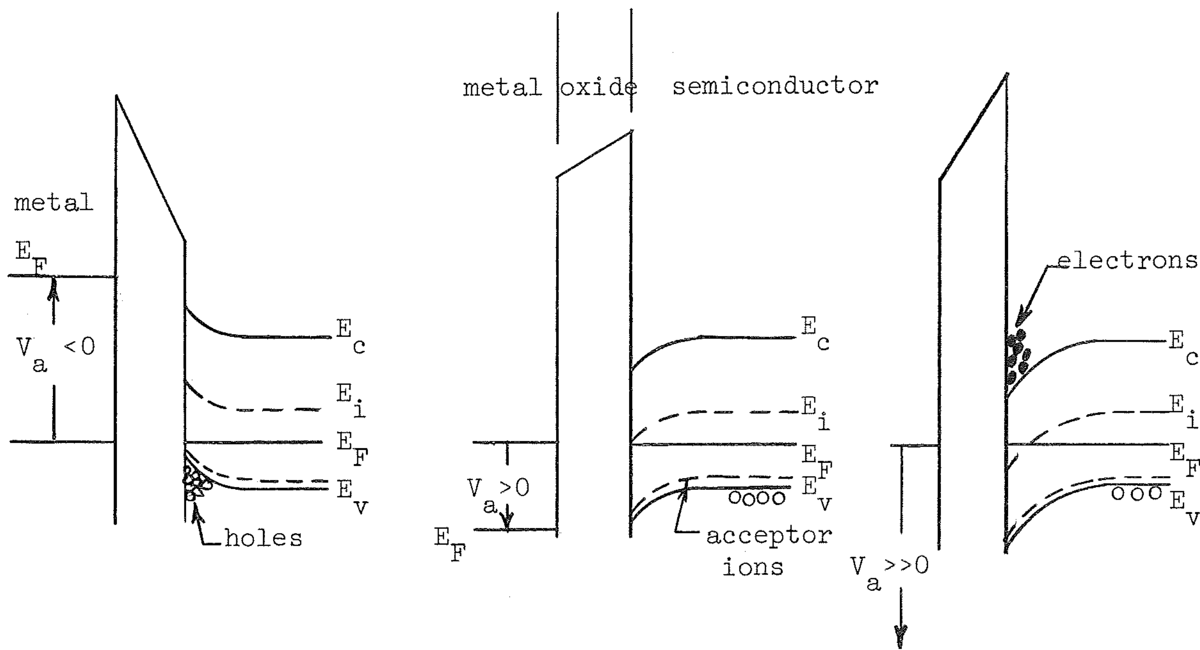

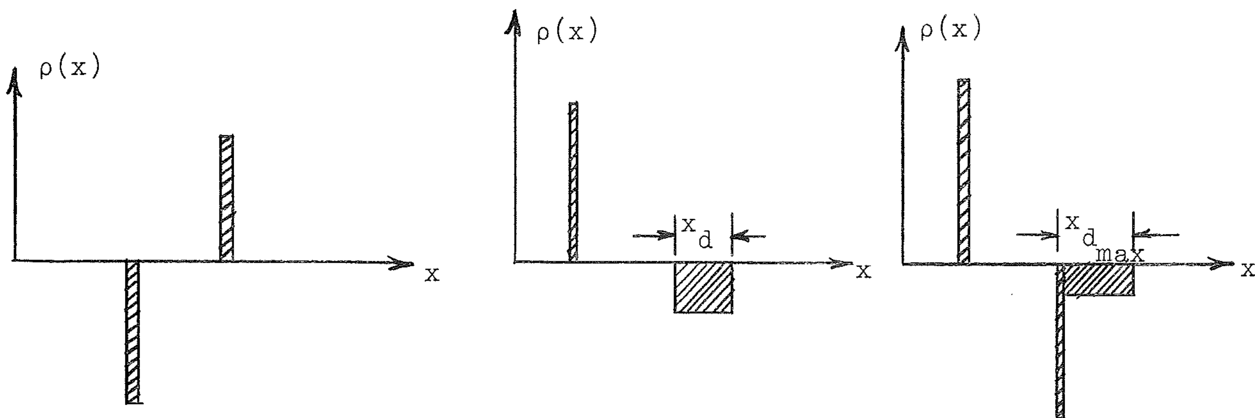

(a) Accumulation (b) Depletion (c) Inversion

Fig. 15 Energy Bands and Charge Distribution of MIS Structure Neglecting Surface States and Work Function Differences

the semiconductor. Figure 15a presents a band picture representing this situation. The applied field causes majority carriers (holes) to drift to the left, but their flow is blocked by the dielectric. As a result, an accumulation of majority carriers forms a very narrow region at the silicon-oxide interface. The ac component of the bias voltage modulates the drift velocity of these carriers, but this modulation is small. The capacitance measured is that of the oxide and is given by

$$C_o = \frac{\varepsilon_o \kappa A}{d} \qquad [37]$$

The charge in the space charge region of the semiconductor is equal and opposite to the charge on the metal plate due to the requirement of charge conservation. The capacitance of the oxide is independent of bias. In view of the forward bias, the only carriers of interest in this region are the majority carriers. The mobility of these is such that at all frequencies of interest they will reach equilibrium throughout the semiconductor very quickly. This situation can be considered one of quasi equilibrium.

2. Flat Band Region.

The flat band case results at zero bias. As the name implies, the bands are flat up to the edge of the semiconductor with no bending for this condition.

3. Depletion Region.

As the bias becomes positive, the band picture appears similar to figure 15b and a space charge region appears in the semiconductor. The space charge consists of uncompensated acceptor ions and the total charge in the space charge region is just equal and opposite to the charge on the metal electrode. The capacitor which is being measured consists now of two dielectrics, the oxide and the depletion zone of the semiconductor. The expression

for the capacitance of a capacitor with this configuration is the same as for two parallel plate capacitors in series,

$$C = C_o C_{sp}/(C_o + C_{sp}) \quad [38]$$

where C_o is given by equation 37 and

$$C_{sp} = \varepsilon_o \kappa_s A/X_d \quad [39]$$

as the bias is increased the depletion width increases and C decreases.

4. Inversion Region.

At some positive bias point the potential of the silicon-oxide interface is such that the band is bent sufficiently to force the Fermi level above midgap (the intrinsic level), causing the concentration of electrons at the interface to increase sharply. This is in effect n-type material and for a small, but finite, distance into the semiconductor the majority carriers are now electrons. This is called an inversion layer and is shown in figure 15c. The net charge of electrons in the inversion layer has the same sign as the uncompensated acceptor charge in the space charge region.

a. Low Frequency Case.

The low frequency inversion layer charge distribution appears in figure 16a. At large positive bias the charge in the inversion layer dominates and the capacitance approaches that of the accumulation region if the measurements are carried out at sufficiently low frequencies so that minority carriers are generated fast enough to keep up with the small signal variation. In this case the generated holes will replenish the holes pulled out of the edge of the depletion region and the extra electrons will appear in the inversion layer. The capacitance curve is similar to curve "a" in figure 16c for the low frequency case because the incremental negative charge will

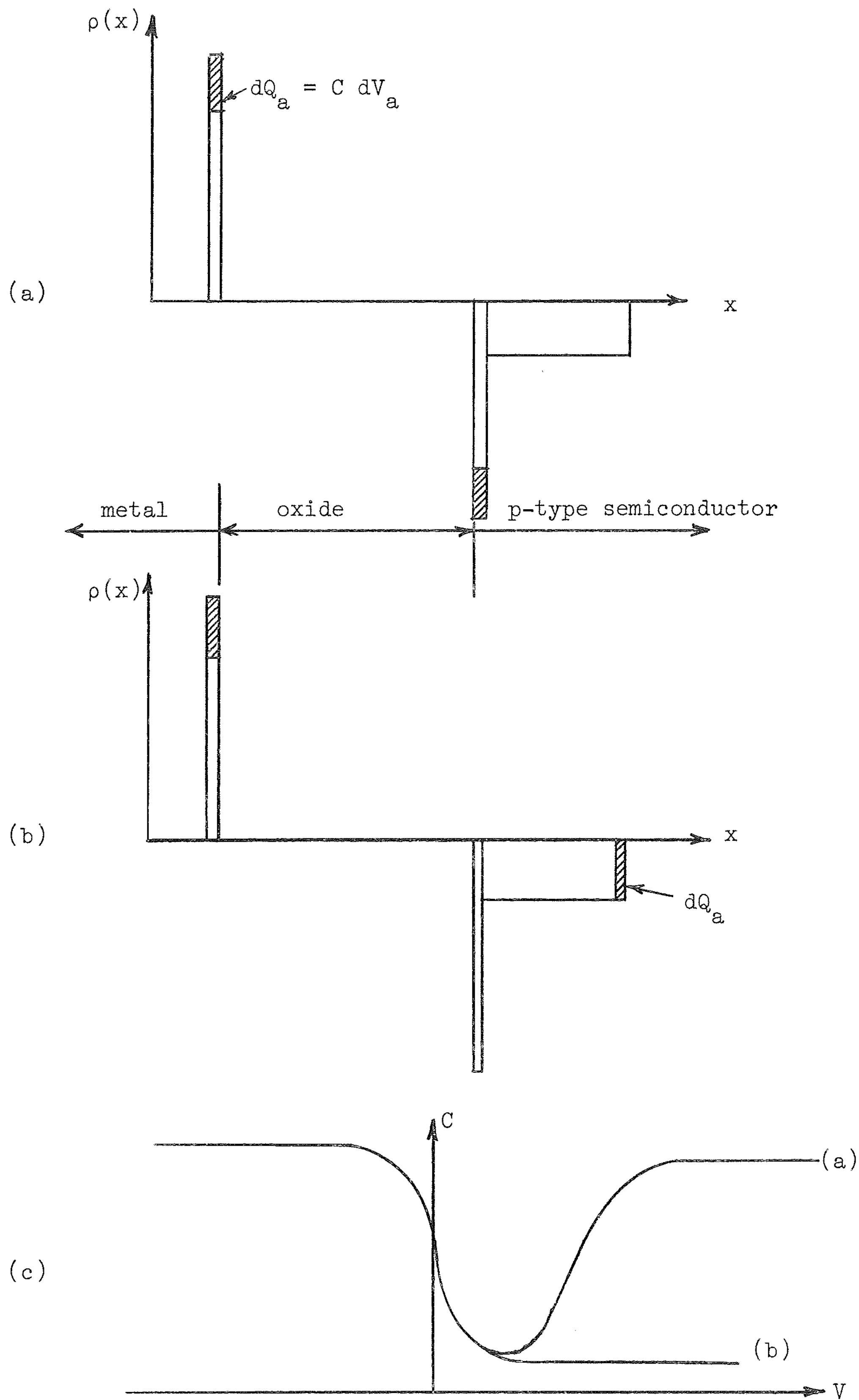

Fig. 16 Charge Distribution and Capacitance Variation for (a) Low Frequencies (b) High Frequencies

appear at the oxide-silicon interface.

b. High Frequency Case.

At high frequencies sufficient minority carriers cannot be generated within a cycle of the ac signal, thus, the charge in the inversion region is constant (as determined by the dc bias) and has no effect on the capacitance readings. The only charge distribution in this case is at the bulk semiconductor end of the depletion region. Figure 16b illustrates this point. The depletion width continues to increase with large positive bias as holes are pulled out of the semiconductor and the total capacitance continues to decrease. When the width of the depletion layer no longer increases with bias, the capacitance value again becomes constant. The capacitance curve is similar to the curve "b" in figure 16c.

5. The Effect of Surface States.

Surface states exhibit energy levels within the forbidden band of the semiconductor. These are associated with the atoms on or very near the surface of the silicon at the silicon-oxide interface. Tamm and Shockley[87] predicted these states theoretically because of a break in the periodicity of the lattice at the interface. They represent a source (or sink) or charge and therefore may alter the electric field within the device.

Not all of the surface states are filled; those above the Fermi level having a low occupation probability and those below the Fermi level having a high occupation probability as in figure 17. Ionized donor atoms at the interface are a source of positive charge, while the filled donor states are neutral. Unionized acceptor atoms are neutral, and when ionized acceptor atoms represent a source of negative charge at the interface. When a bias shift modulates the energy bands relative to the Fermi level a change in total

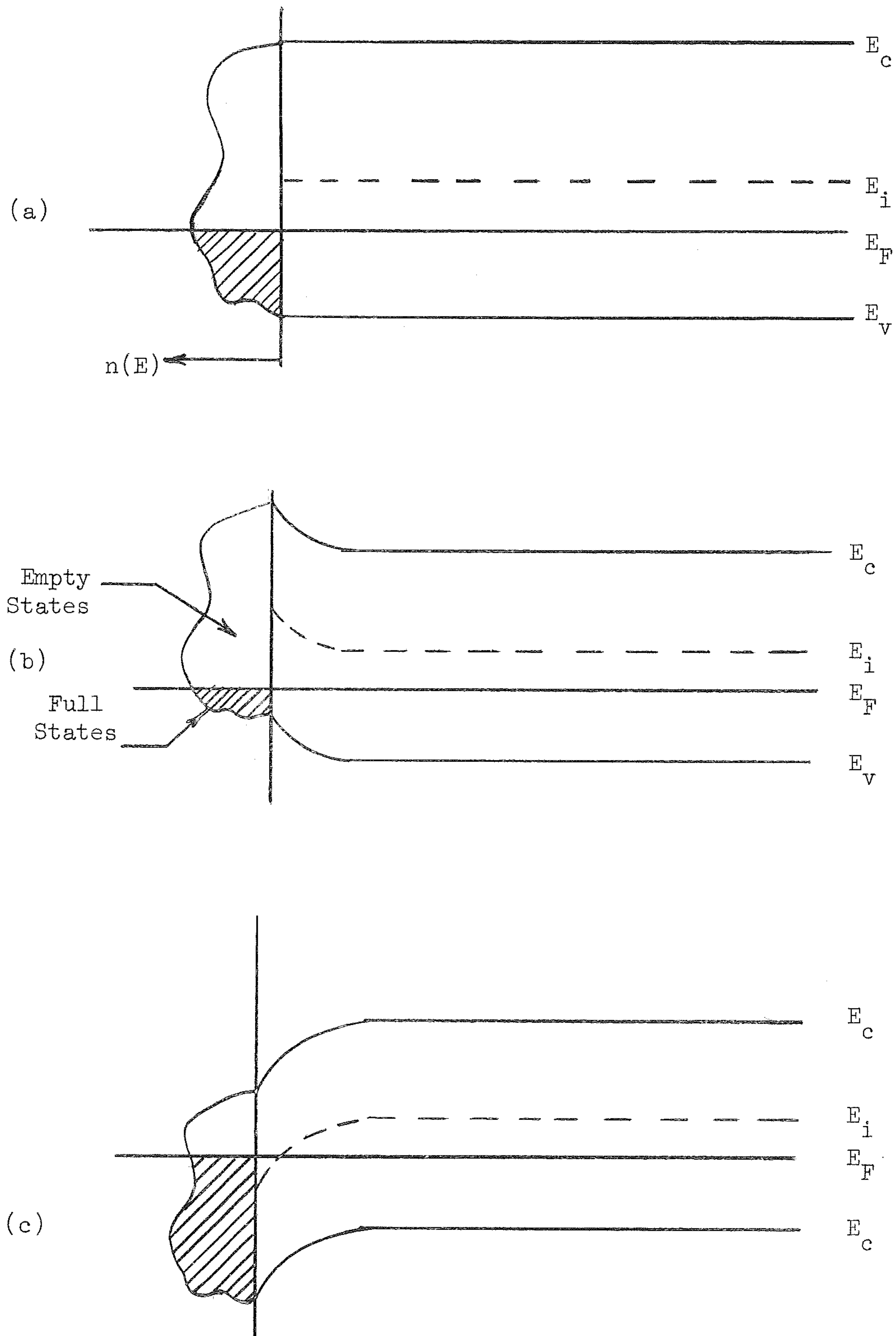

Fig. 17 Surface State Occupancy in Regions of
(a) Flat-Band (b) Accumulation (c) Inversion

charge present at the interface reveals the presence of the surface states. As the surface is accumulated, the states are lifted far above the Fermi level and their probability of occupation by electrons is small. As the surface is depleted and inverted, the states are pulled way below the Fermi level and their probability of occupation is high. Such states whose charge can be readily exchanged with the semiconductor are called fast surface states. Since the charge in these states varies with the band bending, the capacitance-voltage characteristics will be displaced from the theoretical by an amount which itself varies with the surface potential. This may appear as steps or kinks or as a gradual distortion of the characteristics.

Some charges exist in the insulator which, although close to the silicon interface, cannot respond fast enough to keep up with the band bending caused by the modulation described above. These are called oxide surface states or slow states. To see how these affect the capacitance-voltage curves, consider a charge sheet per unit area Q within the insulator as shown in figure 18a. With zero gate voltage this charge will induce an image charge partly in the metal and partly in the semiconductor. To obtain a flat-band condition (i.e., no charge induced in the semiconductor), a negative voltage must be applied to the metal as in figure 18b. Increasing negative voltage puts more negative charge on the metal and thereby shifts the electric field distribution downwards until the electric field at the silicon surface is zero. The area contained under the electric field distribution is the flat-band voltage, V_{FB}. Using Poisson's equation, V_{FB} is given by

$$V_{FB} = - \frac{xQ}{dC_o/A} \qquad [40]$$

where x is the distance from the metal to the charge and d is the distance

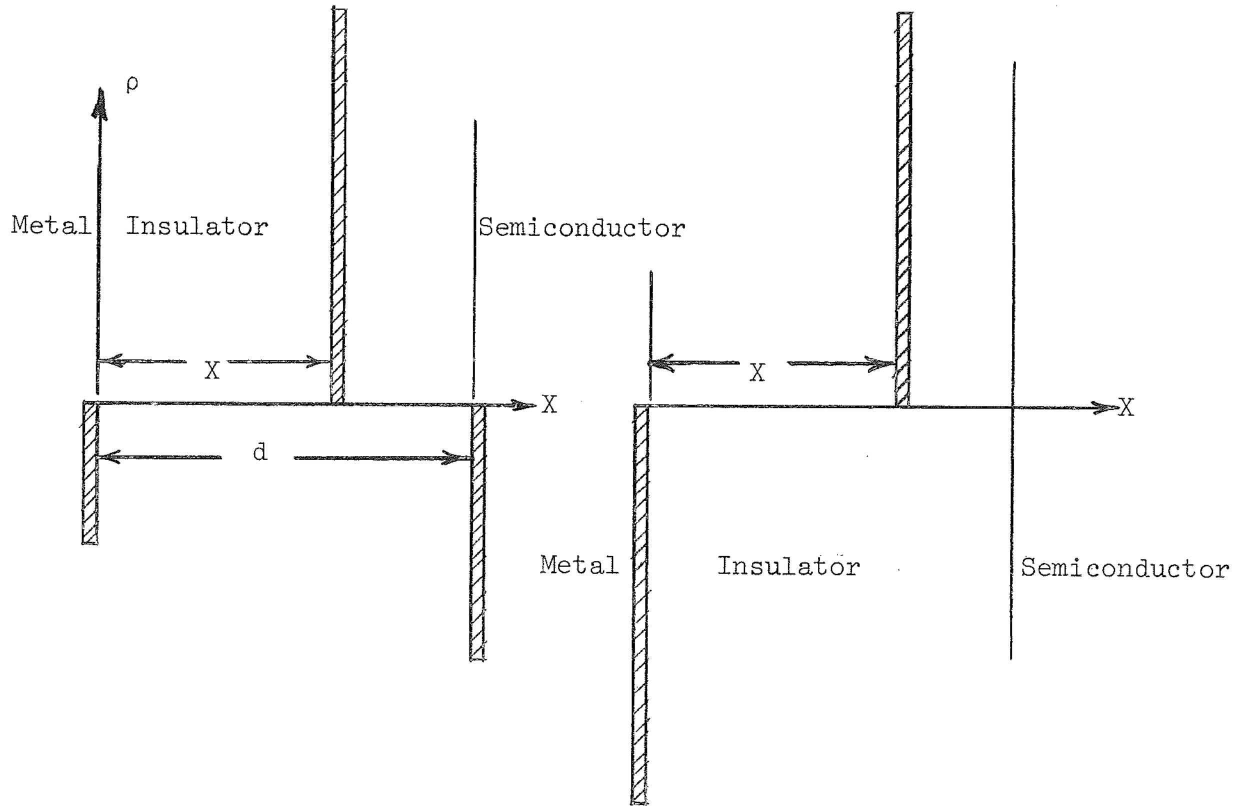

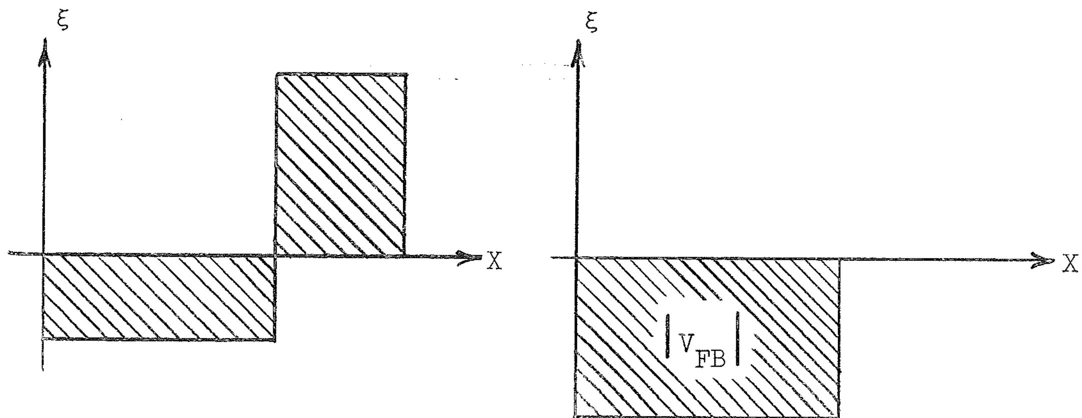

Fig. 18 Effect of a Charge Sheet Within the Insulator

(a) $V_a = 0$

(b) Flat-Band Condition

from the metal to the semiconductor. Therefore, the flat-band voltage depends on the density of the charge and on its location within the insulator. When the sheet of charge is next to the semiconductor, as in the case for most of the oxide surface states, the maximum influence is exerted and the flat band voltage is

$$V_{FB} = - \frac{Q}{C_o/A} \qquad [41]$$

For an arbitrary distribution of charges within the insulator, the flat-band voltage is[61]

$$V_{FB} = - \frac{1}{C_o/A} \int_o^d \frac{x}{d} \rho(x)dx \qquad [42]$$

Hence, positive surface states which, when emptied, represent a source of positive charge such as used in the above illustration, cause the capacitance-voltage curve to be shifted to the left. The flat-band voltage, which would normally be zero, will now have to be translated to some negative value to maintain the flat-band condition. For negative surface states, such as electron traps, the reverse argument holds and the curve shifts to the right. Figure 19 shows this point. Note that the entire capacitance-voltage characteristic shifts by the same amount as the flat-band point.

At higher frequencies the time constants of some of the surface states are sufficiently long that charge from these states does not enter into the capacitance measurement. This is especially true of the deeper states, and the space charge region starts predominanting at a less positive bias for negative surface states than at lower frequencies. This means that the equivalent capacitance starts to decrease for lower bias levels. As a consequence, the high frequency capacitance versus voltage curve lies below the low frequency curve. The capacitance continues to decrease until inversion takes over. Inversion does not depend on the charge in the surface

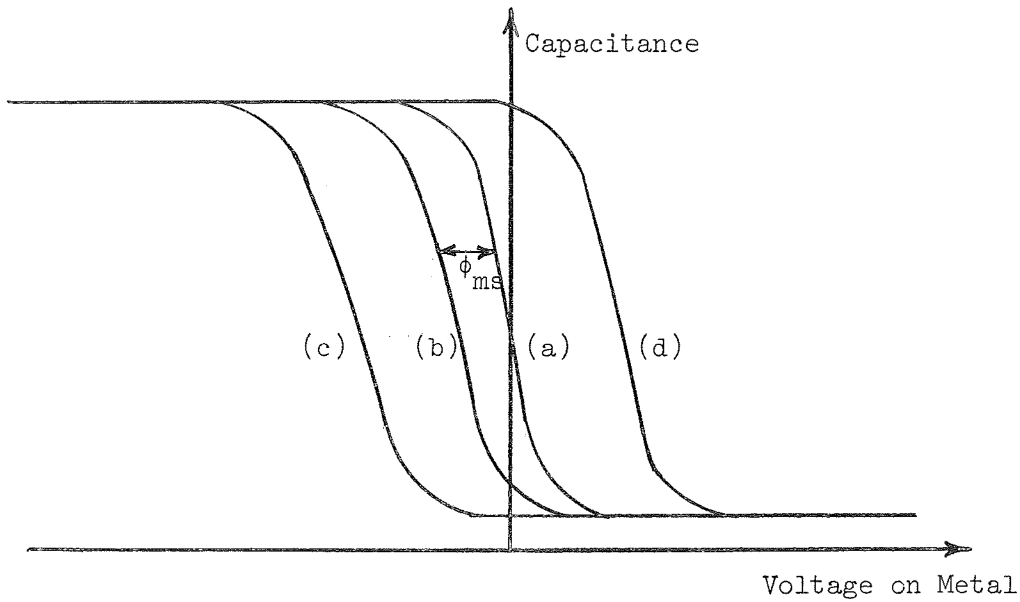

Fig. 19 Effect of Surface States and Work Functions on C-V Curve

(a) Theoretical Curve, $\phi_{ms} = 0$, No Surface States
(b) ϕ_{ms} negative
(c) Positively charged States
(d) Negatively Charged States

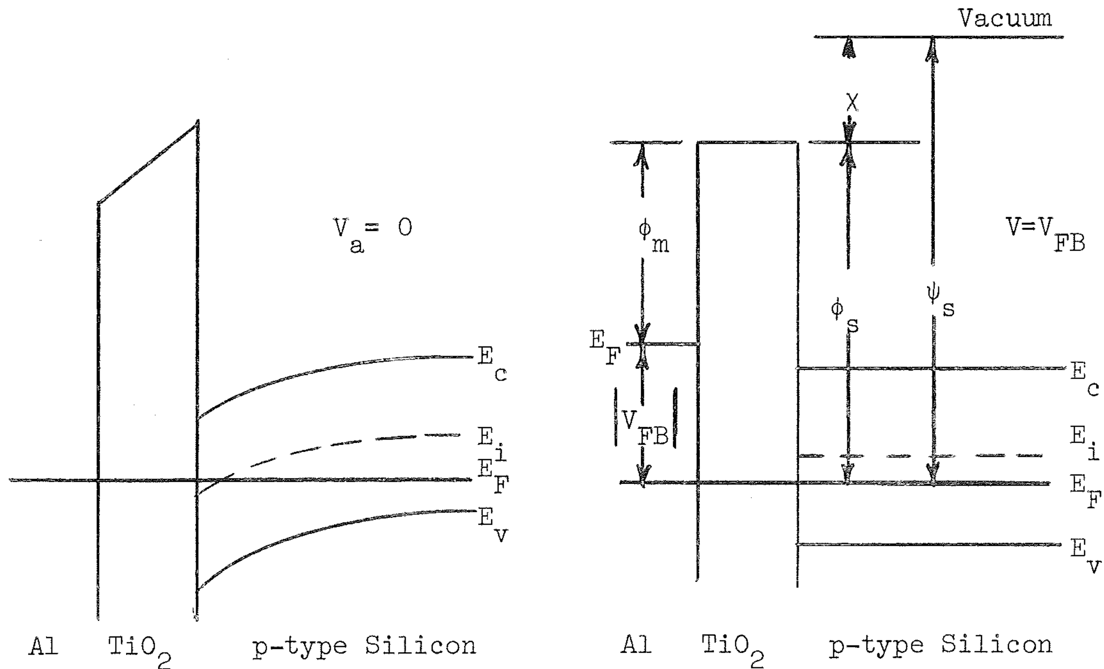

Fig. 20 Effect of Metal-Semiconductor Work Function Difference

(a) $V_a = 0$ (b) Flat-Band Condition

states but only on the surface potential and, therefore, begins at the same value of bias as in the low frequency case.

Grove[61] presents additional information on surface states in the Si-SiO_2 system. Many, Goldstein, and Grover[87] present a more comprehensive treatment of the theory of semiconductor surfaces.

6. Effect of Inteface Contact Polarization Potentials.

Upon making contact, the mutual interaction of two materials results in the formation of an interfacial contact polarization potential. This potential can arise from a transfer of electrons from surface states on one material to surface states on the other or from a perturbation of the surface states themselves. Schmidlin[111] considers the possible shift of energy bands of the mating materials with respect to each other by an amount equal to this polarization potential. Donating this potential drop by Δ_{ai}, the resultant interfacial barrier height ϕ_{oa} for the MIM structure of figure 5 is given by

$$\phi_{oa} = \psi_{ma} - \chi - \Delta_{ai} \qquad [43]$$

where ψ_{ma} is the work function of metal a, and χ is the electron affinity of the dielectric. An analogous case exists for the silicon-TiO_2 system of figure 20 giving an interfacial barrier height of

$$\phi_{os} = \psi_s - \chi - \Delta_{si} \qquad [44]$$

where the subscript "s" denotes the semiconductor.

Thus, an impurity at the interface can be polarized and the associated potential step becomes part of Δ_{si}, causing a change in the interfacial barrier height.

7. Effect of Work Function Difference.

The difference in electron energies at the Fermi level in the metal and in the semiconductor of an MOS structure is expressed as a difference

in work functions, which is the energy required to move an electron from the Fermi level in a given material to vacuum. Figure 20a shows the effect of bringing together an aluminum/titanium dioxide/p-type silicon structure. Electrons will flow to counterbalance the difference in work functions until the Fermi level in the metal is lined up with the Fermi level in the semiconductor. Consider the condition of figure 20b when just enough gate voltage is applied to counterbalance the work function difference and a flat-band condition is maintained in the semiconductor. The gate voltage required to bring about the flat-band condition is the flat-band voltage V_{FB}. Figure 20b gives this flat-band voltage as

$$V_{FB} = \phi_m - \phi_s \equiv \phi_{ms} \qquad [45]$$

B. Experimental Results and Discussion.

This section discusses the experimental results obtained from the capacitance-voltage data. The data yield dielectric constants, surface charge and surface state density numbers. Frequency effects due to various source materials and C-V shifts due to various electrode materials are discussed.

1. Dielectric Constant.

The dielectric constant of titanium dioxide films prepared on platinum as described in Chapter IV is 80. This agrees with the value reported by Feuersanger[50] for films prepared at low temperatures. The dielectric constant of films deposited on silicon is 50 as obtained by measuring the capacitance at 1 kHz of an MIS structure under bias conditions corresponding to strong accumulation of the silicon surface. Using the approximation of 2000 Å of TiO_2 ($\kappa = 80$) in series with d Å of SiO_2 ($\kappa = 4$), one obtains d = 60 Å for the thickness of the SiO_2. This is reasonable since some SiO_2 would form in the atmosphere and the growth process takes place in an oxidizing

atmosphere at 900°C. The dissipation factor for TiO_2 on platinum is between 1% and 4% for frequencies from 1 kHz to 100 kHz. The dissipation factor seems to be minimum at 10 kHz, somewhat higher at 1 kHz, and highest at 100 kHz. On silicon tan δ is less than 10% in the accumulation region, less than 4% in the inversion region, and reaches a peak as the device depletes. The 4% value in the inversion region corresponds closely to values of tan δ found in the inversion region for SiO_2 devices[69]. The 10% value in the accumulation region is higher than the 1% value found for the SiO_2 devices in the accumulation region. This might imply that the loss is the least for SiO_2, somewhat more for the silicon space charge region, and the most for the TiO_2. Figure 21 illustrates this behavior with the corresponding C-V curve at 1 kHz. The cause of this dissipation factor (loss) is discussed further in connection with the density of fast surface states in the next section.

2. Surface Charge and Surface States.

The total charge per unit area, Q_{ss}, associated with MOS structures results[33] from a combination of oxide space charge, or slow outer oxide states caused by ions or charged oxide defect centers, Q_{so}, and fast interface states which are located at the interface of the silicon and the oxide, Q_{FS}. As pointed out previously, the oxide space charge is not normally altered by the voltages required to trace C-V curves, therefore, the oxide space charge offsets the theoretical C-V curve along the voltage axis without changing their shape while surface charge in the fast states causes distortion in the C-V curve because the charge is quickly altered by varying the applied voltage and therefore the amount of charge in the fast states is a function of surface potential.

a. Oxide Space Charge, Q_{so}

Consider first the oxide space charge. This is an important

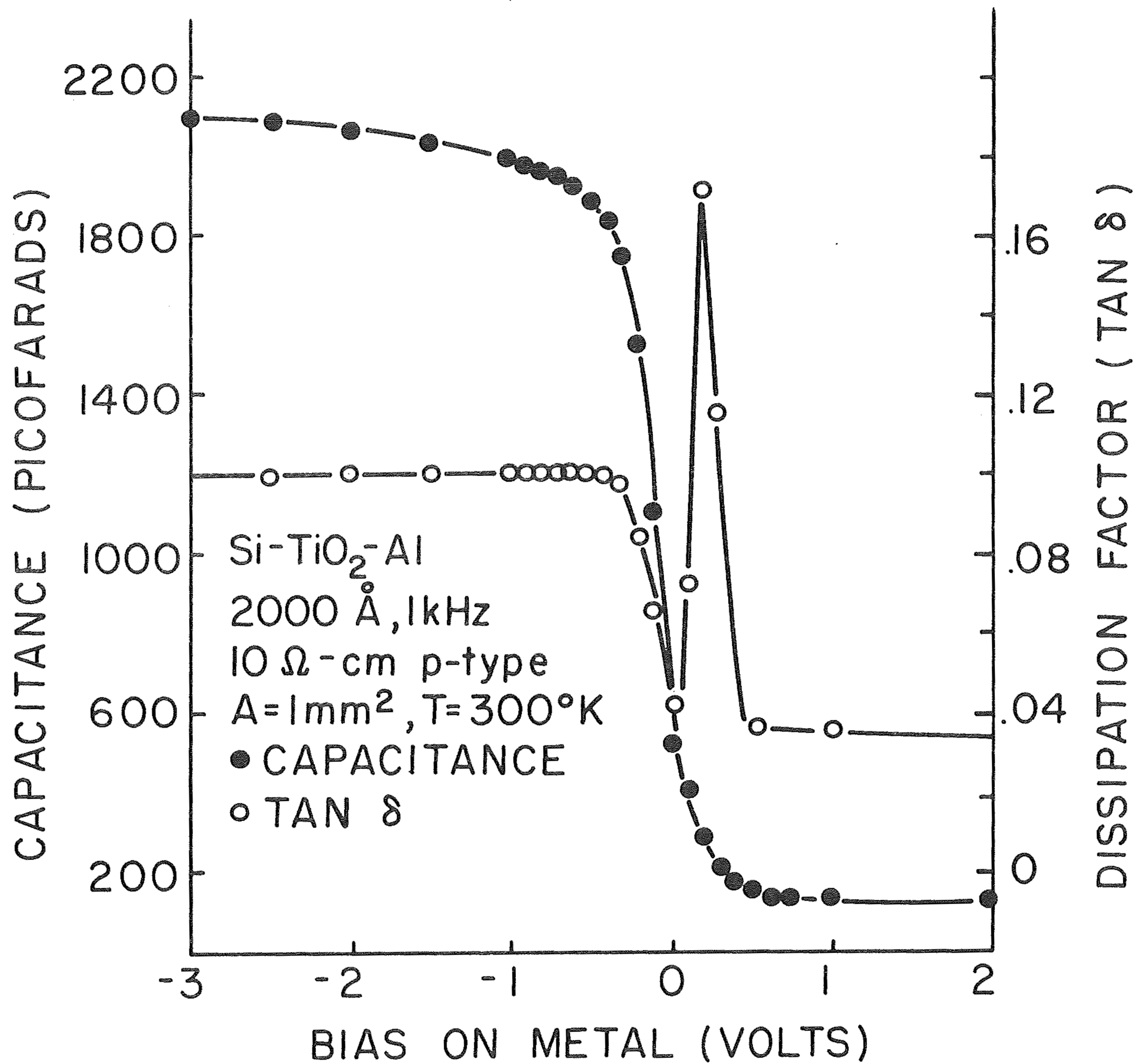

Fig. 21 Capacitance and Dissipation Factor vs. Bias

MOS parameter because it is one of the parameters which controls the threshold of MOS enhancement mode FET* switches, the operating point of MOS depletion mode FET* amplifiers, and the PNP transistor collector junction leakage and parasitic surface capacitances. The capacitance-voltage characteristics of MIS structures yield information about this charge[61]. From equation 45, one determines the flat-band voltage, V_{FB}, of the measured C-V curve. Using equation 41 the oxide space charge is then given by

$$Q_{so} = (\phi_{ms} - V_{FB})C_o/A \qquad [46]$$

Figure 22 shows a typical C-V plot for p-type silicon. The accumulation capacitance gives $C_o/A = 0.21\mu F/cm^2$. Determination of the flat-band voltage requires calculation of the flat-band capacitance. From Frankl[53], the surface charge density is

$$Q_s = \kappa_s \varepsilon_o \xi_s = \kappa_s \varepsilon_o \, (kT/qL_D)F(u_s, u_b) \qquad [47]$$

where

$$F(u_s, u_b) = \pm \sqrt{2} \, [(u_b - u_s) \sinh u_b + \cosh u_s - \cosh u_b]^{1/2} \qquad [48]$$

---

*An enhancement mode MOSFET is a common type metal-oxide-semiconductor field-effect-transistor where the source -to-drain conduction is dependent upon a channel which is electrostatically induced by the gate potential. In a depletion mode MOSFET a shallow, electrically-conductive channel connecting the source and drain is diffused into the device during fabrication. This channel, of the same conductivity type as the source and drain, can be made more resistive by voltage-biasing the gate. In both of these devices, the output current is controlled by an electric field.

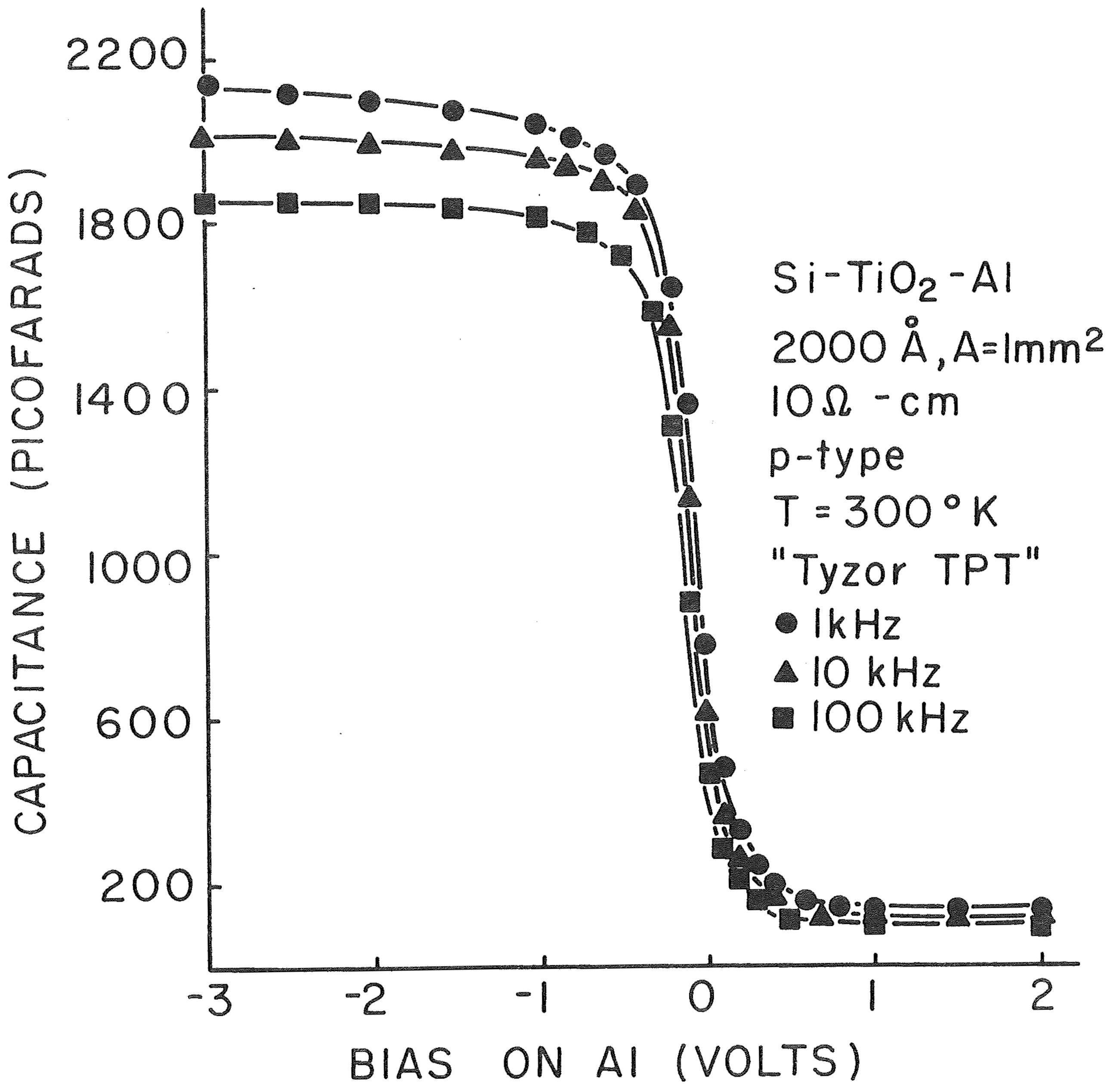

Fig. 22 Capacitance vs. Bias for p-type Sample

where the (-) is for $u_s > u_b$ and the (+) is for $u_s < u_b$, and where

$$u = (E_F - E_i)/kT \qquad [48]$$

where b denotes bulk, s denotes surface and L_D is the intrinsic screening length, (Debye Length)

$$L_D = L_B\ (\cosh u_b)^{1/2} = \left(\frac{\kappa_s \varepsilon_o kT}{2e^2 n_i}\right)^{1/2} \qquad [50]$$

The capacitance per unit area of the space charge layer is

$$C_{sp} = \frac{dQ_s}{du_s} = -\frac{\kappa_s \varepsilon_o}{L_D}\ \frac{\partial F}{\partial u_s} \qquad [51]$$

$$= -\frac{\kappa_s \varepsilon_o}{L_D}\ \frac{\sinh u_s - \sinh u_b}{F(u_s,\ u_b)} \qquad [52]$$

The flat-band condition occurs when $u_s = u_b$, and

$$C_{SFB} = \kappa_s \varepsilon_o\ (\cosh u_b)^{1/2}/L_D = \kappa_s \varepsilon_o / L_B \qquad [53]$$

which gives for p-type material with N_A carriers/cm^3

$$C_{SFB} = q(\kappa_s \varepsilon_o N_A/kT)^{1/2} \qquad [54]$$

$$C_{SFB} = 7.4 \times 10^{-16}\ (300\ \kappa_s N_A/T)^{1/2} \quad \text{farads/cm}^2 \qquad [55]$$

For 10Ω-cm p-type silicon, $N_A = 1.35 \times 10^{15} cm^{-3}$, which gives C_{SFB}=0.095 μF/cm^2.

The MOS flat-band capacitance is then

$$C_{FB} = \frac{C_o C_{SFB}}{C_o + C_{SFB}} \qquad [56]$$

Using the above values for C_o and C_{SFB} gives C_{FB} = 645 pF. Then, from figure 22, this capacitance yields the flat-band voltage, V_{FB} = 0.

Determination of Q_{so} now requires the metal-semiconductor work function difference, ϕ_{ms}, from

$$\phi_{ms} = \phi_m - \phi_s \qquad [57]$$

From Grove[61], for aluminum and 10Ω-cm p-type silicon $\phi_{ms} = -1.05$. These values and equation 46 yield $Q_{so} = 2.2 \times 10^{-7}$ coulombs/cm^2 or a density of states $N_{so} = 1.38 \times 10^{12}$ states/cm^2. Figure 23 shows a typical C-V plot using n-type, 10Ω-cm silicon. In this case, $V_{FB} = 0.57$ volt and $\phi_{ms} = -0.53$ volt. This yields $Q_{so} = 2.3 \times 10^{-7}$ coulombs/cm^2 and $N_{so} = 1.45 \times 10^{12}$ states/cm^2. Note from the direction of the C-V shift that these are negative surface charges (figure 19). For the p-type silicon, the work function difference tries to shift the curve to the left, but the negative surface charges try to shift the curve to the right. The result, for this particular case, is that these two effects exactly compensate each other and the flat-band voltage remains at zero. For the n-type material, the work function difference is less than above and the negative surface state density is about the same, with the net result being a shift in the flat-band voltage to the right. The n-type silicon seems to have more negative surface charges than the p-type which would be expected qualitatively since a higher Fermi level would allow more negative states to exist below the Fermi level, and the n-type material has a higher Fermi level than p-type material.

b. Fast Interface Surface States, Q_{FS}

Consider now the fast surface states. Fast interface state levels alter the performance of MOS devices by altering the reactance of the MOS varactor by filling and emptying in and out of these states at the ac measuring frequency and the charge in these states is an added component to the surface charge at the insulator-semiconductor interface. These fast

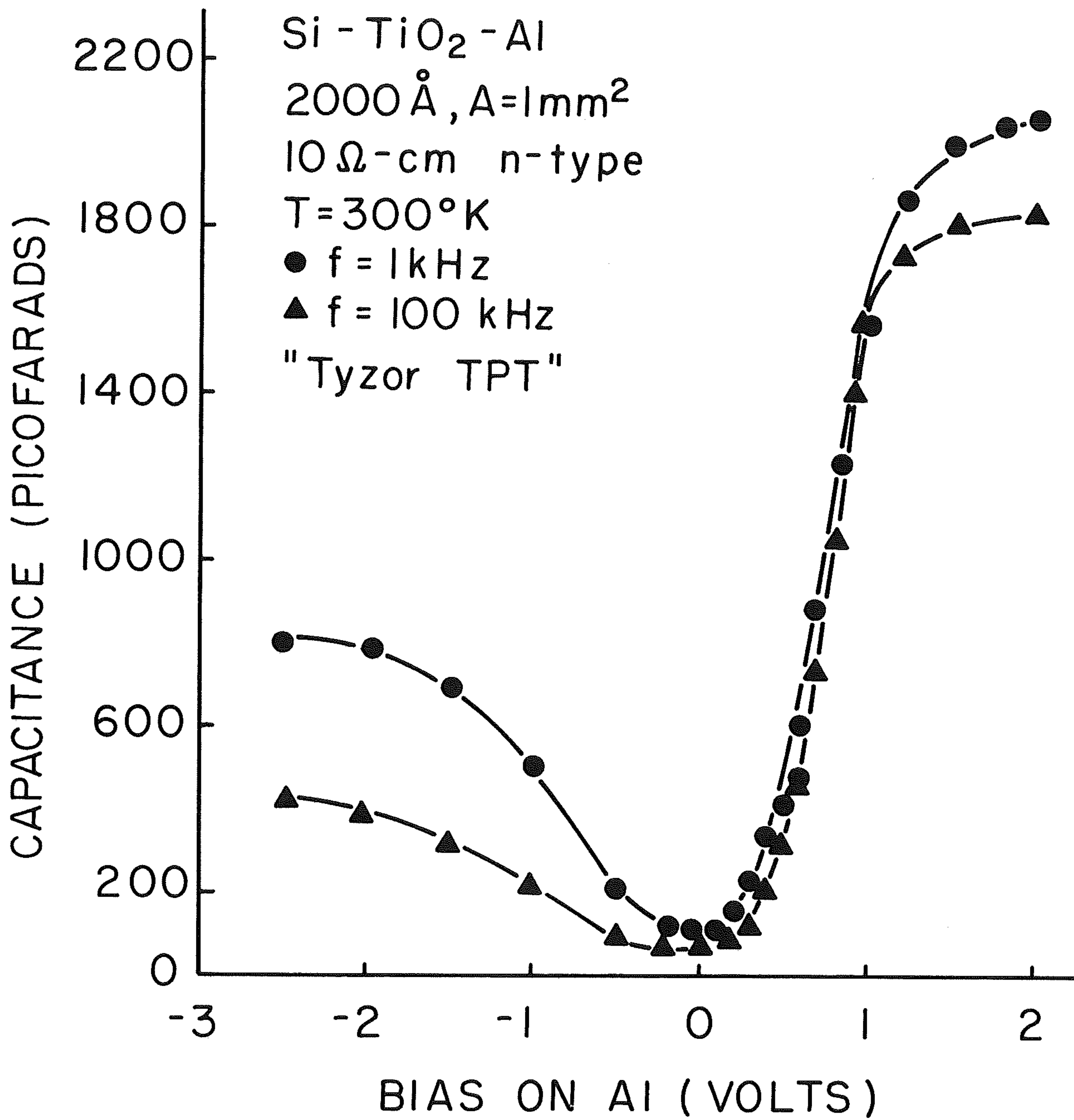

Fig. 23 Capacitance vs. Bias for n-type Sample

states can increase the switching voltage of enhancement mode field effect transistors and decrease the channel mobility causing lower gain-bandwidth products in MOSFET's.

Fast interface surface states cause distortion in the C-V curve. The experimental C-V curves follow the shape of the theoretical curve closely, implying that the density of fast states is not too high. Grove[61] says that a high degree of parallelism of experimental characteristics indicates that the total density of surface states in the middle 0.7 eV portion of the silicon energy band is less than 5×10^{10} cm^{-2}. Grove[61] says also that only those states which are within a few kT in energy of the middle of the energy gap contribute effectively to surface recombination and generation and hence the C-V characteristics will not be affected much by states near the band edges. There are three techniques for measuring these fast states. The method of Nicollian and Goetzberger[100,101] gives the density of states in the center half of the band using MOS surface conductance measurements. The method of Terman[125] uses the capacitance dispersion technique. The method of Gray and Brown[60] gives the density of states in the top quarter and bottom quarter of the band by scanning the forbidden gap using C-V measurements with temperature. The method of measurement for the Gray and Brown technique is that of determining the change in voltage and hence the change in surface charge required to maintain the flat-band condition as the Fermi level within the silicon is varied by changing the sample's temperature from 300°K to 100°K. Performing the measurements at 100 kHz insures that any charge in the interface states does not contribute appreciably to the ac capacitance so the measured ac capacity is almost entirely due to free carriers.

For the p-type samples, it requires less positive or more negative voltage on the metal electrode to reach the flat-band condition as the temperature decreases. The reason for this is that the Fermi level moves closer

to the valence band in a p-type material as the temperature decreases. At higher temperatures, the Fermi level is above some interface states. These are filled with electrons and are neutral. It takes a positive gate voltage to deplete partially the hole concentration at the surface. When the temperature decreases, the Fermi level moves closer to the valence band and some of the interface states lose electrons and become positively charged. In this instance, the interface states control the surface potential, and it requires a large negative gate voltage to deplete the interface states of their electrons in order to reach the flat-band condition.

Changes in the flat-band voltage as the temperature is changed give the change in interface state charge directly since there is no band bending for this condition. In the flat-band condition, the surface potential is equal to the bulk Fermi level which is given by Grove[61]. The procedure is to vary the temperature while maintaining the flat-band capacity, which is also temperature dependent and is calculable from equation 56 at various temperatures, by continuously adjusting the bias. Figure 24 illustrates the results of this measurement. This line represents the surface charge, Q_{FS}, as a function of the surface potential ϕ_s, which is equal to the Fermi level. The density of states, N_{FS}, is given by $\frac{\partial Q_{FS}}{\partial \phi_s}$. These results show that the density of fast states is relatively constant over the range of measurement and is approximately 8.5×10^{11} states/eV-cm^2.

Consider now the method of Nicollian and Goetzberger[100,101]. By this method, a measure of the MOS varactor impedance gives the interface state density, N_{FS}, near the middle of the gap. Both the capacitance and equivalent parallel conductance as functions of voltage and frequency contain identical information about the interface states. Figure 21 shows that the conductance technique is potentially more accurate, because of the sharp

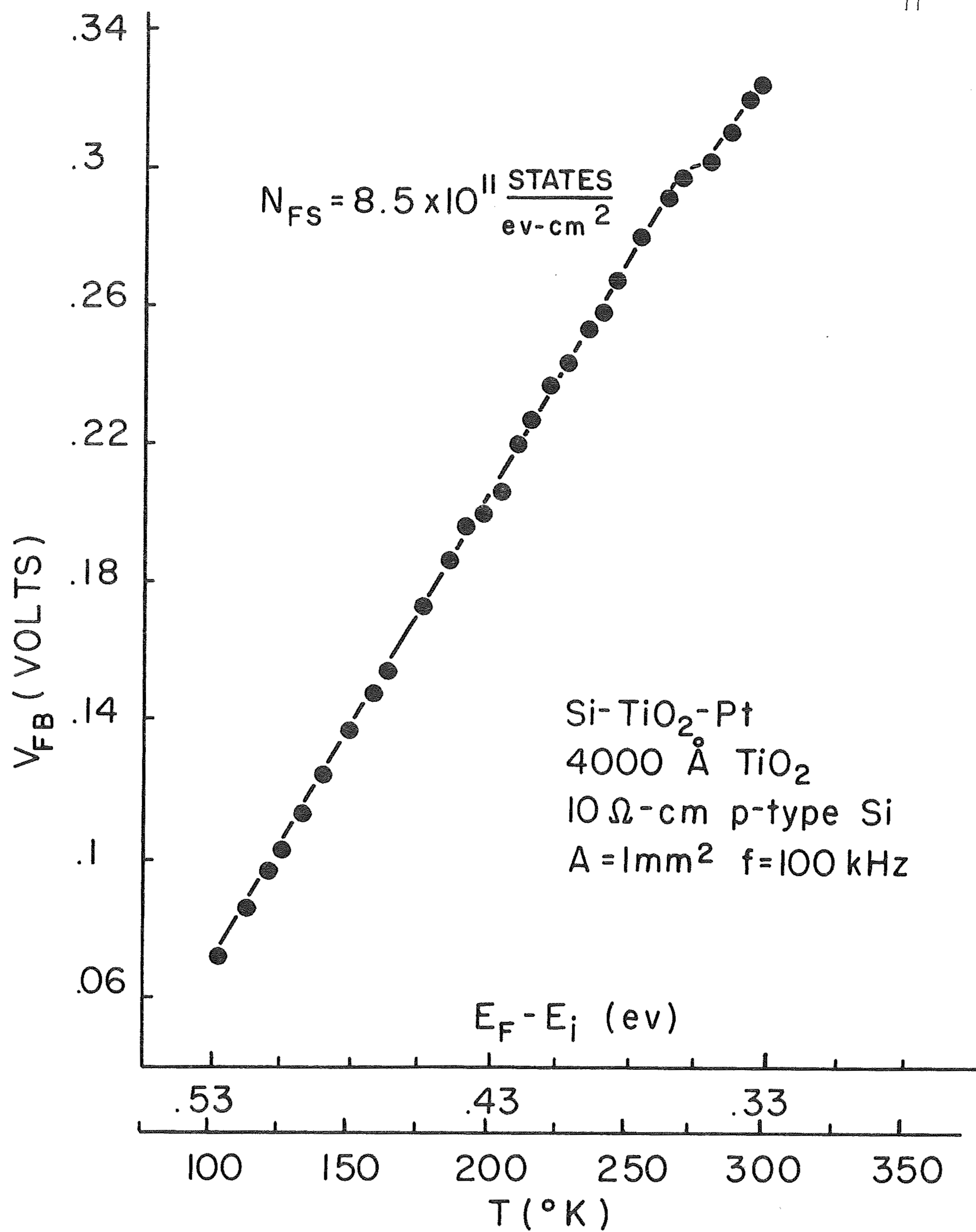

Fig. 24 Flat-Band Voltage vs. Change in Fermi Level with Temperature

peak exhibited by the conductance (directly related to the dissipation factor, $\tan\delta$), than the capacitance technique.

The loss arises in the following manner: When the ac signal moves the conduction band toward the Fermi level in the first half of the cycle, the average energy of the electrons in the silicon is increased. Because a conductance is observed, it is evident that the interface states do not respond immediately, but lag behind. Therefore, electrons at a higher average energy in the silicon are captured by interface states at a lower average energy. This process results in an energy loss. On the other half of the cycle when the ac signal moves the valence band toward the Fermi level, the electrons in filled interface states have higher average energy than the electrons in the silicon. As the electrons are emitted by the interface states into the silicon, they lose energy again. Therefore, there is an energy loss on both halves of the cycle. The energy required for transitions between the band edge and an interface state is much higher than this and is supplied by phonons. The dominant loss mechanism is the capture and emission of majority carriers. The interface states store charge and therefore have a capacitance C_s associated with them which is proportional to their density. The interface states reach equilibrium with the silicon exponentially with time τ. The conductance related to the loss is $G_s = C_s/\tau$. Therefore, measurement of equivalent parallel conductance yields the interface state τ and C_s.

The equivalent circuit of figure 25 illustrates the origin of the loss ($\tan\delta$). The dissipation factor is defined as

$$\tan\delta = \frac{1}{Q} = \frac{1}{2\pi}\,\frac{\text{energy loss per cycle}}{\text{maximum energy stored}} \qquad [58]$$

The equivalent impedance, z, of this circuit is

$$z = \text{Real Part} + \text{Imaginary Part} \qquad [59]$$

$$\text{Energy dissipated} = 1/2\ I_m^2\ [\text{Real Part of } z] \qquad [60]$$

and

$$\text{Energy stored} = 1/2\ I_m^2\ [\text{imaginary Part of } z] \qquad [61]$$

hence from equation 58

$$\tan\delta = \frac{1}{2\pi}\ \frac{z_R}{z_{IM}} = \frac{1}{2\pi}\ \left[\frac{\omega R_s C_s^2}{\omega^2 R_s^2 C_s^2 C_{sp}\ (\frac{C_{sp}}{C_o} + 1) + \frac{(C_{sp}+C_s)^2}{C_o} + (C_{sp} + C_s)}\right. \qquad [62]$$

This equation is of the form

$$\tan\delta = \frac{A\omega}{B+C\omega^2} \qquad [63]$$

where A,B, and C are constants

This same result is obtained by considering the Debye equations for a dielectric in which the polarization can relax exponentially with characteristic time τ after a change in applied electric field occurs. The complex dielectric constant may be written

$$\varepsilon^* = \varepsilon' - j\varepsilon'' \qquad [64]$$

where

$$\varepsilon' = \varepsilon_\infty + \frac{\varepsilon_o - \varepsilon_\infty}{1+\omega^2\tau^2} \qquad [65]$$

and

$$\varepsilon'' = \frac{(\varepsilon_o - \varepsilon_\infty)\omega\tau}{1+\ \omega^2\tau^2} \qquad [66]$$

yielding

$$\tan\delta = \frac{\varepsilon''}{\varepsilon'} = \frac{(\varepsilon_0 - \varepsilon_\infty)\omega\tau}{\varepsilon_o + \varepsilon_\infty(\omega\tau)^2} \qquad [67]$$

The equivalent circuit of figure 25 illustrates the principle of the MIS conductance technique.

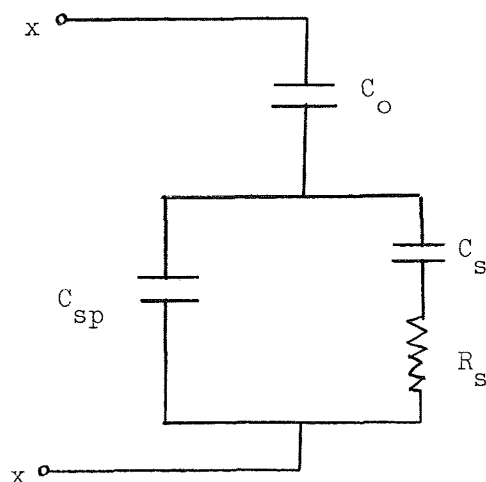

Figure 25. Equivalent Circuit of MIS Capacitor.

A bridge measures the admittance of the capacitor across terminals X-X. The oxide capacitance is measured in the region of strong accumulation. The admittance of the network is then converted into an impedance. The reactance of the oxide capacitance is substrated from this impedance and the resulting impedance converted back into an admittance giving[101]

$$\frac{G_p}{\omega} = \frac{\omega C_o^{\,2}\, G_m (G_m^{\,2} + \omega^2\, C_m^{\,2})}{\omega^2 C_o^{\,2} G_m^{\,2} + [\omega^2 C_m (C_o - C_m) - G_m^{\,2}]^2} \qquad [68]$$

and

$$C_p = \frac{C_o (G_m^{\,2} + \omega^2 C_m^{\,2})\ [\omega^2 C_m\ (C_o - C_m) - G_m^{\,2}]}{\omega^2 C_o^{\,2} G_m^{\,2} + [\omega^2 C_m (C_o - C_m) - G_m^{\,2}]^2} \qquad [69]$$

from the measured capacitance and conductance. This leaves C_{SP} in parallel with the series RC network of the interface states. The equivalent parallel conductance divided by ω is

$$\frac{G_p}{\omega} = \frac{C_s \omega \tau}{1 + \omega^2 \tau^2} \qquad [70]$$

This equation depends only on the interface state branch of the equivalent circuit. G_p/ω goes through a maximum when $\omega\tau = 1$. The value of G_p/ω at the maximum is $C_s/2$. Therefore, C_s is calculated from the peak of G_p/ω which yields N_{FS}. From figure 22 at the peak of tan δ, $C_m = 300$ pF, tan $\delta = D_m = 0.17$. The dissipation factor relates to the conductance by

$$G_m = \frac{1}{R_P} = \omega C_m D_m/(1+D_m^2) \simeq \omega\ C_m D_m \qquad [71]$$

This yields $G_m = 0.32$ μmhos. $C_o = 2000$ pF. These values yield $N_{FS} = 1.25 \times 10^{11}$ states/eV-cm^2. This value is about on order of magnitude less than the value obtained from the method of Gray and Brown[60]. This is expected, however, since both Gray[60] and Nicollian[101] predict that the density of states reaches a minimum very close to midband and Grove[61] states that there should be less than 10^{11} states/eV-cm^2 in order to maintain parallelism between the theoretical and experimental curves.

The other method of calculating N_{FS} involves the capacitance dispersion method of Terman[125]. From the equivalent circuit of figure 25, the equivalent parallel capacitance is

$$C_p = C_{sp} + \frac{C_s}{1+\omega^2\tau^2} \qquad [72]$$

where C_p is given by equation 69. To extract C_s from C_p using equation 72, C_{sp} must be known. C_{sp} can be calculated using an estimated doping density to find X_d and equation 39. However, the doping density is not accurately known near the silicon surface because of pile up or depletion of the dopant during the growth of the insulator. However, this discrepancy should not be as great for TiO_2 as for SiO_2 because of the lower temperatures and shorter times involved. The major difficulty arises from the fact that the interface state capacitance must be extracted from measured capacitance which consists of oxide capacitance, depletion layer capacitance, and

interface state capacitance. Using the same parameters as above, equation 72 gives $C_s = 490$ pF and $N_{FS} = 3.06 \times 10^{11}$ states/eV-cm^2. This value is only about a factor of two different from that obtained by the Nicollian method.

The major conclusions drawn by Nicollian and Goetzberger[101] about the interface follow.

(i) A continuum of states closely spaced in energy exists across the energy gap.

(ii) The dominant contribution to the conductance arises from majority carrier transitions to and from interface states. Thus, the conductance arises solely from the steady-state loss due to capture and emission of carriers by interface states and not states in the silicon space charge region.

(iii) The fluctuating surface potential causes a dispersion of interface state time constants in the depletion region. This fluctuation can arise from various sources, but is primarily due to a random distribution of surface charge.

(iv) In the weak inversion region the dispersion is eliminated by interaction between interface states and the minority carrier band resulting in a single time constant due to the fast response time of the minority carriers.

(v) Capture cross sections for electrons and holes are independent of energy over large portions of the silicon bandgap.

(vi) For a continuum of states, the peak in conductance occurs when the response time of the interface states, which is being varied by the bias, equals the period of the applied signal frequency multiplied by a constant. When generation-recombination

through interface states dominates the loss, the conductance goes through a peak as a function of bias in weak inversion because the time constant varies inversely with majority carrier density at the surface. If generation-recombination through bulk states dominates the loss, this peak will not occur. When the frequency is increased, this peak shifts to a bias value corresponding to a surface potential nearer to flat-band. For the C-V curve of figure 22, the peaks in dissipation factor occur at + 0.2, +0.1 and 0 for 1 kHz, 10 kHz and 100 kHz, respectively, illustrating this point.

3. Frequency Effects.

A difference between the TPT and PB prepared samples occurs in the frequency effects. Figure 22 and figure 26 illustrate that on p-type silicon the TPT samples exhibit the high frequency characteristic in the inversion region between 1 kHz and 100 kHz, while the PB samples exhibit the lower frequency characteristic; i.e., the capacitance rises toward the oxide value as the frequency decreases from 100 kHz to 1 kHz due to a higher generation-recombination rate[61]. This difference occurs because the PB is a partially hydrolyzed organometallic and contains an excess of water molecules. The presence of excess water vapor has been shown to affect MOS C-V curves[69]. Figure 23 illustrates that the TPT formed n-type samples exhibit a frequency characteristic somewhere between the two cases above. The high frequency case results because the measurement frequency is much greater than the generation-recombination rate so that all the charge appears at the edge of the depletion region. If the frequency is low enough for generation-recombination to keep up with the small signal variation, the generation-recombination mechanism leads to charge exchange with the inversion

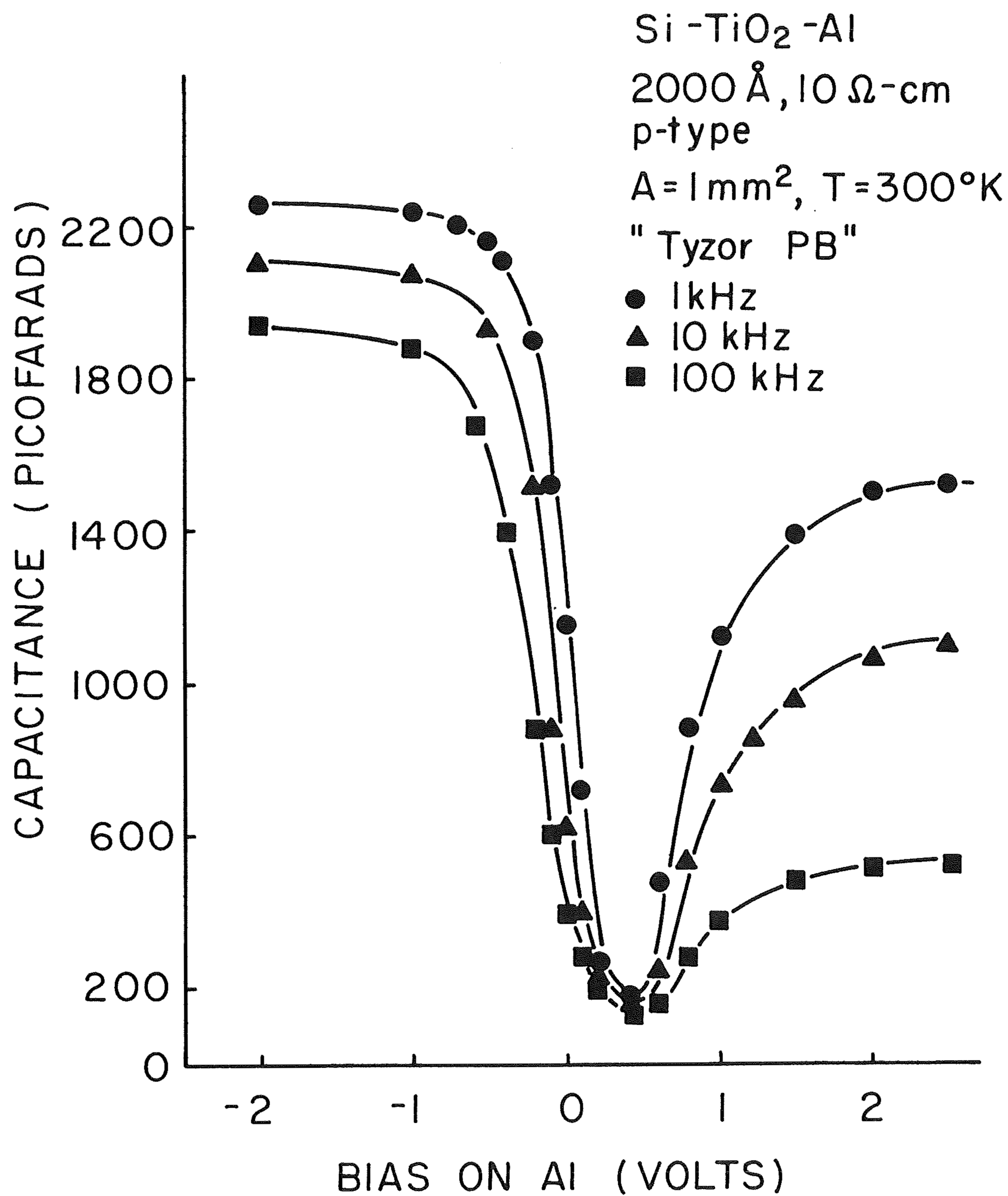

Fig. 26 Capacitance vs. Bias for "PB" Prepared Sample

layer in step with the measurement signal and C will approach C_o. The inversion side of the C-V curves can also be affected by surface charge migration over the oxide around the field plate[99].

Another frequency sensitive effect occurs in the accumulation region of these curves. The oxide capacity or the dielectric constant appears to be frequency sensitive, which is not too likely in the frequency range of measurement and it is more likely that the surface states are at least partially in electrical contact with the silicon and are able to supply a frequency sensitive charge to the capacitance measurements effectively changing the thickness of the film.

4. C-V Shifts.

The high dielectric constant of this material which causes the abrupt change in capacitance to occur near zero volts bias, instead of offset several volts as in SiO_2 and Si_3N_4, offers unique possibilities to the device operation. Figure 27 illustrates the effect of a different work function by changing from aluminum to platinum electrodes to go from a depletion mode device to an enhancement mode device, because with platinum electrodes a channel will form on p-type material with positive bias. With aluminum, the channel is already formed at zero bias. It has not been possible to build an enhancement mode device on p-type material with other insulators, such as SiO_2. Figure 28 shows that additional possibilities exist by growing layers of other dielectric materials under the TiO_2. In this case, SiO_2 was allowed to grow in the deposition chamber from H_2 + CO_2 at 930°C for 5, 10 and 15 minutes prior to TPT being introduced. Since the TiO_2 has negative charge states associated with it and SiO_2 has positive surface states the effect is to shift the flat-band voltage from positive toward negative by having the positive states cancel some of the

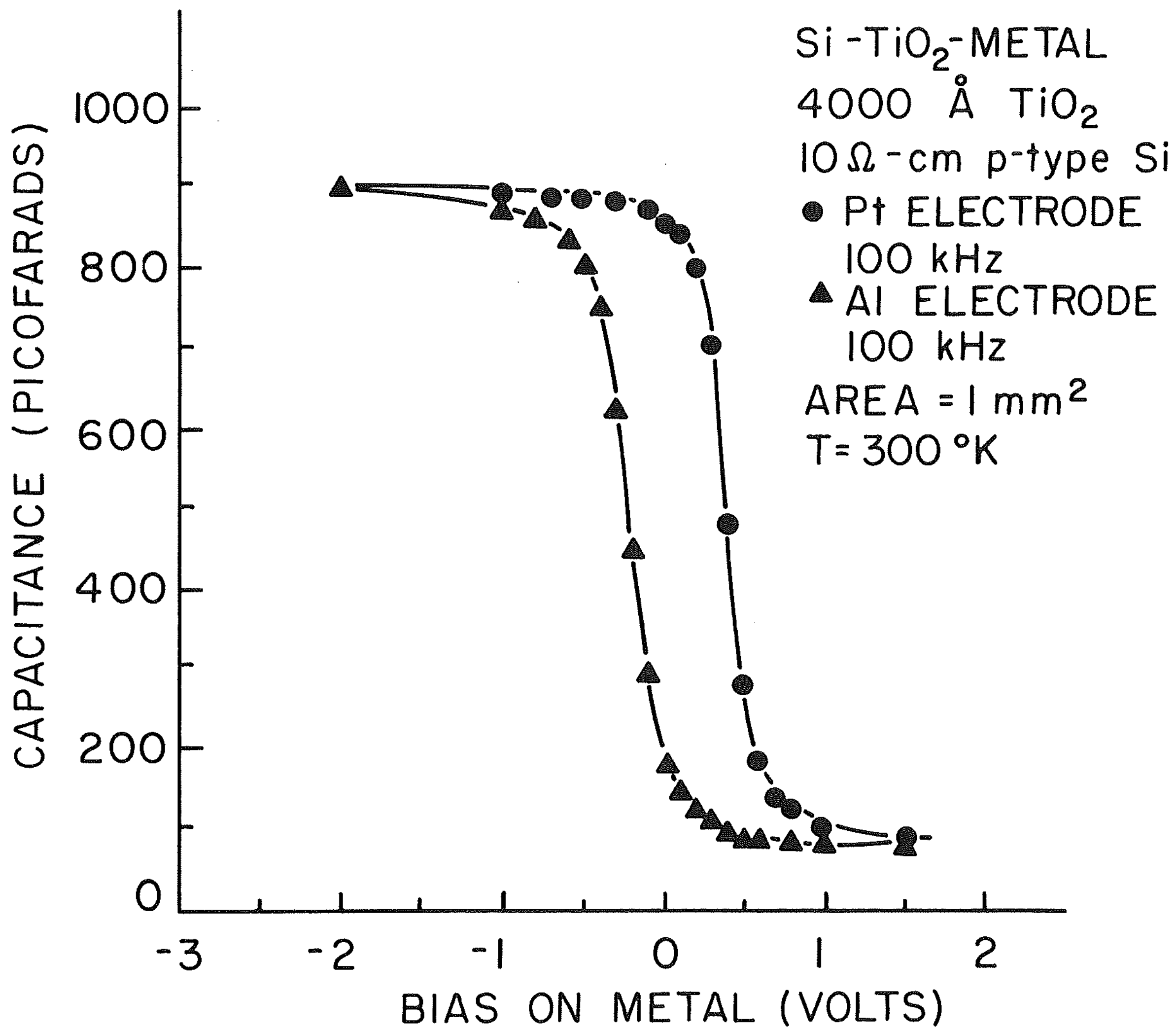

Fig. 27 Electrode Effects on Capacitance vs. Bias

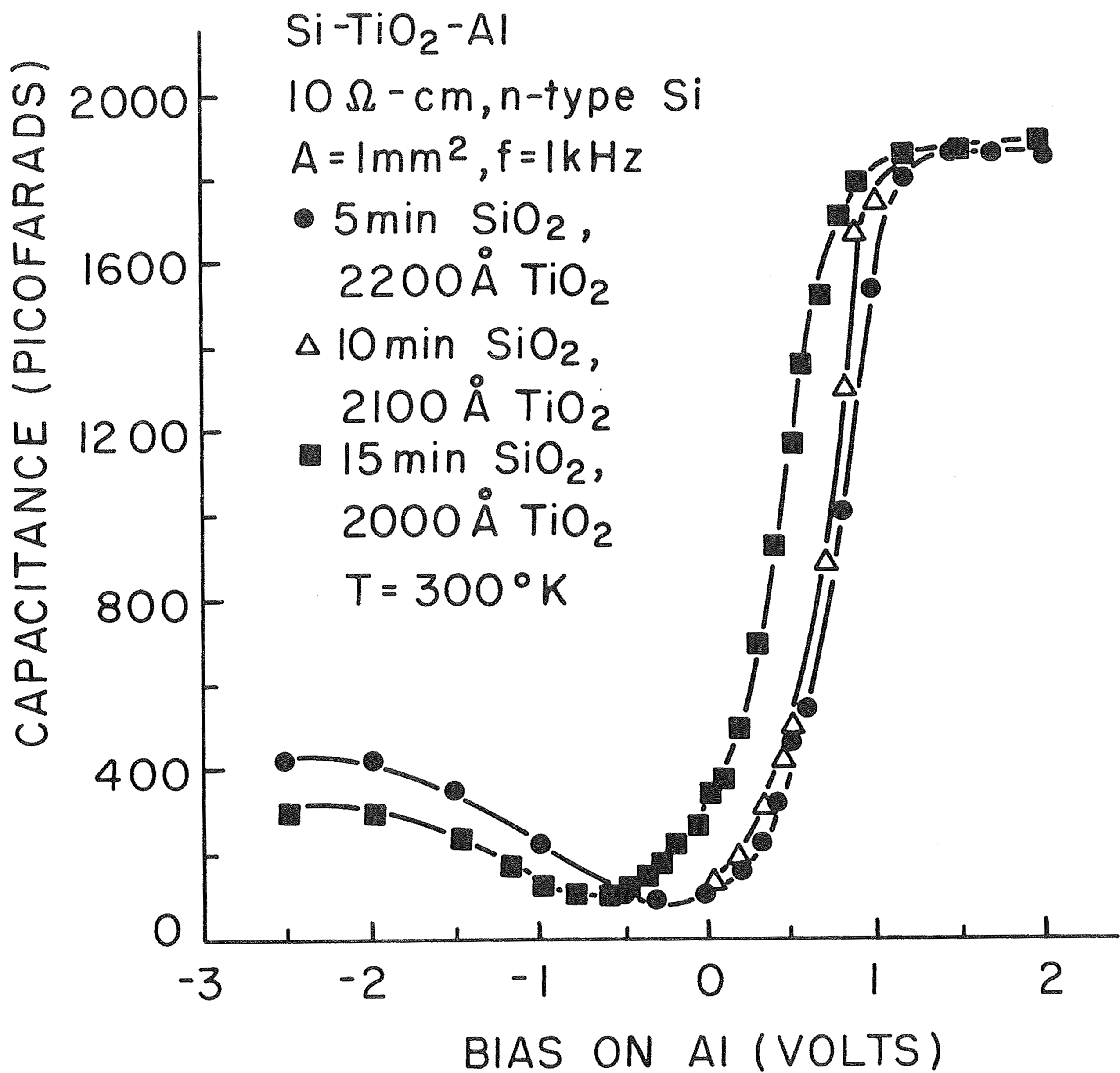

Fig. 28 SiO_2 Effects on Capacitance vs. Bias

negative states. Analogous effects are seen for silicon dioxide-silicon nitride mixtures[43].

No hysteresis effect is observed in making the C-V measurements as with Si_3N_4. Hysteresis would be observed when there is an appreciable density of states deep in the oxide having time constants longer than the time it takes to vary the bias because the charging and discharging of these states would lag behind the bias variation[101]. The fact that no hysteresis is observed means that the density of states in the oxide having time constants of the order of minutes is negligible.

The preceding considerations indicate that negative surface charges exist within the TiO_2 film. The density of slow oxide surface states is approximately 10^{12} states/cm^2. The density of fast interface surface states is about 10^{12} states/eV-cm^2 near the band edge and about 10^{11} states/eV-cm^2 near the center of the band. Different frequency characteristics are observed depending on the organometallic used to form the films. Shifts in the capacitance-voltage characteristics near V = 0 with different metal electrodes and with mixtures of TiO_2 - SiO_2 indicate unique device possibilities.

CHAPTER VII

SUMMARY AND CONCLUSIONS

The results of this work form a consistent picture of the growth and behavior of the titanium dioxide films formed by chemical vapor deposition. Hydrolysis of titanium organometallics in a hydrogen and carbon dioxide atmosphere at high temperature forms physically and electrically satisfactory titanium dioxide films.

This research includes the design and construction of a vapor deposition system to grow TiO_2. The growth technique is new, however, it is similar to a technique used by Feuersanger[50]. The thermodynamic considerations aid in the analysis of the process and lead to the determination of the optimum operating conditions. The reaction utilized various organometallics of titanium, and tetraisopropyl titanate proves to be the most suitable due to its high vapor pressure.

Substrates are platinum coated quartz and polished silicon, both n-type and p-type. Fast neutron activation analysis finds that the stoichiometry of the films depends on the deposition conditions. Films formed at temperatures less than 850°C are oxygen deficient.

A study of the physical properties of the films indicates that the films appear hard, smooth, and reflective. An x-ray study indicates that the films are polycrystalline TiO_2. The film adherence to the substrate is entirely satisfactory. Forty-eight per cent hydrofluoric acid etches the films at about 700 angstroms per minute and tends to cause some peeling. The electrical characteristics do not change during room temperature storage and moisture tests. The refractive index, as determined by ellipsometry, is about 2.0.

A major result of this work is a knowledge of the conduction behavior of titanium dioxide films on silicon and metal substrates. The

deposition temperature strongly influences the conductivity of these films. The oxygen deficient films are more semiconducting than insulating. Experimentally, the current is proportional to exp $(mE^{1/2})$ where m is a constant and E is the electric field. The current-voltage characteristics for MIM structures are independent of polarity for metals with different work functions indicating bulk controlled emission. These considerations indicate that the dominant conduction mechanism in titanium dioxide is Poole-Frenkel emission from donor and acceptor sites and traps within the bulk of the TiO_2 film. The sites lie approximately 0.25 eV from the band edge. Both donor and acceptor sites are present creating a compensating effect. The breakdown strength of these films is 5×10^5 volts/cm.

Another major result of this work is a knowledge of the silicon-titanium dioxide system as determined from capacitance-voltage characteristics of an MOS capacitor structure. Energy states exist at the interface between the silicon and the titanium dioxide. These states become sources of charge strongly affecting the device's properties. The C-V data indicate that negative surface charges exist within the TiO_2 film. The density of slow oxide surface states is approximately 10^{12} states/cm^2. The density of fast interface surface states is about 10^{12} states/eV-cm^2 near the band edge and about 10^{11} states/eV-cm^2 near the center of the band as determined by the flat-band variation with temperature method of Gray and Brown[60], the equivalent parallel conductance method of Nicollian and Goetzberger[100,101] and the capacitance dispersion method of Terman[125].

The dielectric constant of these films is 80 on platinum and 50 on silicon due to the presence of a thin layer of SiO_2 on the silicon. Different frequency characteristics are observed in the C-V curves depending on the organometallic used to form the films.

Shifts in the capacitance-voltage characteristics near V = 0 with different metal electrodes and with mixtures of TiO_2 - SiO_2 indicate unique device possibilities. Herein lies a very promising area for further study. The high dielectric constant causes the abrupt change in the C-V curve to occur very near zero volts even for rather large densities of surface states. Figure 27 illustrates the effect of a different work function on the C-V curves. By changing from aluminum to platinum electrodes one can go from a depletion mode device to an enhancement mode device because with platinum electrodes a channel will form on p-type material with positive bias. With aluminum the channel is already formed at zero bias. This means that TiO_2 could be used to make an n-channel enhancement mode MOSFET which is nearly impossible to do with SiO_2. Building such a device would lead to such device parameters as channel conductivity and turn-on voltage.

Figure 28 shows the effect of growing a layer of SiO_2 under the TiO_2. Possibilities exist for further work here by studying mixtures of SiO_2 - TiO_2 - Si_3N_4. Certainly, the different types of states and mechanisms associated with these three insulators could create interesting shifts and effects on the MOS characteristics and perhaps lead to very useful device applications.

APPENDIX I

ATTEMPTS TO GROW LEAD TITANATE

Having established the optimum conditions for the deposition of TiO_2, attempts were made to grow $PbTiO_3$ which might yield improved dielectric properties. The alkyl derivatives of lead have sufficient volatility and stability to be very promising for such an application. Tetraethyl lead, $(C_2H_5)_4Pb$, and Tetraisopropyl titanate, $(C_3H_7O)_4Ti$, should form $PbTiO_3$. The lead and titanium compounds are liquids at room temperature and have sufficient vapor pressure to permit the rate of delivery of the respective gas to the reactor to be controlled by regulation of the flow of carrier gas over the liquid. The vapor pressure and properties of tetraethyl lead are closely similar to tetraisopropyl titanate. The source of the tetraethyllead is the Ethyl Corporation.

The plan of attack was to grow lead oxide from the tetraethyllead and establish a growth rate similar to that of the already studied TiO_2 and then combine the two to form $PbTiO_3$. Problems occurred in the growth of the PbO due to the low melting points of various forms of lead oxide. When operating at temperatures around 900°C, required for the $H_2 + CO_2$ reaction to go to completion, no lead oxide is formed because the melting is between 300°-800°C for various forms of lead oxide. At temperatures around 500°C a cloudy film of poor appearance is formed, but it is suspected that this film could be oxygen deficient as were TiO_2 films formed at low temperatures.

With equal flow rates of tetraisopropyl titanate (TPT) and tetraethyllead (TEL) at 900°C nothing forms. Turning off the TEL allows a film of TiO_2 to form, but turning on the TEL again stops the growth. The PbO is apparently keeping the TiO_2 and $PbTiO_3$ from forming at high temperatures.

The conclusion of this attempt is that lead titanate cannot be grown easily in a $H_2 + CO_2$ atmosphere because of the low melting point of the PbO and the high temperature required for the $H_2 + CO_2$ reaction. Lower temperature deposition in an oxygen atmosphere or in a moist atmosphere from a water bubbler might be a plausible approach to this problem.

BIBLIOGRAPHY

History and Review

1. J.N. Blicker and J.H. Oxley, "CVD Opens New Horizons in Ceramic Technology," Bull. Am. Ceram. Soc. 41 (2), 81 (1962).

2. R. Glang and S. Wajda, "Vapor Growth in Semiconductor Technology," Met. Soc. Conf. 15, 27 (1961).

3. A.J. Mountvala and S.L. Blum, "Chemical Vapor Deposition for Electron Devices," Research/Development, 34 (July 1966).

4. H.E. Podall and M.M. Mitchell, Jr., "The Use of Organometallic Compounds in Chemical Vapor Deposition," Ann. N.Y. Acad. Sci. 125 (1), 218 (1965).

5. C.F. Powell, I.E. Campbell, B.W. Gonser, Vapor Plating, John Wiley and Sons, Battelle Memorial Institute, Electrochemical Series (1955).

6. C.F. Powell, J.H. Oxley, J.M. Blocher, Vapor Deposition, John Wiley and Sons, Battelle Memorial Institute, Electrochemical Series (1966).

7. E.M. Sherwood (Battelle), "Vapor Plating," Plating 52, 667 (1965).

8. E.M. Sherwood and J.M. Blocher, Jr. (Battelle), "Vapo-Metallurgy: I Vapor Deposition [of Metals]: The First Hundred Years," J. Metals 17 (6), 594 (1965).

Dielectric Review

9. P.A. Larssen, "Non-linear Dielectrics," Insulation 338 (May/June 66).

10. A.R. von Hippel, et al., "High Dielectric Constant Materials and Ferroelectricity" - Final Report No. AFCRL 6392 Contract AF 1906-6155, AD 404776 (Mar., 1963).

11. A.R. von Hippel, "High-Dielectric Constant Materials as Capacitor Dielectrics," Technical Report 145, MIT Lab Insul. Res. (Dec. 1959).

12. A.R. von Hippel Ed., Dielectric Materials and Applications, Technical Press, MIT, Wiley, (1954).

Thermodynamics

13. American Chemical Society, Metal-Organic Compounds, a collection of papers composing the Symposium on Metal-Organic Compounds of the Am. Chem. Soc. April, 1957. Adv. Chem. Ser. 23.

14. D.C. Bradley, R. Gaze and W. Wardlaw, "Structure Aspects of the Hydrolysis of Titanium Alkoxides," J. Chem. Soc., 469 (1957).

15. R.W. Coutant, N. Albon, J.F. Miller, "Study of the Mechanisms of Pyrolytic Deposition," (Battelle) AD 468055 (August 1965).

16. H.C. Brill, "Organo-titanates," TAPPI 38, No. 5, 141A (1955).

17. Bulletin of the Titanium Pigment Corp. (National Lead Co.)

18. Dow Chemical Company, JANAF Thermochemical Tables (1960 to date).

19. Handbook of Chemistry and Physics, 39th edition, Chemical Rubber Publishing Co., 1958.

20. H.C. Kaufman, Handbook of Organometallic Compounds, Van Nostrand, Inc., New York, (1961).

21. Parks, Free Energies of Some Organic Compounds, N.Y.: Chemical Catalog Co. (1932).

22. K.S. Pitzer and L. Brewer, Thermodynamics (Lewis and Randall), New York: McGraw-Hill (1961).

23. E.G. Rochow, Organometallic Chemistry, Reinhold Publ. Co., N.Y. (1964).

24. F.D. Rossini, et al., Selected Values of Physical and Thermodynamic Properties of Hydrocarbons and Related Compounds, Pittsburgh: Carnegie Press, (1953).

25. H. Schaffer, Chemical Transport Reactions, Academic Press, N.Y. (1964).

CVD and Dielectric Materials

26. Roger Argenal-Arauz, "Composition of Thin Ti_mO_n Films by Fast Neutron Activation Analysis," Master Thesis, University of Texas at Austin (June, 1968).

27. T. Arizumi and T. Nishinaga, "Transport Reaction in a Closed Tube Process," Japan JAP 4(3), 165 (1965).

28. C.R. Barnes and C.R. Gasner, "Pyrolytic Deposition of SiO_2 for 600°C Thin Film Capacitors," J. Electrochemical Soc. 110, 361 (May 1963).

29. K.E. Bean, P.S. Gleim and W.R. Runyan, "Some Properties of Vapor Deposited Si_3N_4 Films Using SiH_4-NH_3-H_2 System," presented at Electrochemical Society Meeting in Philadelphia, October 9-14, 1966.

30. K.E. Bean and P.S. Gleim, "Some Properties of Vapor Deposited SiC," J. Electrochem. Soc. 114, 1158 (1967).

31. J. Black, D. Peterson, W. Brand, "Vapor Phase Deposition Methods for Metal Oxide Based Dielectrics," AD 450131 (Oct., 1964).

32. J. Black, D. Peterson, W. Brand, "Vapor Phase Deposition Techniques for Fabrication of Microelectronic Circuitry Thin Film Elements," AD 456793 (Jan. 1965).

33. D.M. Brown and P.V. Gray, "MOS Science and Technology," General Electric Research and Development Center, Rept. #67-C-026 (1967).

34. G.A. Brown, W.C. Robinette, Jr. and H.G. Carlson, "Electrical Characteristics of Si_3N_4 Films," J. Electrochem. Soc. 115, 948 (1968).

35. R.M. Burger and R.P. Donovan, Fundamentals of Silicon Integrated Device Technology, Prentice Hall, Englewood, N.J., (1967).

36. E.G. Bylander, "Kinetics of Silicon Crystal Growth from $SiCl_4$ Decomposition," J. Electrochem. Soc., 109, 1171 (1962).

37. D.R. Callaby, "Surface Layer of $BaTiO_3$, JAP, 37, 2295 (May 1966).

38. R.W. Christy, "Electrical Properties of Thin Polymer Films, Part II, Thickness 50-150A," J. Appl. Phys., 35, 2179 (1964).

39. T.L. Chu and G.A. Grubec, "Silica Films by Chem-Transport," Trans. AIME 223, 568 (1965).

40. T.L. Chu, C.H. Lee, J.R. Szedon, "Films of Silicon Nitride-Silicon Dioxide Mixtures," presented at the Dallas Meeting of the Electrochemical Society, May 10, 1967, Abstract No. 83.

41. B.J. Curtis and J.A. Wilkinson, "Preparation of Mixed Oxide Crystals by Chemical Transport Reactions," J. Am. Ceram. Soc. 48 , 49 (1965).

42. P.D. Davidse and L.I. Maissel, "Dielectric Thin Films through rf Sputtering," JAP 37, 574 (1966).

43. B.E. Deal, P.J. Fleming and P.L. Castro, "Electrical Properties of Vapor Deposited Si_3N_4 and SiO_2 Films," J.Electrochem. Soc. 115, 300 (1968).

44. A.J. Dekker, Solid State Physics, Prentice-Hall, Englewood Cliffs, New Jersey (1957).

45. R.P. Donovan, Integrated Silicon Device Technology, Vol. XIII, Intraconnections and Isolation, RTI, AD 655 081 (May 1967).

46. P.R. Emtage, "Enhancement of Metal to Insulator Tunneling by Optical Phonons," J. Appl. Phys., 38, 1820 (1967).

47. P.R. Emtage and W. Tantraporn, "Schottky Emission Through Thin Insulating Films," Phys. Rev. Lett., 8, 267 (1962).

48. G. Ferment and N.J. Haskell, "Fabrication of Beryllium Oxide Radomes by Pyrolytic Deposition," AD 608486 (June 30, 1964).

49. A.E. Feuersanger and D.R. Frankl, "High Frequency Surface Varactors," IEEE Trans. on Electron Devices, ED-10, 143 (1963).

50. A.E. Feuersanger, "Titanium Dioxide Dielectric Films Prepared by Vapor Reaction," Proc. IEEE 52 (12), 1463 (1964).

51. E.T. Fitzgibbons, Current Mechanisms in Thin Polymer Films, Master's Thesis, The University of Texas at Austin, Austin, Texas, June, 1967.

52. R.I. Frank and J.G. Simmons, "Space-Charge Effects on Emission-Limited Current Flow in Insulators," J. Appl. Phys., Vol. 38, No. 2, Feb. 1967, pp. 832-840.

53. D.R. Frankl, "Some Effects of Material Parameters on Surface Varactors," Solid State Electronics 2, 71 (1961).

54. J. Frenkel, "Pre-Breakdown Phenomena, Insulators and Semiconductors," Phys. Rev., 54, 657 (1938).

55. R.E. Gannon, R.C. Foliveiler, T. Vasilos, "Pyrolytic Synthesis of Titanium Diboride," J. Am. Ceram. Soc. 46 (10), 496 (1963).

56. G.C.B. Garrett and W.H. Brattain, "Physical Theory of Semiconductors Surfaces," Phys. Rev., Vol. 99, No. 2, pp. 376-388, July 15, 1955.

57. J.J. Gebhardt and R.F. Cree, "Vapor Deposited Borides of Group IVA Metals," J. Am. Ceram. Soc. 48, 262 (1965) and AD 601861.

58. R.M. Glaister, "Solid Solution Dielectrics Based on Sodium Niobate," J. Am. Ceram. Soc. 43, 348 (1960).

59. F.R. Gleason, Jr. and L.R. Watson, "Ferrite Films Prepared by Pyrohydrolytic Deposition," JAP 34, 1217 (1963).

60. P.V. Gray and D.M. Brown, "Density of SiO_2-Si Interface States," Appl. Phys. Letters 8, 31 (1966).

61. A.S. Grove, Physics and Technology of Semiconductor Devices, Wiley, Ch. 9 (1967).

62. A.E. Grove, E.H. Snow, B.E. Deal and C.T. Sah, "Simple Physical Model of the Space Charge Capacitance of Metal-Oxide-Semiconductor Structures," J. Appl. Phys., Vol. 35, No. 8, pp. 2458, Aug., 1964.

63. G. Haas, "Preparation, Properties and Optical Application of Thin Films of TiO_2," Vacuum, 2, 331 (1952).

64. L.E. Hallander, Jr. and P.L. Castro, "Dielectric Properties of Single Crystal Nonstoichiometric Rutile, TiO_2," JAP 33, 3421 (1962).

65. L. Holland, Vacuum Deposition of Thin Films, Wiley: New York, N.Y. 473 (1960).

66. J.J. Hanak, K. Strater, G.W. Cullen, "Preparation and Properties of Vapor Deposited Niobium Stannide (Nb_3Sn)," RCA Rev. 25 (3), 342 (1964).

67. D.R. Harbison and H.L. Taylor, "Chemical Vapor Deposition of Thin Film Dielectrics," Southwestern IEEE Conference Record, Houston, Texas

68. D.R. Harbison and H.L. Taylor, "Chemical Vapor Deposition of Thin Film Titanium Dioxide, " J. Electrochem. Soc. 115, 238C (August, 1968) to be published in Deposited Thin Film Dielectric Materials by the Electrochemical Society.

69. D.R. Harbison, J.R. Yeargan, and H.L. Taylor, "MOS Capacitance-Dissipation Properties," Southwestern IEEE Conference Record, Dallas, Texas (1966).

70. T.E. Hartman, J.C. Blair, and R. Bauer, "Electrical Conduction Through SiO Films," J. Appl. Phys., 37, 2468 (1966).

71. T.E. Hartman and J.S. Chivian, "Electron Tunneling Through Thin Aluminum Oxide Films," Phys. Rev., 134, A1094 (1964).

72. W.H. Hartwig and R.R. Richard, "MIS ADC and Digital Transducer Concepts," Government Microcircuit Applications Conference Digest of Papers, 1, 378 (Oct. 1-3, 1968).

73. S.M. Hu, D.R. Kerr, and L.V. Gregor, "Evidence of Hole Injection and Trapping in Silicon Nitride Films Prepared by Reactive Sputtering," Appl. Phys. Lett., 10, 97 (1967).

74. F. Huber, "Thin Films of Ti Oxide for Microminiaturization," IEEE Trans. Component Pts. CP-11, #2, 38 (1964).

75. IIT Research Institute, "Characterization of Ceramic Materials for Microelectronic Applications," Project G 6006-6, Rept. #2 (June 1966).

76. V.J. Jennings, A Sommers, H.C. Chang, "Epitaxial Growth of SiC," J. Electrochem. Soc. 113, 728 (1966).

77. I.T. Johansen, "Electrical Conductivity in Evaporated Silicon Oxide Films, J. Appl. Phys., 37, 499 (1966).

78. B.A. Joyce, et al., "The Epitaxial Deposition of Si on Quartz and Alumina," Trans AIME 233, 556 (1965).

79. I.L. Kalnin and J. Rosenstock, "Vapor Deposition of Ge on Mo," J. Elecchem. Soc. 112, 329 (1965).

80. J. Klerer, "On the Mechanism of the Deposition of Silica by Pyrolytic Deposition of Silanes," J. Electrochem. Soc. 112, 503 (1965).

81. T.K. Lakshmanan, "Chemical Formation of Microcircuit Elements," AD 428590 (Dec. 1963).

82. D.R. Lamb, Electrical Conduction Mechanisms in Thin Insulating Films, London, Methuen, 1967.

83. K. Lehovec, A. Slobodskoy and J.L. Sprague, "Field Effect Capacitance Analysis of Surface States on Silicon," Phys. Stat. Soc., Vol. 3, pp. 447-464, 1963.

84. R. Lindner, "Semiconductor Surface Varactor," B.S.T.J., Vol. 41, No. 3, May, 1962.

85. M. Macha, "A Review of Ceramic Thin Film Technology," Tech. Report, No. AFML-TR-67-226 (1967).

86. H.T. Mann, "Electrical Properties of Thin Polymer Films, Part I. Thickness 500-2500A," J. Appl. Phys., 35, 2173 (1964).

87. A. Many, Y. Goldstein, N.B. Grover, Semiconductor Surfaces, North-Holland Publishing Co. Amsterdam 1965.

88. Paul M. Marcus, "Calculation of the Capacitance of a Semiconductor Surface, with Application to Silicon," I.B.M. Journal, Vol. 8, No. 5, pp. 496-505, Nov., 1964.

89. H.B. Martin, "Development of Microelectronic Circuits for Linear Applications," AD 287650 (Oct. 1962).

90. J. Maserjian and C.A. Mead, "Conduction through TiO_2 Thin Films with Large Ionic Space Charge," J. Phys. Chem. Solids 28, 1971 (1967).

91. K.H. Maxwell and L.H. Robouin, "Chemical Vapor Deposition of Oxide Films from Volatile Chlorides I SiO_2," Electrochem. Technol, 3, 37 (1965).

92. F.L. McCrackin, E. Passaglia, R.R. Stromberg and H.L. Steinberg, "Measurement of the Thickness and Refractive Index of Very Thin Films and the Optical Properties of Surfaces by Ellipsometry," J. of Research, A. Phys. and Chem., Vol. 67A, No. 4, July-Aug., 1963, pp. 363-377.

93. C.A. Mead, "Electron Transport Mechanisms in Thin Insulating Films, Phys. Rev., 128, 2088 (1962).

94. D. Meyerhofer and S. Ochs, "Current Flow in Very Thin Films of Al_2O_3 and BeO," J. Appl. Phys., 34, 2535 (1963).

95. J.J. Mitchell, "Preparation and Dielectric Properties of a Multi-component Metallic Oxide Film," AD 416330 (March. 1963).

96. N.F. Mott and R.W. Gurney, Electronic Processes in Ionic Crystals, Dover Publications, Inc., New York (1964).

97. E.K. Muller, B.J. Nicholson, G. L'E Turner, "The Expiaxy of $BaTiO_3$ Films by Vapor Deposition," Brit. JAP 13, 486 (1962).

98. E.K. Muller, B.J. Nicholson, G. L'E Turner, "The Epitaxial Vapor Deposition of Perovskite Materials," J. Electrochem. Soc. 110, 969 (1963).

99. E.H. Nicollian and A. Goetzberger, "Lateral AC Current Flow Model for MOS Capacitors," IEEE Trans. E.D., ED-12, 108 (1965).

100. E.H. Nicollian and A. Goetzberger, "MOS Conductance Technique for Measuring Surface State Parameters," App. Phys. Lett. 7, 216 (1965).

101. E.H. Nicollian and A. Goetzberger, "The Si-SiO_2 Inteface - Electrical Properties as Determined by the Conductance Technique," BSTJ 46, 1055 (1967).

102. J.J. O'Dwyer, "Current-Voltage Characteristics of Dielectric Films," J. Appl. Phys., 37, 599 (1966).

103. D. Peterson, J. Black, W. Brand, D. Dulaney, "Non Vacuum Deposition Technique for Use in Fabricating Thin Film Circuits," AD 462743 (April 1965).

104. D.R. Peterson, Black, Brand, Tolliver (Motorola S/C Div.) "Techniques for Vapor Plating Passive Film Components on Silicon Integrated Circuit Wafers," AD 475622. (Nov. 1965).

105. S.R. Pollack and C.E. Morris, "Electron Tunneling Through Asymmetric Films of Thermally Grown Al_2O_3," J. Appl. Phys., 35, 1503 (1964).

106. S.R. Pollack, "Schottky Field Emission Through Insulating Layers," J. Appl. Phys., 34, 877 (1963).

107. M. Rand and J.L. Ashworth, "Deposition of Silica Films on Ge by the CO_2 Process," J. Electrochem. Soc. 113, 48 (1966).

108. H.G. Rylander III, "Ellipsometric Measurements," Internal Report, Electronic Materials Research Lab, The University of Texas, Austin, Texas.

109. C.T. Sah, R. Noyce, and W. Shockley, "Carrier Generation and Recombination in P-N Junctions," Proc IRE 45, 1228 (1957).

110. P.S. Schaffer, "Evaluation of Vapor Deposition Growth of Oxide Single Crystals from Metal Halides," AD 616914 (May, 1965).

111. F.W. Schmidlin, "Enhanced Tunneling Through Dielectric Films due to Ionic Defects," J. Appl. Phys. 37, 2823 (1966).

112. A.C. Schaffhauser, ed. Proceedings of the Conference on Chemical Vapor Deposition of Refractory Metals, Alloys, and Compounds, held at Gatlinburg, Tenn., September 12-14, 1967.

113. M.S. Seltzer, N. Albon, B. Paris, R.C. Himes, "Microscopic Measurement of Step Movement During Crystal Growth by Chemical Vapor Deposition," Rev. Sci. Instr. 36, 1423 (1965).

114. W.H. Shepherd, "Vapor Phase Deposition and Etching of Silicon," J. Electrochem. Soc. 112, 988 (1965).

115. V.J. Silvestri, "Growth Rate and Doping in the $GeCl_4$-H_2 System," presented at the Dallas Meeting of the Electrochemical Society Meeting, Abstract No. 104, May 12, 1967.

116. J.G. Simmons, "Generalized Formula for the Electric Tunnel Effect Between Similar Electrodes Separated by a Thin Insulating Film," J. Appl. Phys., Vol. 34, No. 6, June, 1963, pp. 1793-1803.

117. J.G. Simmons, "Poole-Frenkel Effect and Schottky Effect in Metal-Insulator-Metal Systems," Phys. Rev., 155, 657 (1967).

118. J.G. Simmons, "Potential Barriers and Emission-Limited Current Flow Between Closely Spaced Parallel Metal Electrodes," J. Appl. Phys., Vol. 35, No. 8, Aug. 1964, pp. 2472-2481.

119. R.A. Smith, Semiconductors, Cambridge Univ. Press, Cambridge, (1959).

120. S. Steele, J. Poppis, R. Ellis, L. Hagen, H. Schiller, "Progress Report on Chemical Vapor Deposited Materials for Electron Tubes," AD 477126.

121. H.F. Sterling and R.C.G. Swann, "Chemical Vapor Deposition Promoted by RF Discharge," Solid State Electron 8, 653 (1965).

122. H.F. Sterling and R.C.G. Swann, "RF Initiated Vapor Deposition of Glassy Layer," Phys. Chem. Glasses 6, 109 (1965).

123. R. Stratton, "Volt-Current Characteristics for Tunneling Through Insulating Films," J. Phys. Chem. Solids, Vol. 23, 1963, pp. 1177-1190.

124. S.M. Sze, "Current Transport and Maximum Dielectric Strength of Silicon Nitride Films," J. Appl. Phys. 38, 2951 (1967).

125. L.M. Terman, "An Investigation of Surface States at a Silicon/Silicon Oxide Interface Employing M-O-S Diodes," Dissertation, University Microfilms, Inc., Ann Arbor, Michigan.

126. H.C. Theurer, "Epitaxial Si Films by Hydrogen Reduction of $SiCl_4$," J. Electrochem. Soc. 108, 649 (1961).

127. H.C. Theurer and H. Christensen, "Epitaxial Films of Si and Ge by Halide Reduction," J. Electrochem. Soc. 107, 268c (1960).

128. J.J. Tietjen and J.A. Amick, "The Preparation and Properties of Vapor Deposited Epitaxial GaAs by Using Arsine and Phosphine," J. Electrochem. Soc. 113, 724 (1966).

129. S.K. Tung and R.E. Caffrey, "The Deposition of Oxide on Si by Reaction of a Metal Halide with a Hydrogen/Carbon Dioxide Mixture," Trans. Met. Soc. AIME 233, 572 (1965).

130. "Tyzor" Organic Titanates, Bulletin of E.I. duPont de Nemours and Company, Wilmington, Delaware.

131. J.A. van Raalte, "Conduction Phenomena in Rutile Single Crystals," AD 610101, (1964).

132. A.R. von Hippel, "Studies on the Formation and Properties of High Temperature Dielectrics," AD 459511 (1964).

133. L.C. Wang, "Electrical Conduction Mechanisms in Metal-Polymer-Semiconductor Thin Film Structures," Master's Thesis, The University of Texas at Austin, Austin, Texas (1968).

134. C.W. Wilmsen, "Tunneling from a Metal into a Semiconductor," Dissertation, The University of Texas, January, 1967.

135. J.J. Wortman, Integrated Silicon Device Technology, Vol. III -- Photoengraving, AD 603715 (1964).

136. J.R. Yeargan and H.L. Taylor, "Conduction Mechanisms of Pyrolytic Silicon Nitride Films," J. Electrochem. Soc. 115, 273 (1968).

137. J.R. Yeargan and H.L. Taylor, "The Poole-Frenkel Effect with Compensation Present," J. Appl. Phys. (Nov. 1968).

138. M. Yokozawa, "Vapor Deposition of TiO_2," Japan JAP 7, 96 (1968).

139. A. Zawadowski, "General Theory of Tunneling in Oxide Diodes," Phys. Rev. 163, 341 (1967).

140. C. Ziegler, "Epitaxial In-Sb Films by Vapor Phase Transport Reaction," Solid State Electronics 6, 680-81 (1963).